PHASE EQUILIBRIA

IN

THE SYSTEM $NaAlSi_3O_8$-$NaAlSiO_4$-H_2O

EXPERIMENTAL AND THEORETICAL STUDIES OF PHASE EQUILIBRIA IN THE SYSTEM $NaAlSi_3O_8$-$NaAlSiO_4$-H_2O WITH SPECIAL EMPHASIS ON THE STABILITY OF ANALCITE

By

KI-TAE KIM, B.Sc., M.Sc.

A Thesis

Submitted to the School of Graduate Studies

in Partial Fulfilment of the Requirements

for the Degree

Doctor of Philosophy

McMaster University

September, 1970

Dedicated to

My Wife and Our Parents

DOCTOR OF PHILOSOPHY (1970) McMASTER UNIVERSITY
(Geology) Hamilton, Ontario.

TITLE: Experimental and Theoretical Studies of Phase Equilibria in the System $NaAlSi_3O_8$-$NaAlSiO_4$-H_2O with Special Emphasis on the Stability of Analcite

AUTHOR: Ki-Tae Kim, B.Sc., Seoul National University (1959)
M.Sc., Seoul National University (1962)

SUPERVISOR: Professor B. J. Burley.

NUMBER OF PAGES: xx, 151.

SCOPE AND CONTENTS: Phase equilibria in the system $NaAlSi_3O_8$-$NaAlSiO_4$-H_2O were determined in the P-T range of 0.5-10Kb and 150-900°C. The T-X stability fields of analcite were established and the petrogenetic implication of analcite was discussed. The compositions of a number of univariant phases were determined in this P-T range. A method has been developed for the determination of H_2O- content in melts and hydrous minerals.

By adding $KAlSiO_4$ component to this system, the sequence of P-T curves around a quaternary invariant point was theoretically deduced.

In the P-T region above 10Kb, phase equilibria in the ternary system were theoretically reviewed in the light of compositional data of invariant phases. The P-T stability fields of subsolidus analcite and liquidus analcite were deduced.

ABSTRACT

Phase equilibrium relations were determined in the system $NaAlSi_3O_8$-$NaAlSiO_4$-H_2O on a P-T projection in the P-T range 0.5-10Kb and 150°-900°C, and on three isobaric (2Kb, 5.15Kb and 7.32Kb) T-X projections. The T-X stability field of analcite determined in this study has a relatively large distorted pentagonal shape. The petrogenetic problem of analcite is fully discussed. On the composition join $NaAlSiO_4$-H_2O, the phase relation is not binary for the transition: nepheline hydrate I = nepheline + H_2O; there exists a narrow three-phase zone for the transition. The true P-T curve was determined in terms of a ternary univariant reaction: nepheline hydrate I + analcite = nepheline + H_2O. Another univariant reaction (zeolite species P. = analcite + nepheline hydrate I + H_2O) was found at 2Kb/215°C and 5.15Kb/235°C and determined on a P-T projection. In the system $NaAlSi_3O_8$-SiO_2-H_2O, albite contains a maximum of about 5 Wt.% silica in solid solution at 5.15Kb/670°C.

The equilibrium compositions of various univariant phases were determined essentially by phase boundary-location on several isobaric T-X projections. Three singular points were determined: two of

them are approximately located at 0.8Kb/390°C and 9.4Kb/475°C on a univariant curve (N-h I + Anl = Ne + H_2O). The other one is approximately located at 6Kb/655°C on the (Ab) univariant curve.

A simple method for determining H_2O-solubility in melts was developed and applied to the study of the system $NaAlSi_3O_8$-$NaAlSiO_4$-H_2O. Using this method, solubility data are simply obtained as by-products of the experimental runs made for the investigation of the phase equilibria. The amount of water required to make an H_2O-saturated melt (from the total amount of water in the original charge) is taken as the dissolved water in the melt; the solubility value is corrected by determining the amount of moisture originally absorbed in the starting powder. The method is generally applicable to the determination of H_2O-content in any hydrous phase. The H_2O-solubility in a melt is not too sensitive to a variation in anhydrous composition of the melt (~6±1Wt.% H_2O at 2Kb and ~11±1 Wt.% H_2O at ~5Kb in the range of compositions $Ab_{100}Ne_0$-$An_{40}Ne_{60}$). H_2O-solubility in the (Anl) and (Ne) univariant melts was determined up to 10Kb (H_2O contents: 4.7 Wt.%/1.1Kb and 852°C, 6.2 Wt.%/2Kb and 804°C, 10.8 Wt.%/5.2Kb and 672°C, 12.2 Wt.%/6.6Kb and 655°C, 13.2 Wt.%/7.3Kb and 652°C and 14(?) Wt.%/10Kb and 632°C). The origin of water bubbles in quenched hydrous glasses is essentially attributed to the exsolution of the dis-

solved water in melts upon quenching.

The sequence of P-T curves around a quaternary invariant point ($\sim$5Kb and $\sim$635°C) in the system $NaAlSiO_4$-$KAlSiO_4$-SiO_2-H_2O was theoretically discussed. The most probable four P-T diagram types are proposed, one of which is expected to be the real one.

Phase relations in the system $NaAlSi_3O_8$-$NaAlSiO_4$-H_2O are theoretically discussed up to $\sim$15Kb. The discussion is largely based on the equilibrium compositions of invariant phases approximately estimated from data presented in Parts 1 and 2. Six invariant points are examined. Two of them, I_5 and I_6, have been predicted to occur; I_5 is inferred to be located at $\sim$13Kb/$\sim$500°C where five phases Jd, N-h I, Anl, Ne and V coexist, and I_6 to be located at $\sim$0.5Kb/$\sim$375°C where Ab, Ne, Anl, N-h I and V coexist. The phase relations around the other four are partly modified. The maximum P-T stability field of analcite is deduced. The stability field of solidus analcite is extremely large, whereas that of liquidus analcite is very much limited. The maximum stability field of liquidus analcite is a small triangular area defined by three invariant points I_1 (5.15Kb/657°C), I_2 (11Kb/650°C) and I_4 (12.5Kb/575°C).

ACKNOWLEDGEMENTS

I am greatly indebted to Dr. B.J. Burley for suggesting many important investigations, for his assistance and constructive criticism throughout this work, and for greatly improving the manuscript through his critical reading and advice.

I wish to thank the National Research Council of Canada and the Geological Survey of Canada for providing research grants.

I am grateful to Mr. F. Tebay for running the X-ray diffraction patterns for the identification of run products, to Mr. J. Cekr for constructing furnaces and controllers, and for repairing various instruments, to Mr. J.R. Muysson for analysing the starting materials, and to Messrs. H.D. and L.J. Falkiner for making fragment sections.

I am also grateful to Miss J. Barrett for ordering the necessary materials and instruments for the present work, and for speedy and careful typewriting of the thesis.

In particular, I am indebted to Drs. D.L. Hamilton, H.P. Schwarcz and D.M. Shaw for critical reading and discussion of the manuscript, and to Drs. R.H. McNutt, C.J.L. Lock and H.D. Grundy for numerous helpful suggestions from the beginning of this study.

I am also grateful to Mr. J. L. Griep for partly reading the manuscript and for suggesting good presentation; to Mrs. H. Elliott for typewriting the manuscript of preliminary results of this work, and to Mr. J. Whorwood for photographic services.

Finally, I wish deeply to express many thanks to my wife, Sun-Young, for her limitless patience and encouragement.

The responsibility for errors, misconceptions and misinterpretations is, of course, my own.

TABLE OF CONTENTS

LIST OF TABLES

LIST OF FIGURES

PART 1

PHASE EQUILIBRIA IN THE SYSTEM $NaAlSi_3O_8$-$NaAlSiO_4$-H_2O UP TO 10Kb WITH SPECIAL EMPHASIS ON THE T-X STABILITY OF ANALCITE

EXPERIMENTAL INVESTIGATION

I. GENERAL STATEMENTS

The various phase relations in the system $NaAlSiO_4$-$KAlSiO_4$-SiO_2 ± H_2O have been investigated experimentally with the aid of synthetic mixtures. Through these studies, invaluable basic knowledge has been established, on which modern petrology is largely based.

The present study was restricted to one of its subsystems $NaAlSi_3O_8$-$NaAlSiO_4$-H_2O as a step towards the study of the total system. The phase relations in this ternary system were studied on a P-T projection up to 10Kb and 900°C and also on isobaric T-X projections.

MacKenzie (1957) synthesized analcite of albitic composition in his study of albite modifications. Burley & Freeman (1959) synthesized silica-rich analcite in their study of the temperature effect on analcite lattice parameters. Saha (1959, 1961) pointed out the extensive solid solutions of synthetic analcites from albitic to natrolitic compositions. Thus it has been demonstrated that analcite forms a wide range of solid solutions. Subsequently, Wilkinson (1963), Wilkinson & Whetten (1964), and Coombs & Whetten (1967), etc. confirmed that natural analcites, especially sedimentary ones, also have a similar range of solid solutions to the synthetic ones.

In order to find out the temperature and pressure dependences of the stability field of analcites of various compositions and also for other purposes, the phase relations on several isobaric T-X diagrams were determined. The theoretical basis for this work was provided by an earlier construction of a hypothetical T-X phase diagram based on data reported by various authors and also data obtained by preliminary experiments in the system SiO_2-$NaAlSiO_4$-H_2O. Actually, this experimental study was a phase-equilibria study of the system SiO_2-$NaAlO_2$-H_2O, but the present report is restricted to the system $NaAlSi_3O_8$-$NaAlSiO_4$-H_2O.

Yoder (1954), Greenwood (1961) and Peters, Luth & Tuttle (1966) have investigated the P-T stability field of phase-equilibria in the system $NaAlSi_3O_8$-$NaAlSiO_4$-H_2O. The former two authors determined a univariant curve (L): analcite $\rightleftharpoons$ albite + nepheline + vapor up to P_{H_2O} = 40,000 psi and 30,000 psi respectively. The last authors, Peters et al. have established the P-T stability field up to 10Kb around an invariant point, where five phases albite, nepheline, analcite, liquid and vapor occur.

The univariant curves (L) of reaction Anl $\rightleftharpoons$ Ab+Ne+V determined independently by the above authors deviate from one another as much as 80°C which seems to be beyond the range of experimental error.

Sand, Roy and Osborn (1957, p.176) found the transition temperature from nepheline to nepheline hydrate I in the presence of excess water to be 460°C at 1Kb. Saha (1961, p.867) determined the transition curve for nepheline + water = nepheline hydrate I + water up to 3.45Kb, and found the transition temperature to be 445°±10°C at 1Kb. He concluded that it was impossible to establish the stability field of nepheline hydrate I.

In order to find and precisely determine the P-T stability fields in this ternary system, the present study was based on 900 data points, including reversible runs, within the P-T range 0.5-10Kb and 150-900°C.

The crystal phases encountered in this study are:

Albite solid solution (intermediate form only, with respect to the value of $2\theta_{131} - 2\theta_{1\bar{3}1}$).

Nepheline solid solution (low nepheline only, hexagonal symmetry)

Nepheline hydrate I solid solution (orthorhombic ?)

Analcite solid solution (cubic, corresponding to Saha's study (1959, 1961) with respect to compositional range and displacement of (639) peak of analcite of different compositions

Zeolite species P solid solution (cubic ?).

In addition to the crystal phases, there are liquid and water vapor phases. H_2O-contents in hydrous phases were based on the data determined in

this study using a method which will be described in Part 2. The composition of the vapor phase was not determined in this study.

Nepheline hydrate I was interpreted as orthorhombic by Barrer and White (1952, p. 1565) and indexed assigning an orthorhombic unit cell by Edgar (1964, p. 1140-41). But it was interpreted to be hexagonal and indexed on the basis of the hexagonal unit cell by Kubo, Yamaguchi and Kasahara (1967, p. 185). In this study, the crystallography was not studied further.

II. EXPERIMENTAL METHODS

For the present study, starting materials mostly consisted of oxide gels which were prepared using the method described by Hamilton and MacKenzie (1960). The composition of the gels was determined by an atomic absorption spectrophotometric method and found to be correct within the limits of analytical accuracy. For the determination of the reversibility of phase-equilibria, synthetic minerals were used as starting materials.

All experiments of phase equilibria were carried out in cold-seal pressure vessels described by Tuttle (1949) and Luth & Tuttle (1963), and using the sealed-tube technique (Goranson, 1931). The size of all the capsules (mostly gold, to a lesser extent platinum) used herein is 2.5mm internal diameter, 3mm external diameter and 18-20mm in length. In order to get simultaneously the data of H_2O-contents in hydrous phases from the study of phase-equilibria, the experimental details to be described in Part 2 (Chapter III) were used. Pressures were measured by a Harwood manganin cell and a Bourdon-tube-type gauge and are believed to be within ±4 percent of the stated values. Temperature measurements were recorded continuously on a Speedomax W recorder and checked by a potentiometer. The temperatures are believed to be correct within $\pm 5^{\circ}C$.

The run products were examined with a petrographic microscope and by filtered CuKα X-ray diffraction.

The determination of the anhydrous composition of a phase was essentially based on the conventional method of phase boundary-location.

III. T-X STABILITY FIELDS OF CRYSTAL PHASES

Two T-X phase diagrams (Figs. 1 and 2) were determined nearly completely at P_{H_2O} = 2Kb and 5.15Kb respectively (see Tables I and II). The phase relations in the liquidus region at 7.32Kb were determined (Figs. 6a & b, etc. and Table IVa). The isobaric T-X phase diagrams were constructed projecting all the phase relations determined in the presence of excess water to the plane consisting of the temperature-axis and the composition-axis of $NaAlSi_3O_8$-$NaAlSiO_4$ (dry base).

It was found that the stability field of analcite has a distorted pentagonal shape which is essentially temperature-dependent but insignificantly pressure-dependent (see Fig. 4). The equilibrium compositions of the univariant phases were determined essentially on the basis of the T-X phase diagrams. The three singular points were also obtained in this way, and two univariant reactions were newly found and their P-T curves were determined on P-T projection.

It is to be noted that below about 500°C (see Figs. 1, 2 and 3c-e and g-j) the phase-equilibrium relations are not restricted to the system $NaAlSi_3O_8$-$NaAlSiO_4$-H_2O but extend towards SiO_2- and $NaAlO_2$-components. Strictly speaking, therefore, the phase relations belong to the system SiO_2-$NaAlO_2$-H_2O, below that temperature.

TABLE I

RUNS FOR THE DETERMINATION OF A T-X PHASE DIAGRAM AT 2 KB IN THE SYSTEM ALBITE-NEPHELINE-WATER(RELEVANT TO FIG.1). THE STARTING MATERIALS USED WERE POWDERED GELS OF VARIOUS COMPOSITION.
AB=ALBITE SOLID SOLUTION(S.S.), NE=NEPHELINE S.S., ANL=ANALCITE S.S., N-H I=NEPHELINE HYDRATE I S.S., ZP=ZEOLITE SPECIES P S.S., GL=GLASS(MELT), V=WATER VAPOR, .=SMALL AMOUNT, ..=VERY SMALL OR TRACE AMOUNT.

RUN	COMPOSITION, Wt %			EXPERIMENTAL CONDITION			RESULTS
	ANHYDROUS		WATER	PRESS	TEMP	TIME	(PHASE)
NO.	AB	NE	AMOUNT	KB	°C	DAY	
277	104.9	-4.9	49.0	2.02	305	16.9	ANL+V
656	100.0	0.0	29.8	1.97	713	8.8	AB+V
659	100.0	0.0	31.5	1.97	594	8.8	AB+V
857	100.0	0.0	25.8	2.02	585	20.2	AB+V
614	100.0	0.0	35.3	2.01	496	5.9	AB+..ANL+V
665	100.0	0.0	32.8	1.97	451	8.8	AB+..ANL+V
611	100.0	0.0	33.2	2.01	420	5.9	AB+..ANL+V
576	100.0	0.0	44.0	2.00	389	7.1	AB+.ANL+V
622	100.0	0.0	31.9	2.04	347	14.8	AB+ANL+V
605	100.0	0.0	37.1	2.01	303	5.9	ANL+V
727	100.0	0.0	32.8	2.01	250	25.9	ANL+V
729	100.0	0.0	28.0	2.01	250	25.9	ANL+V
631	100.0	0.0	36.7	2.04	253	14.8	ANL+ZP+V
743	96.6	3.4	34.1	2.01	775	0.9	AB+..GL+V
734	96.6	3.4	32.4	2.01	762	0.9	AB+V
657	96.6	3.4	31.9	1.97	713	8.8	AB+V
740	96.6	3.4	35.6	2.01	700	5.0	AB+V
660	96.6	3.4	29.7	1.97	594	8.8	AB+..ANL+..NE+V
615	96.6	3.4	30.2	2.01	496	5.9	AB+..ANL+V
735	93.1	6.9	26.5	2.01	762	0.9	AB+..GL+V
741	93.1	6.9	31.5	2.01	700	5.0	AB+..NE+V
235	89.7	10.3	33.0	2.00	880	0.9	GL+V
190	89.7	10.3	31.1	2.00	853	3.8	GL+AB+V
198	89.7	10.3	31.6	2.00	804	3.8	AB+GL+V
228	89.7	10.3	40.3	2.01	786	2.5	AB+GL+V
219	89.7	10.3	34.2	2.02	761	3.9	AB+..GL+V
288	89.7	10.3	37.1	2.02	748	16.9	AB+..NE+..GL+V
207	89.7	10.3	34.1	1.99	737	13.1	AB+..NE+V
282	89.7	10.3	37.5	2.02	690	16.9	AB+.NE+V
210	89.7	10.3	35.0	1.99	612	28.3	AB+.NE+V
188	89.7	10.3	29.2	2.02	497	23.0	AB+ANL+V
247	89.7	10.3	48.0	2.02	311	13.7	ANL+V
263	89.7	10.3	50.0	2.04	277	23.0	ANL+V
266	89.7	10.3	52.6	2.04	256	23.0	ANL+V
253	89.7	10.3	52.6	2.02	165	13.7	ZP+V
211	87.7	12.3	34.5	1.99	612	28.3	AB+..NE+V
623	87.7	12.3	33.7	2.04	347	14.7	ANL+..AB+V
639	87.7	12.3	42.7	2.04	200	14.8	ANL+ZP+V
236	85.9	14.1	36.1	2.00	880	0.9	GL+V
229	85.9	14.1	33.3	2.01	786	2.5	AB+GL+V
220	85.9	14.1	28.3	2.02	761	3.9	AB+.GL+V

TABLE I (Continued)

208	85.9	14.1	35.6	1.99	737	13.1	AB+..NE+V
191	84.0	16.0	31.1	2.00	853	3.8	GL+.AB+V
199	84.0	16.0	28.6	2.00	804	3.8	GL+AB+V
289	84.0	16.0	30.1	2.02	748	16.9	AB+.NE+V
209	84.0	16.0	35.6	1.99	737	13.1	AB+.NE+V
283	84.0	16.0	32.6	2.02	690	16.9	AB+.NE+V
244	84.0	16.0	48.2	2.02	358	13.7	ANL+..AB+V
221	76.7	23.3	29.9	2.02	761	3.9	AB+GL+V
238	76.7	23.3	27.5	2.02	403	10.1	ANL+..AB+V
577	76.7	23.3	35.2	2.00	389	7.1	ANL+..AB+V
624	76.7	23.3	26.0	2.04	347	14.8	ANL+..AB+V
719	76.7	23.3	22.8	2.01	300	25.9	ANL+V
632	76.7	23.3	36.2	2.04	233	14.8	ANL+V
640	76.7	23.3	32.8	2.04	200	14.8	ANL+V
239	70.7	29.3	31.9	2.02	403	10.1	ANL+..AB+V
679	70.7	29.3	21.5	1.97	358	10.1	ANL+V
192	69.1	30.9	26.9	2.00	853	3.8	GL+V
200	69.1	30.9	28.9	2.00	804	3.8	GL+.AB+V
264	69.1	30.9	48.6	2.04	277	23.0	ANL+V
230	66.9	33.1	32.7	2.01	786	2.5	GL+..AB+V
222	66.9	33.1	29.7	2.02	761	3.9	AB+GL+V
292	66.9	33.1	41.0	2.02	506	16.9	ANL+.AB+V
201	64.8	35.2	39.0	2.00	804	3.8	GL+V
744	64.8	35.2	24.3	2.01	775	0.9	GL+V
223	64.8	35.2	38.5	2.02	761	3.9	GL+AB+V
293	64.8	35.2	50.1	2.02	506	16.9	ANL+..AB+V
582	64.8	35.2	26.0	2.00	472	7.1	ANL+..AB+V
666	64.8	35.2	28.0	1.97	451	8.8	ANL+..AB+V
708	64.8	35.2	26.4	2.01	413	25.2	ANL+..AB+V
240	64.8	35.2	39.6	2.02	403	10.1	ANL+V
684	64.8	35.2	25.6	1.97	390	10.1	ANL+V
245	64.8	35.2	53.5	2.02	358	13.7	ANL+V
265	64.8	35.2	51.0	2.04	277	23.0	ANL+V
267	64.8	35.2	55.2	2.04	256	23.0	ANL+V
633	64.8	35.2	37.4	2.04	233	14.8	ANL+V
641	64.8	35.2	41.0	2.04	200	14.8	ANL+V
617	64.8	35.2	40.0	2.04	169	14.8	ANL+V
745	59.8	40.2	24.2	2.01	775	0.9	GL+.NE+V
736	59.8	40.2	20.5	2.01	762	0.9	GL+.NE+V
874	59.8	40.2	25.0	2.00	616	19.1	AB+NE+V
858	59.8	40.2	22.5	2.02	585	20.2	ANL+..AB+V
634	59.8	40.2	34.5	2.04	233	14.8	ANL+V
642	59.8	40.2	35.6	2.04	200	14.8	ANL+V
618	59.8	40.2	34.5	2.04	169	14.8	ANL+V
193	57.0	43.0	30.1	2.00	853	3.8	GL+V
231	57.0	43.0	29.9	2.01	786	2.5	GL+.NE+V
224	57.0	43.0	34.7	2.02	761	3.9	NE+GL+V
349	57.0	43.0	36.9	2.00	664	3.1	AB+NE+V
347	57.0	43.0	41.3	2.00	645	3.1	AB+NE+V
365	57.0	43.0	43.8	2.01	620	2.7	AB+NE+V
363	57.0	43.0	41.7	2.01	602	2.7	ANL+..AB+V
367	57.0	43.0	43.6	2.01	545	2.7	ANL+V
294	57.0	43.0	44.3	2.02	506	16.9	ANL+V
256	57.0	43.0	43.5	1.99	444	20.0	ANL+V
585	54.7	45.3	23.7	2.00	605	7.1	NE+AB+..ANL+V

TABLE I (Continued)

661	54.7	45.3	24.6	1.97	594	8.8	ANL+•NE+••AB+V
859	54.7	45.3	24.8	2.02	585	20.2	ANL+V
606	54.7	45.3	33.3	2.01	303	5.9	ANL+V
663	54.7	45.3	21.6	1.97	284	8.8	ANL+V
635	54.7	45.3	37.0	2.04	233	14.8	ANL+V
643	54.7	45.3	32.2	2.04	200	14.8	ANL+V
619	54.7	45.3	34.9	2.04	169	14.8	ANL+ZP+V
202	49.2	50.8	27.3	2.00	804	3.8	GL+NE+V
350	49.2	50.8	36.2	2.00	664	3.1	NE+AB+V
348	49.2	50.8	30.7	2.00	645	3.1	NE+AB+V
366	49.2	50.8	33.8	2.01	620	2.7	NE+AB+V
586	49.2	50.8	29.8	2.00	605	7.1	NE+AB+••ANL+V
364	49.2	50.8	34.1	2.01	602	2.7	ANL+•NE+V
368	49.2	50.8	33.0	2.01	545	2.7	ANL+••NE+V
616	49.2	50.8	28.8	2.01	496	5.9	ANL+V
583	49.2	50.8	29.5	2.00	472	7.1	ANL+V
257	49.2	50.8	37.4	1.99	444	20.0	ANL+V
625	49.2	50.8	32.0	2.04	347	14.7	ANL+V
248	49.2	50.8	41.6	2.02	311	13.7	ANL+V
730	49.2	50.8	27.8	2.01	250	25.9	ANL+V
878	49.5	50.8	28.7	2.00	194	44.2	ANL+V
612	43.5	56.5	33.0	2.01	420	5.9	ANL+V
608	43.5	56.5	36.6	2.01	379	5.9	ANL+V
626	43.5	56.5	31.6	2.04	347	14.8	ANL+V
720	43.5	56.5	28.3	2.01	300	25.9	ANL+V
808	43.5	56.5	28.0	2.03	249	27.0	ANL+••N-H I+V
644	43.5	56.5	38.7	2.04	200	14.8	ZP+•ANL+V
237	42.3	57.7	24.3	2.00	880	0.9	GL+•NE+V
258	42.3	57.7	37.3	1.99	444	20.0	ANL+••NE+V
709	39.3	60.7	22.8	2.01	413	25.2	ANL+••NE+V
685	39.3	60.7	20.0	1.97	390	10.1	ANL+••N-HI+••NE+V
721	39.3	60.7	28.3	2.01	300	25.9	ANL+••N-HI+V
194	35.4	64.6	30.1	2.00	853	3.8	NE+GL+V
203	35.4	64.6	31.3	2.00	804	3.8	NE+GL+V
232	35.4	64.6	30.3	2.01	786	2.5	NE+••GL+V
225	35.4	64.6	27.0	2.02	761	3.9	NE+••GL+V
259	35.4	64.6	39.8	1.99	444	20.0	ANL+NE+V
613	35.4	64.6	29.7	2.01	420	5.9	ANL+•NE+V
609	35.4	64.6	27.8	2.01	379	5.9	ANL+•N-HI+V
246	35.4	64.6	42.5	2.02	358	13.7	ANL+••N-HI+V
233	32.3	67.7	31.4	2.01	786	2.5	NE+••GL+V
226	32.3	67.7	25.5	2.02	761	3.9	NE+••GL+V
290	32.3	67.7	32.1	2.02	748	16.9	NE+••AB+V
249	32.3	67.7	43.7	2.02	311	13.7	ANL+••N-HI+V
254	32.3	67.7	44.8	2.02	165	13.7	ZP+V
195	29.1	70.9	25.1	2.00	853	3.8	NE+••GL+V
204	29.1	70.9	28.3	2.00	804	3.8	NE+••GL+V
234	29.1	70.9	34.2	2.01	786	2.5	NE+••GL+V
227	29.1	70.9	25.5	2.02	761	3.9	NE+••GL+V
658	29.1	70.9	35.1	1.97	713	8.8	NE+•AB+V
578	29.1	70.9	31.4	2.00	389	7.1	ANL+•N-HI+V
250	29.1	70.9	42.4	2.02	298	13.7	ANL+•N-HI+V
636	29.1	70.9	28.7	2.04	233	14.8	ANL+•N-HI+V
737	25.1	74.9	29.9	2.01	761	0.9	NE+V
742	25.1	74.9	24.0	2.01	700	5.0	NE+••AB+V
196	21.2	78.8	39.2	2.00	853	3.8	NE+••GL+V

TABLE I (Continued)

205	21.2	78.8	41.2	2.00	804	3.8	NE+V
738	21.2	78.8	26.7	2.01	761	0.9	NE+V
587	21.2	78.8	25.2	2.00	605	7.1	NE+V
189	21.2	78.8	33.1	2.02	497	23.0	NE+ANL+V
610	21.2	78.8	33.3	2.01	379	5.9	ANL+N-HI+V
607	21.2	78.8	34.5	2.01	303	5.9	ANL+.N-HI+V
645	21.2	78.8	37.3	2.04	200	14.8	ZP+..ANL+V
861	17.0	83.0	27.1	2.02	585	20.2	NE+V
197	12.7	87.3	41.3	2.00	853	3.8	NE+V
206	12.7	87.3	36.1	2.00	804	3.8	NE+V
295	12.7	87.3	48.9	2.02	506	16.9	NE+V
584	12.7	87.3	32.7	2.00	472	7.1	NE+V
667	12.7	87.3	33.3	1.97	451	8.8	NE+..ANL+V
474	12.7	87.3	46.2	1.98	413	12.0	NE+.ANL+V
579	12.7	87.3	38.2	2.00	399	7.1	N-HI+NE+ANL+V
637	12.7	87.3	33.9	2.04	233	14.8	N-HI+ANL+V
212	5.8	94.2	41.3	1.99	612	28.3	NE+V
296	5.8	94.2	48.9	2.02	506	16.9	NE+V
261	5.8	94.2	54.3	1.99	444	20.0	NE+V
477	5.8	94.2	50.1	1.98	431	12.0	NE+V
475	5.8	94.2	52.2	1.98	413	12.0	NE+N-HI+V
580	5.8	94.2	37.2	2.00	399	7.1	N-HI+NE+V
627	5.8	94.2	28.6	2.04	347	14.8	N-HI+.ANL+V
627	5.8	94.2	51.5	2.02	298	13.7	N-HI+ANL+V
255	5.8	94.2	51.1	2.02	165	13.7	ZP+V
757	0.0	100.0	26.3	2.03	599	8.1	NE+V
680	0.0	100.0	24.0	1.97	375	10.1	N-HI+V
628	0.0	100.0	24.5	2.04	347	14.8	N-HI+..ANL+V
722	0.0	100.0	29.5	2.01	300	25.9	N-HI+..ANL+V
646	0.0	100.0	32.0	2.04	200	14.8	N-HI+..ZP+V
297	-1.0	101.0	49.9	2.02	506	16.9	NE+V
262	-1.0	101.0	51.9	1.99	444	20.0	NE+V
478	-1.0	101.0	52.2	1.98	431	12.0	NE+V
476	-1.0	101.0	42.5	1.98	413	12.0	N-HI+NE+V
252	-1.0	101.0	56.3	2.02	298	13.7	N-HI+..ANL+V
268	-1.0	101.0	52.0	2.04	256	23.0	N-HI+.ANL+V
723	-5.2	105.2	29.0	2.01	300	25.9	N-HI+V
731	-5.2	105.2	23.7	2.01	250	25.9	N-HI+V
800	-9.3	109.3	27.5	2.03	300	27.0	N-HI+V
732	-9.3	109.3	26.4	2.01	250	25.9	N-HI+V

CD TOT 0225

TABLE II

RUNS FOR THE DETERMINATION OF A T-X PHASE DIAGRAM AT 5.15 KB IN THE SYSTEM ALBITE-NEPHELINE-WATER(RELEVANT TO FG.2). THE STARTING MATERIALS USED WERE POWDERED GELS OF VARIOUS COMPOSITION.
AB=ALBITE SOLID SOLUTION(S.S.), NE=NEPHELINE S.S., ANL=ANALCITE S.S., N-H I=NEPHELINE HYDRATE I S.S., ZP=ZEOLITE SPECIES P S.S., GL=GLASS(MELT), V=WATER VAPOR, .=SMALL AMOUNT, ..=VERY SMALL OR TRACE AMOUNT.

RUN	COMPOSITION, Wt%			EXPERIMENTAL CONDITION			RESULTS
	ANHYDROUS		WATER	PRESS	TEMP	TIME	(PHASE)
NO.	AB	NE	AMOUNT	KB	°C	DAY	
777	104.9	-4.9	27.3	5.22	758	0.6	AB+GL+V
781	104.9	-4.9	29.5	5.22	668	0.6	AB+V
778	100.0	0.0	21.1	5.22	758	0.6	AB+V
690	100.0	0.0	36.5	5.17	751	0.9	AB+V
591	100.0	0.0	31.5	5.08	495	3.0	AB+V
650	100.0	0.0	37.5	5.24	375	8.8	AB+..ANL+V
558	100.0	0.0	31.5	5.10	338	6.9	AB+ANL+V
556	100.0	0.0	32.3	5.10	299	6.9	ANL+V
653	100.0	0.0	42.2	5.24	289	8.8	ANL+V
779	96.6	3.4	23.1	5.22	758	0.6	ABP+GL+V
694	96.6	3.4	35.5	5.17	699	0.9	AB+..GL+V
599	96.6	3.4	36.3	5.23	672	2.2	AB+V
594	96.6	3.4	31.7	5.08	653	3.0	AB+V
780	93.1	6.9	22.0	5.22	758	0.6	GL+.AB+V
698	93.1	6.9	29.2	5.17	668	0.9	AB+..GL+V
518	89.7	10.3	36.4	5.10	272	3.9	ANL+..ZP+V
499	89.7	10.3	42.0	5.10	245	7.8	ANL+ZP+V
496	89.7	10.3	42.0	5.10	227	7.8	ZP+ANL+V
559	87.7	12.3	32.3	5.10	338	6.9	ANL+.AB+V
654	87.7	12.3	32.7	5.24	289	8.8	ANL+V
520	84.0	16.0	34.2	5.10	349	3.9	ANL+.AB+V
691	76.7	23.3	28.1	5.17	751	0.9	GL+V
651	76.7	23.3	32.6	5.24	375	8.8	ANL+..AB+V
854	76.7	23.3	23.5	5.15	251	7.5	ANL+V
523	69.1	30.9	28.1	5.10	482	3.9	ANL+.AB+V
428	66.9	33.1	42.4	5.12	468	1.5	ANL+..AB+V
695	64.8	35.2	30.8	5.17	699	0.9	GL+V
302	64.8	35.2	51.2	5.10	675	0.7	GL+.AB+V
299	64.8	35.2	49.2	5.10	661	0.7	GL+AB+V
592	64.8	35.2	29.3	5.08	496	3.0	ANL+..AB+V
429	64.8	35.2	47.0	5.12	468	1.5	ANL+V
500	64.8	35.2	47.5	5.10	245	7.8	ANL+V
497	64.8	35.2	44.8	5.10	227	7.8	ANL+V
570	64.8	35.2	35.6	5.14	178	8.6	ANL+V
600	59.8	40.2	28.5	5.23	672	2.2	GL+V
596	59.8	40.2	28.2	5.23	626	2.2	ANL+..AB+V
361	57.0	43.0	50.4	5.29	669	0.8	GL+V
380	57.0	43.0	45.1	5.17	658	1.0	ANL+GL+V
379	57.0	43.0	45.3	5.17	651	1.0	ANL+..AB+V
359	57.0	43.0	51.4	5.29	645	0.8	ANL+V
696	54.7	45.3	30.8	5.17	699	0.9	GL+V
601	54.7	45.3	32.9	5.23	672	2.2	GL+..NE+V

TABLE II (Continued)

597	54.7	45.3	33.4	5.23	626	2.2	ANL+V
519	54.7	45.3	34.3	5.10	272	3.9	ANL+V
573	54.7	45.3	34.4	5.14	225	8.6	ANL+V
527	54.7	45.3	33.4	5.19	176	5.8	ZP+ANL+V
602	49.2	50.8	26.6	5.23	695	2.2	GL+.NE+V
303	49.2	50.8	36.4	5.10	675	0.7	GL+.NE+V
362	49.2	50.8	41.6	5.29	669	0.8	GL+..NE+V
300	49.2	50.8	41.4	5.10	661	0.7	GL+.NE+V
360	49.2	50.8	36.6	5.29	645	0.8	ANL+.NE+V
311	49.2	50.8	40.9	5.36	537	2.6	ANL+V
308	49.2	50.8	44.0	5.36	462	2.6	ANL+V
655	49.2	50.8	35.2	5.24	289	8.8	ANL+V
848	49.2	50.8	23.2	5.15	220	7.5	ANL+V
692	43.5	56.5	35.6	5.17	751	0.9	GL+V
430	42.3	57.7	33.8	5.12	468	1.5	ANL+.NE+V
816	43.5	56.5	31.9	5.12	463	7.8	ANL+V
820	43.5	56.5	24.9	5.12	419	7.8	ANL+V
652	43.5	56.5	34.3	5.24	375	8.8	ANL+V
521	42.3	57.7	24.0	5.10	349	3.9	ANL+..N-HI+V
855	43.5	56.5	20.0	5.15	250	7.5	ANL+..N-HI+V
312	35.4	64.6	47.5	5.37	537	2.6	ANL+.NE+V
524	35.4	64.6	25.1	5.10	482	3.9	ANL+.NE+V
588	35.4	64.6	23.8	5.08	437	3.0	ANL+.NE+V
647	35.4	64.6	25.1	5.24	415	8.8	ANL+..N-HI+V
522	35.4	64.6	26.5	5.10	349	3.9	ANL+.N-HI+V
603	29.1	70.9	24.4	5.23	695	2.2	NE+GL+V
525	29.1	70.9	24.7	5.10	482	3.9	ANL+.NE+V
589	29.1	70.9	30.4	5.08	437	3.0	ANL+.NE+V
648	29.1	70.9	38.5	5.24	415	8.8	ANL+..N-HI+V
571	29.1	70.9	28.7	5.14	178	8.6	ZP+V
604	21.2	78.8	34.4	5.23	695	2.2	NE+.GL+V
699	21.2	78.8	28.0	5.17	668	0.9	NE+..GL+V
598	21.2	78.8	28.2	5.23	626	2.2	NE+.ANL+V
590	21.2	78.8	36.8	5.08	437	3.0	ANL+NE+..N-HI+V
649	21.2	78.8	31.1	5.24	415	8.8	ANL+N-HI+V
574	21.2	78.8	30.2	5.14	225	8.6	ZP+.ANL+V
528	21.2	78.8	29.1	5.19	176	5.8	ZP+V
783	17.0	83.0	19.7	5.22	668	0.6	NE+V
787	17.0	83.0	23.8	5.22	647	0.6	NE+V
697	12.7	87.3	29.6	5.17	699	0.9	NE+V
700	12.7	87.3	33.0	5.17	668	0.9	NE+V
309	12.7	87.3	57.9	5.36	462	2.6	NE+ANL+V
452	12.7	87.3	54.4	5.14	441	2.0	ANL+N-HI+NE+V
575	12.7	87.3	39.0	5.14	225	8.6	ZP+..N-HI+V

TABLE II (Continued)

693	5.8	94.2	34.0	5.17	751	0.9	NE+V
593	5.8	94.2	30.2	5.08	496	3.0	NE+V
455	5.8	94.2	53.5	5.14	452	2.0	NE+.ANL+V
453	5.8	94.2	50.4	5.14	441	2.0	N-HI+.NE+.ANL+V
572	5.8	94.2	35.1	5.14	178	8.6	ZP+V
313	-1.0	101.0	55.8	5.36	537	2.6	NE+V
310	-1.0	101.0	53.2	5.36	462	2.6	NE+V
456	-1.0	101.0	53.9	5.14	452	2.0	NE+..N-HI+V
454	-1.0	101.0	49.3	5.14	441	2.0	N-HI+.NE+..ANL+V
427	-1.0	101.0	59.5	5.12	429	1.5	N-HI+.ANL+V
501	-1.0	101.0	41.3	5.10	245	7.8	N-HI+ANL+V
498	-1.0	101.0	41.7	5.10	227	7.8	ZP+N-HI+V
670	-9.3	109.3	24.8	5.17	342	7.7	N-HI+V
856	-9.3	109.3	19.3	5.15	250	7.5	N-HI+V

TABLE III

REVERSAL RUNS FOR PHASE-EQUILIBRIA(RELEVANT TO FIGS.1,2 AND 5). SYNTHETIC MINERALS WERE USED AS STARTING MATERIALS IN THE PRESENCE OF EXCESS WATER(WATER-CONTENTS=20-40 WEIGHT PERCENT). AB=ALBITE S.S., NE=NEPHELINE S.S., ANL=ANALCITE S.S., N-HI= NEPHELINE HYDRATE I S.S., ZP=ZEOLITE SPECIES P.S.S., GL=GLASS (MELT), V=WATER VAPOR, .=SMALL AMOUNT, AND ..=VERY SMALL OR TRACE AMOUNT. * DENOTES THAT EQUILIBRIUM WAS NOT REVERSED.

RUN	COMPOSITION STARTING MATERIAL ANHYDROUS,Wt%			RUN CONDITION RESULTS			
				PRESS	TEM	TIME	(PHASES)
NO.	AB	NE		KB	°C	DAY	
886	12.7	87.3	ANL+N-HI+V	7.34	482	19.1	NE+ANL+V
887	5.8	94.2	N-HI+.ANL+V	7.34	482	19.1	NE+.ANL+V
888	-1.0	101.0	N-HI+.ANL+V	7.34	482	19.1	NE+V
882	5.8	94.2	NE+V	7.34	445	19.1	NE+N-HI+ANL+V
883	0.0	100.0	NE+V	7.34	445	19.1	NE+V *
890	100.0	0.0	AB+..ANL+V	5.15	510	10.5	AB+V
673	AMELIA AB		AB+V	5.17	303	7.7	AB+V *
676	AMELIA AB		AB+V	5.17	249	7.7	AB+V *
812	96.6	3.4	AB+V	5.12	561	7.8	AB+..ANL+V
850	89.7	10.3	ZP+ANL+V	5.15	295	7.5	ANL+V
851	76.7	23.3	ANL+.AB+V	5.15	295	7.5	ANL+..AB+V
819	66.9	33.1	ANL+..AB+V	5.12	419	7.8	ANL+V
891	64.8	35.2	ANL+V	5.15	510	10.5	ANL+..AB+V
813	59.8	40.2	ANL+.AB+V	5.12	561	7.8	ANL+..AB+V
782	57.0	43.0	ANL+V	5.22	668	0.6	GL+V
786	57.0	43.0	HYDROUS GL +V	5.22	647	0.6	ANL+V
814	49.2	50.8	ANL+V	5.12	561	7.8	ANL+..NE+V
892	49.2	50.8	ANL+..NE+V	5.15	510	10.5	ANL+V
818	21.2	78.8	ANL+N-HI+V	5.12	463	10.5	ANL+NE+V
815	12.7	87.3	NE+V	5.12	561	7.8	NE+..ANL+V
821	12.7	87.3	ANL+NE+V	5.12	419	7.8	ANL+NE+N-HI+V
853	12.7	87.3	ZP+.N-HI+V	5.15	250	7.5	ANL+N-HI+V
893	5.8	94.2	NE+..ANL+V	5.15	510	10.5	NE+V
846	-1.0	101.0	N-HI+ANL+V	5.15	220	7.5	N-HI+ANL+..ZP+V
842	57.0	43.0	ANL+..AB+V	4.80	654	2.7	ANL+..AB+..NE+V
839	49.2	50.8	NE+AB+V	4.80	664	2.7	NE+AB+GL+V
845	49.2	50.8	NE+AB+V	4.80	645	2.7	ANL+..NE+..AB+V
875	89.7	10.3	ANL+ZP+V	2.00	194	44.2	ANL+V
862	85.9	14.1	AB+NE+V	2.02	585	20.2	AB+ANL+V
867	64.8	35.2	ANL+.AB+V	2.02	388	49.2	ANL+V
872	57.0	43.0	ANL+V	2.00	616	19.1	AB+NE+V
864	49.2	50.8	NE+AB+V	2.02	585	20.2	NE+AB+..ANL
876	49.2	50.8	ANL+V	2.00	194	44.2	ANL+V *
868	42.3	57.7	ANL+.NE+V	2.02	388	49.2	ANL+V
873	21.2	78.8	NE+.ANL	2.00	616	19.1	NE+V
865	21.2	78.8	NE+V	2.02	585	20.2	NE+..ANL
879	21.2	78.8	ANL+.N-HI+V	2.00	425	44.2	ANL+.NE+V
880	12.7	87.3	NE+V	2.00	425	44.2	NE+.ANL+V
869	12.7	87.3	NE+V	2.02	388	49.2	NE+.ANL+.N-HI+V
877	12.7	87.3	ANL+N-HI+V	2.00	194	44.2	ANL+N-HI+V *
881	5.8	94.2	NE+N-HI+V	2.00	425	44.2	NE+V
871	0.0	100.0	N-HI+..ANL+V	2.02	388	49.2	N-HI+V
870	-1.0	101.0	NE+V	2.02	388	49.2	NE+.N-HI+V

FIG. 1. T-X (TEMPERATURE-COMPOSITION) PHASE DIAGRAM AT P_{H_2O} = 2Kb IN THE SYSTEM $NaAlSi_3O_8$-$NaAlSiO_4$-H_2O

Based on the experimental data presented in Table I.

Equilibrium phase relations in the presence of excess water were projected to the dry base, which was defined by two axes temperature and anhydrous composition. The equilibrium phase boundary is denoted by thick solid line. The phase boundary denoted by fine solid line is determined but uncertain with respect to the reversibility of phase-equilibria. Data were incomplete where dashed. Big open circle accompanied with run number represents a reversal run, given in Table III.

L = liquid, Ab = albite solid solution, Ne = nepheline s. s., Anl = analcite s. s., N-hI = nepheline hydrate I s. s., Zp = zeolite species P. s. s.

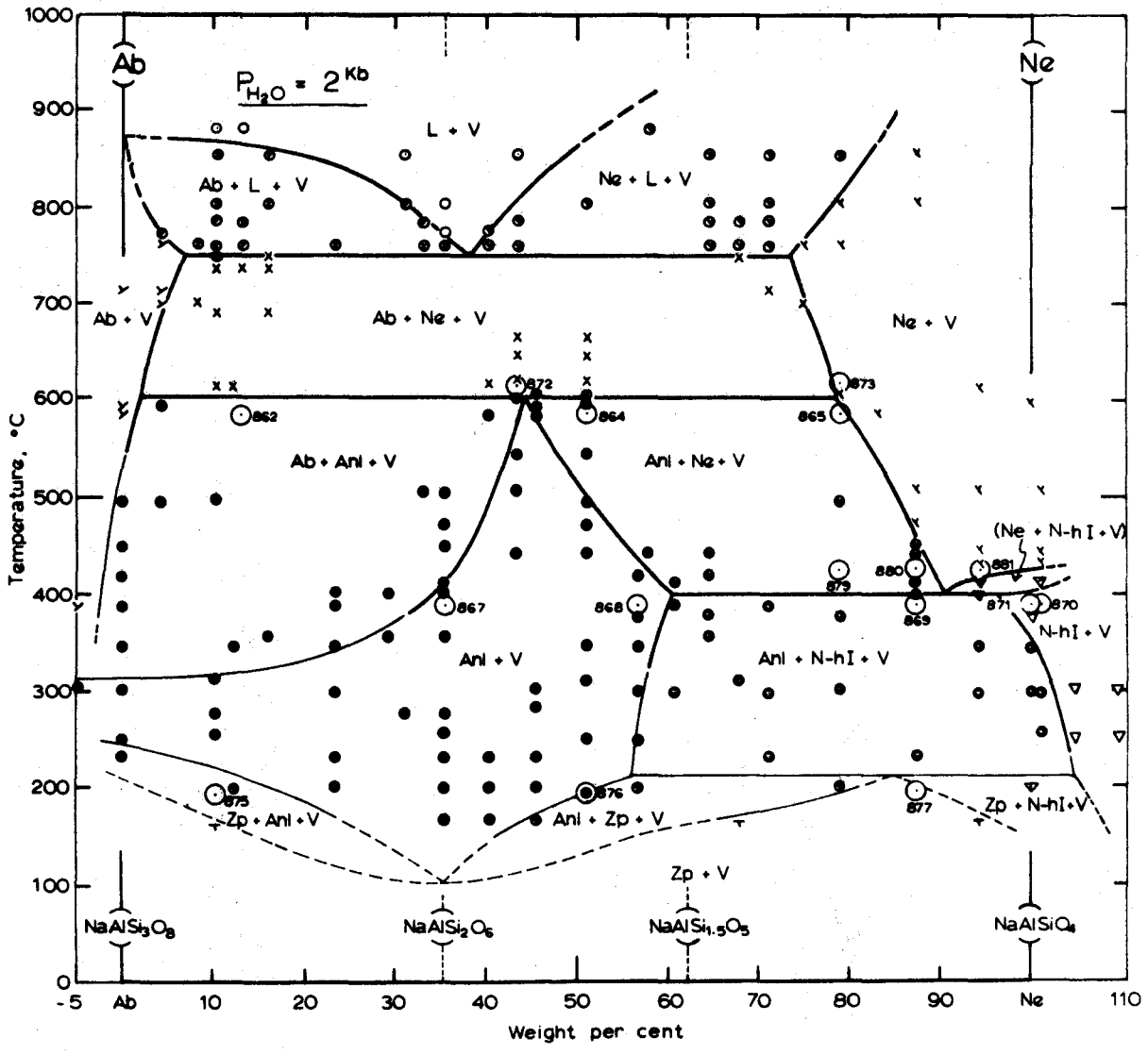
Ab
Ne
P_{H_2O} = 2 Kb
L + V
Ab + L + V
Ne + L + V
Ab + V
Ab + Ne + V
Ne + V
Ab + Anl + V
Anl + Ne + V
(Ne + N-hl + V)
Anl + V
Anl + N-hl + V
N-hl + V
Zp + Anl + V
Anl + Zp + V
Zp + N-hl + V
Zp + V
$NaAlSi_3O_8$
$NaAlSi_2O_6$
$NaAlSi_{1.5}O_5$
$NaAlSiO_4$
Temperature, °C
Weight per cent
-5
Ab
10
20
30
40
50
60
70
80
90
Ne
110
0
100
200
300
400
500
600
700
800
900
1000

FIG. 1

FIG. 2. T-X PHASE DIAGRAM AT P_{H_2O} = 5.15KB IN THE SYSTEM $NaAlSi_3O_8$-$NaAlSiO_4$-H_2O

Constructed projecting the equilibrium phase-boundaries determined in the presence of excess water to the dry base.

Experimental data are presented in Table II.

Equilibrium phase boundary is drawn with thick solid line, and the phase boundary drawn with fine solid line is also determined but uncertain with regard to reversibility of phase-equilibria. Data were incomplete where dashed. Big open circle denotes reversal run whose number is placed near the circle. For the details of reversal runs, see Table III.

L = liquid, Ab = albite solid solution, Ne = nepheline s.s.,

Anl = analcite s.s., N-h I = nepheline hydrate I, Zp = zeolite species P. s.s.

and V = water vapor phase.

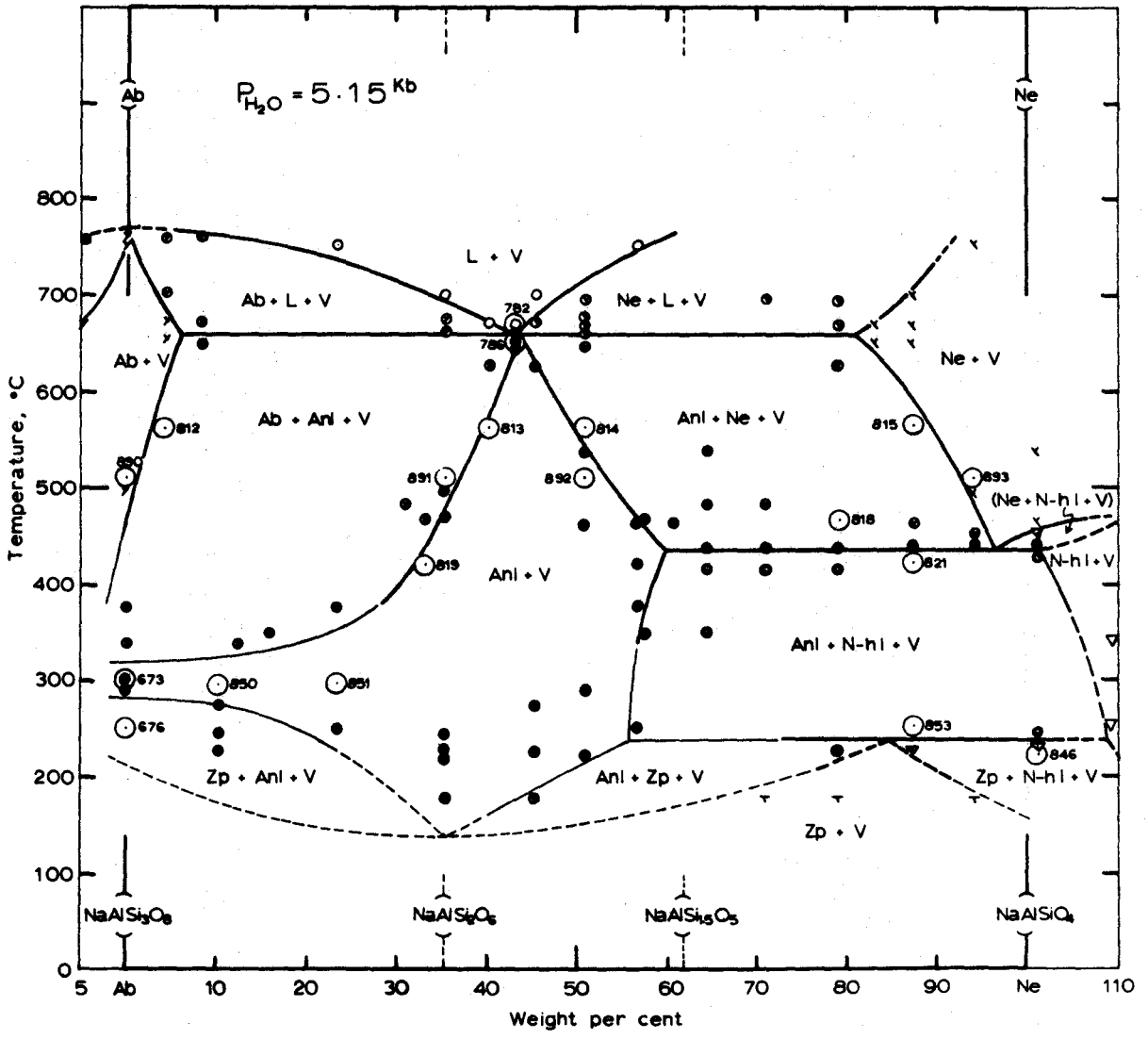
P_{H_2O} = 5.15 Kb
Ab
Ne
L + V
Ab + L + V
Ne + L + V
Ab + V
Ne + V
Ab + Anl + V
Anl + Ne + V
Anl + V
(Ne + N-hl + V)
N-hl + V
Anl + N-hl + V
Zp + Anl + V
Anl + Zp + V
Zp + N-hl + V
Zp + V
782
812
813
814
815
818
819
821
846
850
851
853
890
891
892
893
673
676
$NaAlSi_3O_8$
$NaAlSi_2O_5$
$NaAlSi_{1.5}O_5$
$NaAlSiO_4$
Temperature, °C
Weight per cent
0
100
200
300
400
500
600
700
800
5
10
20
30
40
50
60
70
80
90
110

FIG. 2

FIG. 3. ISOBARIC - ISOTHERMAL SECTIONS AT P_{H_2O} = 2Kb and 5.15Kb.

The sections a-e are showing phase relations at 2Kb and the ones f-j are representing phase-relations at 5.15Kb (invariant pressure).

Note that (1) section f is an invariant chemogram;

(2) where univariant reaction occurs at a given P & T, the reaction equation is given below the section;

(3) the successive isobaric-isothermal sections illustrate the compositional range of analcite solid solution;

(4) the phase-equilibria in the water-deficient region are not considered.

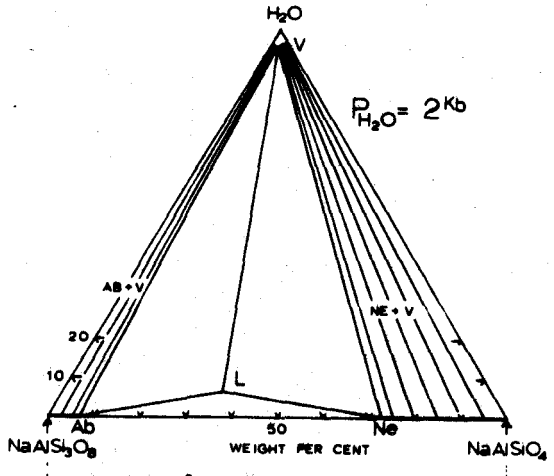

a) At 750°C, Ab + Ne + V = L

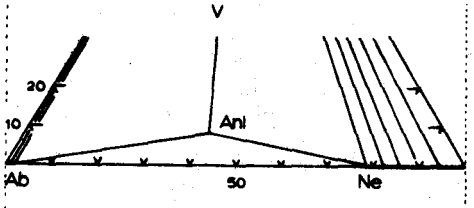

b) At 600°C, Ab + Ne + V = Anl

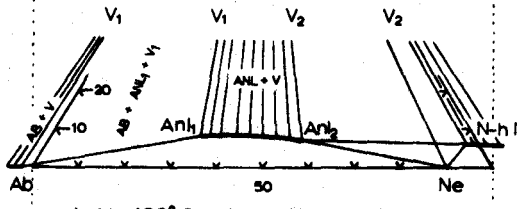

c) At 400°C, Anl_2 + N-hl = Ne + V_2

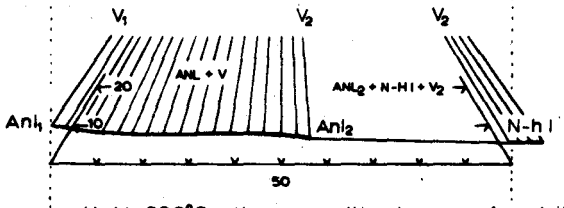

d) At 300°C, the compositional range of analcite solid solutions is the widest

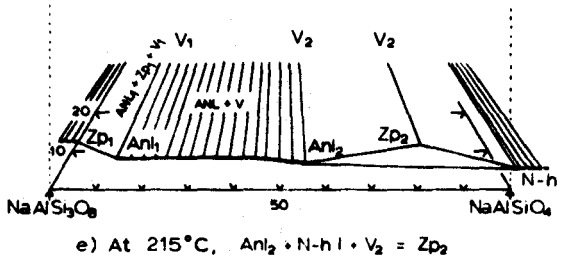

e) At 215°C, Anl_2 + N-hl + V_2 = Zp_2

f) At 657°C, an invariant temperature, the five phases, Ab, Ne, Anl, L & V, occur.

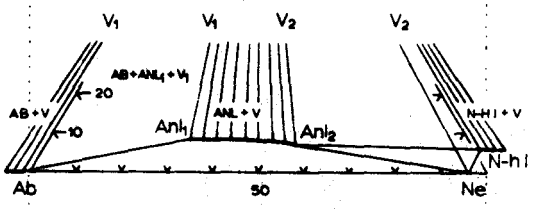

g) At 435°C, Anl_2 + N-hl = Ne + V_2

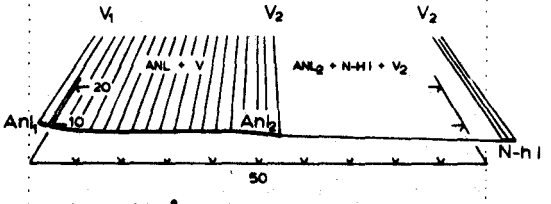

h) At 300°C, the widest compositional range of analcite solid solutions

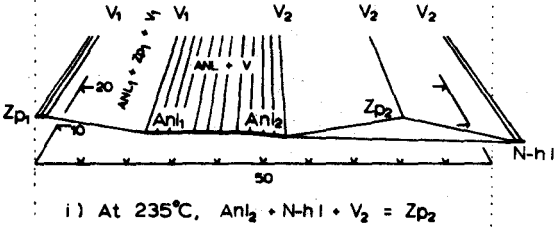

i) At 235°C, Anl_2 + N-hl + V_2 = Zp_2

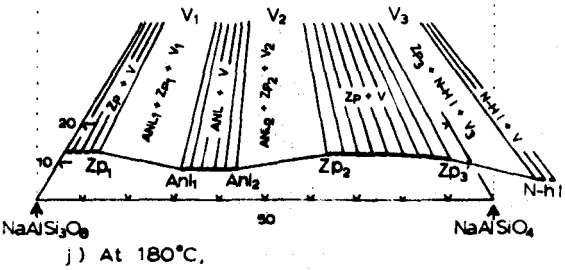

j) At 180°C.

FIG. 3

Fig. 4. THE STABILITY FIELD OF ANALCITE SOLID SOLUTIONS AS A FUNCTION OF TEMPERATURE AT EACH GIVEN PRESSURE

The analcite stability fields at P_{H_2O} = 2Kb and 5.15Kb were determined. The one at P_{H_2O} = 7.32Kb was approximately estimated.

Each of the stability fields has a distorted pentagonal shape.

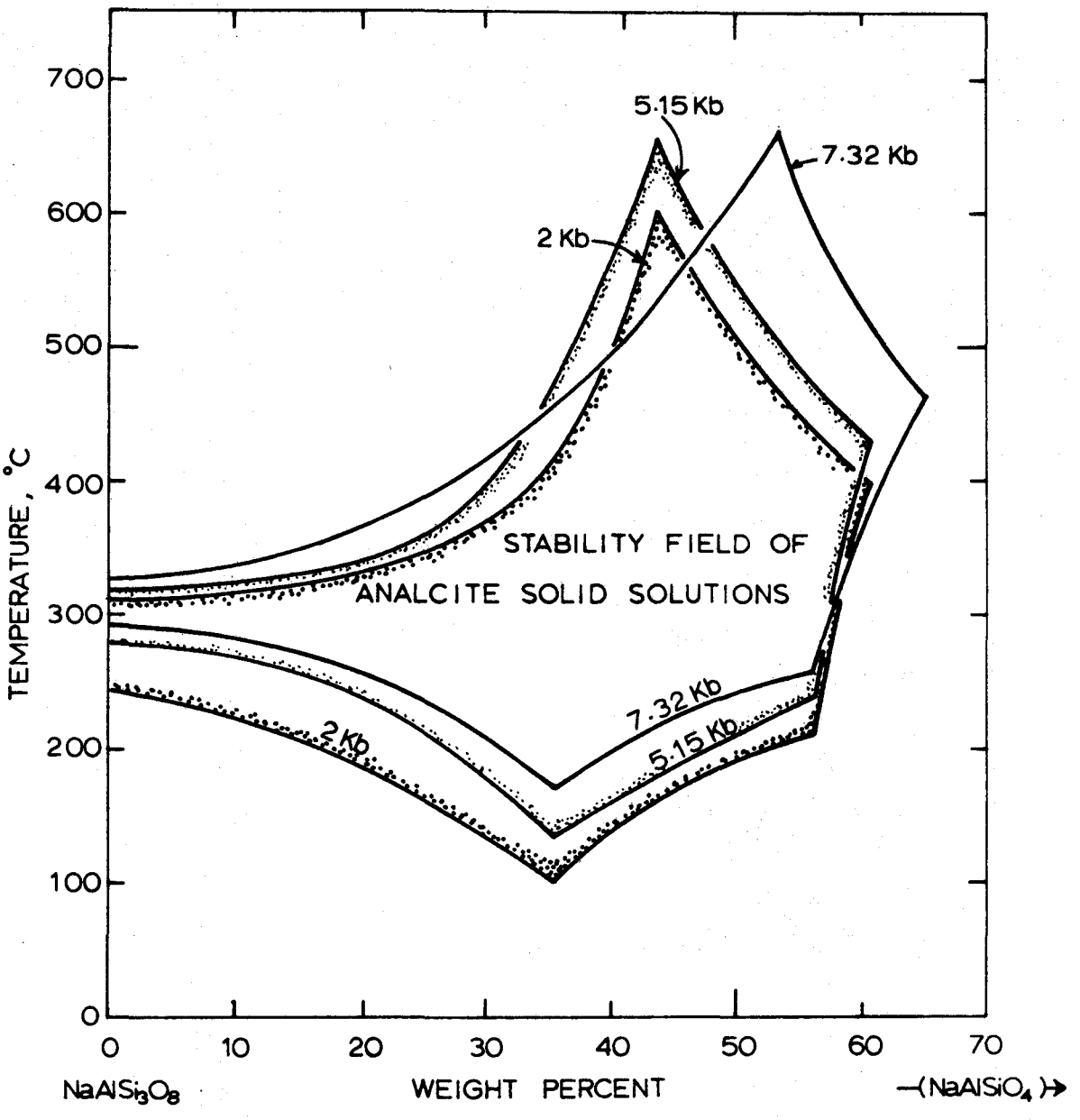
700
600
500
400
300
200
100
0
TEMPERATURE, °C
5.15 Kb
7.32 Kb
2 Kb
STABILITY FIELD OF
ANALCITE SOLID SOLUTIONS
7.32 Kb
5.15 Kb
2 Kb
0
10
20
30
40
50
60
70
NaAlSi3O8
WEIGHT PERCENT
(NaAlSiO4)

FIG. 4

In this chapter the stability fields of mineral phases only are studied. Further discussion of the phase equilibria will be presented in more detail in the chapter following.

1. Analcite Solid Solution

The stability field of analcite solid solutions has the shape of a distorted pentagon, situated in the central region of the T-X phase diagram (Figs. 1, 2 and 4). At the thermal peak of its stability field, analcite has the composition (Ne_{44}. Ab_{56}, 8 Wt. % H_2O) which does not vary with water vapor pressure up to the invariant pressure (5.15 ± 0.25Kb). But at pressures above the invariant point, the analcite changes drastically towards a natrolitic composition, and it nearly approaches the natrolite one at 10Kb (see Fig. 4).

The analcite composition at the thermal trough of its stability field seems to be of the ideal formula, $NaAlSi_2O_6 . H_2O$, and the temperature is approximately 100°C at 2Kb and 140°C at 5.15Kb. The most silica-deficient analcite at 2Kb has a nearly natrolitic composition (Ne_{59}. Ab_{41}, 7.3 Wt. % H_2O at 400±5°C) and this is constant at pressures below 5.15Kb. But at 7.32Kb, the composition of the most silica deficient analcite is Ne_{65}. Ab_{35} with 7.3 Wt. % H_2O, which is richer in $NaAlSiO_4$ than that of the natrolitic one. At about 300°C, silica-rich analcite richer in silica even than $NaAlSi_3O_8$

was formed. At this temperature (up to 10Kb), analcite has a compositional range from Ab_{105}. Ne_{-5} to $Ne_{56}Ab_{44}$ (anhydrous), which is the widest range of analcite solid solution synthesized at a given P-T (see Figs. 3d & h).

In this study, it was made certain that the analcite solid solutions at temperatures above 350°C (at 2Kb and 5.15Kb) are equilibrium phases (see Figs. 1 and 2). But below this temperature, it is simply a T-X field of analcite-synthesis because it is difficult to prove experimentally whether it is at equilibrium or not.

In order to investigate the stability of analcite of albite-composition, several long runs (3 months, at 2Kb and 300°C) were made by Saha (1961, p. 871) using natural albites as starting materials, but analcite was not synthesized. In the present study, an attempt was made to synthesize analcite from natural albite at high pressure (7.7 days run at 5.17Kb and 249°C & 303°C) but also failed (see No. 673 and 676 in Table III). Two reversal runs in the region of albite-rich composition and low temperature (7.5 days run at 5.15Kb and 295°C) were made using synthetic crystalline mixtures for the reactions: Zeol. P. + Anl (silica-poor) → Anl (silica-rich) + V (see No. 850) and Anl (silica-poor) + Ab + V → Anl (silica-rich) (see No. 851). The results show that the first reversal reaction (No. 850) was completely attained, and the second one (No. 851) was partly attained (Table VIII). From the result of run

No. 850, the analcite solid solution of $Ab_{90} \cdot Ne_{10}$ composition seems to be an equilibrium phase. This agrees fairly well with the composition of a natural analcite (approximately $Na_{13}Al_{13}Si_{35}O_{96} \cdot n\ H_2O$) reported by Coombs and Whetten (1957, p. 273) as the most silica-rich analcite found in sedimentary and metamorphic rocks.

Thus it is interpreted that the stability field of Na-rich analcite solid solutions may not be very much different from the one determined in this study (see Figs. 1, 2 and 4).

2. Albite Solid Solution

Greig & Barth (1938) found that albite forms a solid solution with nepheline. In the present study, the limit of albite solid solution was determined to be $Ab_{94.5} \cdot Ne_{5.5}$ at P_{H_2O} = 2Kb and $Ab_{95} \cdot Ne_5$ at 5.15Kb. These are univariant albite for the reaction (Anl): L = Ab + Ne + V up to the invariant point, the limit of albite s.s. changes along the curve labelled as $Ab_{(Anl)}$ in Fig. 7 as a function of water vapor pressure. Above the invariant pressure (5.15 Kb), it changes along the curve $Ab_{(Ne)}$.

The melting temperature of albite was estimated to be around 872°C at P_{H_2O} = 2Kb and 770°C at 5.15Kb (Fig. 2).

An interesting feature to note is that the albite solid solution seems to be extended towards the SiO_2-component past the $NaAlSi_3O_8$ composition. The albite contains around 5 Wt.% quartz in solid solution

at the minimum temperature of melting at 5.15Kb where the univariant reaction Quartz + Albite + Water = liquid occurs in the system $NaAlSi_3O_8$-SiO_2-H_2O.

It is also noteworthy that the minimum temperature of albite formation of $NaAlSi_3O_8$ composition is around 530°C/2Kb and around 470°C/5.15Kb. At temperatures lower than 530°C/2Kb (or 470°C/5.15Kb) the composition of the albite solid solution, which is at equilibrium with an analcite solid solution and water vapor, is richer in silica than $NaAlSi_3O_8$. Such a compositional departure, from $NaAlSi_3O_8$ towards a SiO_2-rich composition may explain why MacKenzie (1957, p. 487) obtained, below about 530°C (at around 1Kb), a reversal of the general tendency of $2\theta_{131}$-$2\theta_{1\bar{3}1}$ values of albite to decrease with lowering temperatures.

3. Nepheline Solid Solution

The largest range of nepheline solid solution forms at one temperature minimum of melting at each given pressure in the system. At this temperature, a univariant reaction (Anl): Ab + Ne + V = L occurs. Nepheline on the (Anl) univariant curve contains the largest amounts of albite in solid solution. The composition of the univariant nepheline is $Ab_{26}.Ne_{74}$ at 750°C and 2Kb, and $Ab_{21}Ne_{79}$ at 657°C and 5.15Kb (Figs. 3a & f, and 7). In the dry system, the nepheline is of $Ab_{33}.Ne_{67}$ composition as determined by Greig & Barth (1938). Therefore, the curve $Ne_{(Anl)}$ in Fig. 7 represents the limit of nepheline solid solution as a function of water vapor pressure up to the invariant pressure. Above the invariant pressure, the limit of nepheline s.s. is represented by the curve $Ne_{(Ab)}$.

Consequently, the limit of the nepheline s. s. decreases drastically as pressure increases, especially up to 5.15Kb.

The minimum temperature of the nepheline stability field is controlled by the univariant reaction Anl + Ne-hy I = Ne + V within the H_2O pressure range between 0.8Kb and 9.4Kb. The composition of the nepheline stability trough changes along the curve given in Fig. 9a. But below 0.8Kb and above 9.4Kb, the minimum temperature of nepheline stability is lower than the univariant temperature.

4. Nepheline Hydrate I Solid Solution

The stability field of nepheline hydrate I solid solution exists in a small area near the $NaAlSiO_4$ component in this system. Most of its stability field exists in the system $NaAlSiO_4$-$NaAlSiO_2$-H_2O. Its stability range is also controlled by the univariant temperature where Anl, Ne, N-h I and V are involved in reaction.

The limit of nepheline hydrate I s. s. towards albite changes along the curve shown in Fig. 9a, as a function of water vapor pressure.

5. Zeolite Species P Solid Solution

The T-X field of zeolite species P is wide with respect to composition below approximately 200°C. Below the temperatures of analcite stability field and nepheline hydrate I stability field, the mineral phase encountered in this study was only the zeolite species P. over the whole range of the system as shown in Figs. 1 and 2. Since it is very difficult to achieve equilibrium in this low temperature range, it may be metastable.

However, the reversibility for the univariant reaction zeolite species P. = analcite + nepheline hydrate I + water was held (see run Nos. 853 and 846 in Table III). The univariant temperature is 235°C at P_{H_2O} = 5.15Kb. At least, therefore, the univariant zeolite P. must be an equilibrium phase. Its anhydrous composition is $Ab_{16}.Ne_{84}$ with 11.6 weight percent water (for details see Chapter IV, § 6).

IV. INVARIANT, UNIVARIANT AND SINGULAR EQUILIBRIA

Since the preliminary study on the univariant curve (L): Anl = Ab + Ne + V at 1Kb indicated some disagreement with those of Greenwood (1961), and Peters, Luth and Tuttle (1966) but good agreement with that of Yoder (1954), a decision was made to redetermine all the univariant curves including the invariant point, determined to be at 4.75 ± 0.25Kb and 665 ± 5°C by Peters et al. The experimental results as shown in Figs. 5 and 10 give good agreement with that of Peters et al. The experimental data are selectively presented in Table IV.

1. Invariant Point (Figs. 2, 3(f) & 5).

The invariant point determined in this study is located at 5.15±0.25Kb and 657±5°C which is a slightly higher pressure and a slightly lower temperature than that of Peters et al. (1966). The compositions of the five invariant phases were determined as shown in Table V, where the present data are presented on the left side and those of Peters et al. are given on the right side for comparison.

TABLE IV

RUNS FOR THE DETERMINATION OF UNIVARIANT CURVES UP TO 10 KB IN THE SYSTEM ALBITE-NEPHELINE-WATER(RELEVANT TO FIG.5). THE STARTING MATERIALS USED WERE POWDERED GELS OF VARIOUS COMPOSITION.
AB=ALBITE SOLID SOLUTION(S.S.), NE=NEPHELINE S.S., ANL=ANALCITE S.S., N-H I=NEPHELINE HYDRATE I S.S., ZP=ZEOLITE SPECIES P S.S., GL=GLASS(MELT), V=WATER VAPOR, .=SMALL AMOUNT, ..=VERY SMALL OR TRACE AMOUNT.

TABLE IVa
DATA FOR THE (NE),(AB) AND (V) UNIVARIANT CURVES

RUN	COMPOSITION, Wt% ANHYDROUS		WATER	EXPERIMENTAL CONDITION PRESS	TEMP	TIME	RESULTS (PHASE)
NO.	AB	NE	AMOUNT	KB	°C	DAY	
703	64.8	35.2	25.9	10.34	543	3.6	ANL+.AB+V
704	54.7	45.3	27.6	10.34	543	3.6	ANL+V
488	64.8	35.2	46.5	9.65	632	0.8	GL+.AB+V
489	54.7	45.3	50.0	9.65	632	0.8	GL+V
485	64.8	35.2	49.0	9.65	619	0.8	ANL+AB+V
486	54.7	45.3	46.4	9.65	619	0.8	ANL+.AB+V
434	64.8	35.2	50.0	9.20	607	0.6	ANL+AB+V
435	49.2	50.8	44.8	9.20	607	0.6	ANL+V
436	35.4	64.6	39.0	9.20	607	0.6	ANL+.NE+V
431	64.8	35.2	46.5	9.20	588	0.6	ANL+.AB+V
432	49.2	50.8	47.8	9.20	588	0.6	ANL+V
433	42.3	57.7	39.6	9.20	588	0.6	ANL+..NE+V
414	57.0	43.0	50.0	9.03	625	3.5	ANL+AB+V
415	49.2	50.8	43.8	9.03	625	3.5	ANL+V
471	64.8	35.2	50.0	9.00	642	1.7	GL+.AB+V
472	64.8	35.2	5.7	9.00	642	1.7	ANL+.AB
473	49.2	50.8	50.0	9.00	642	1.7	GL+V
468	64.8	35.2	48.7	9.00	630	1.7	ANL+AB+V
469	49.2	50.8	49.4	9.00	630	1.7	ANL+..GL+V
470	35.4	64.6	38.2	9.00	630	1.7	ANL+.NE+V
493	54.7	45.3	50.0	8.80	660	2.0	GL+V
494	54.7	45.3	3.9	8.80	660	2.0	NE+AB+.GL+..ANL
495	35.4	64.6	46.5	8.80	660	2.0	GL+..NE+V
490	64.8	35.2	46.8	8.80	650	2.0	GL+.AB+V
491	54.7	45.3	48.7	8.80	650	2.0	GL+V
492	54.7	45.3	2.8	8.80	650	2.0	ANL+NE+AB
460	64.8	35.2	50.0	8.14	647	1.5	GL+.AB+V
461	49.2	50.8	50.0	8.14	647	1.5	GL+V
462	35.4	64.6	45.0	8.14	647	1.5	GL+.NE+V
457	64.8	35.2	50.0	8.14	632	1.5	ANL+.AB+V
458	49.2	50.8	45.0	8.14	632	1.5	ANL+V
459	35.4	64.6	49.3	8.14	632	1.5	ANL+.NE+V
747	64.8	35.2	7.6	8.02	669	2.9	AB+.NE+.GL
748	59.8	40.2	27.5	8.02	669	2.9	GL+V
749	54.7	45.3	26.5	8.02	669	2.9	GL+V

412	49.2	50.8	11.7	7.60	668	0.9	GL+•NE
413	49.2	50.8	49.0	7.60	668	0.9	GL+V
410	49.2	50.8	12.0	7.60	627	0.9	ANL+•NE+V
446	64.8	35.2	50.0	7.33	645	1.6	GL+•AB+V
447	49.2	50.8	40.1	7.33	645	1.6	ANL+•GL+V
448	35.4	64.6	42.0	7.33	645	1.6	ANL+•NE+V
443	64.8	35.2	50.0	7.33	637	1.6	ANL+AB+V
444	49.2	50.8	39.0	7.33	637	1.6	ANL+V
445	42.3	57.7	39.9	7.33	637	1.6	ANL+••NE+V
403	49.2	50.8	3.4	7.31	652	0.9	ANL+•NE+•AB
404	49.2	50.8	46.0	7.31	652	0.9	GL+V
405	42.3	57.7	49.0	7.31	652	0.9	GL+•NE+V
401	49.2	50.8	43.3	7.31	635	0.9	ANL+V
402	42.3	57.7	47.0	7.31	635	0.9	ANL+••NE+V
408	49.2	50.8	6.8	6.62	655	0.8	ANL+•NE+••AB
409	49.2	50.8	37.2	6.62	655	0.8	GL+V
407	49.2	50.8	46.3	6.62	646	0.8	ANL+V
331	57.0	43.0	50.0	5.91	661	1.1	GL+V
316	64.8	35.2	50.0	5.78	650	3.5	ANL+•AB+V
317	49.2	50.8	41.7	5.78	650	3.5	ANL+V
341	64.8	35.2	49.5	5.64	658	1.7	GL+AB+V
342	57.0	43.0	45.2	5.64	658	1.7	GL+V
343	49.2	50.8	41.8	5.64	658	1.7	GL+••NE+V

TABLE IVb
DATA AROUND THE INVARIANT POINT(5.15KB/657°C)

RUN	COMPOSITION, Wt% ANHYDROUS		WATER	EXPERIMENTAL CONDITION PRESS	TEMP	TIME	RESULTS (PHASE)
NO.	AB	NE	AMOUNT	KB	°C	DAY	
361	57.0	43.0	50.4	5.29	669	0.8	GL+V
362	49.2	50.8	41.6	5.29	669	0.8	GL+••NE+V
359	57.0	43.0	51.4	5.29	645	0.8	ANL+V
360	49.2	50.8	36.6	5.29	645	0.8	ANL+••NE+V
600	59.8	40.2	28.5	5.23	672	2.2	GL+V
601	54.7	45.3	32.9	5.23	672	2.2	GL+••NE+V
380	57.0	43.0	45.1	5.17	658	1.0	ANL+GL+V
379	57.0	43.0	45.3	5.17	651	1.0	ANL+V
595	54.7	45.3	28.3	5.08	658	3.0	GL+•AB+•NE+V
398	49.2	50.8	13.6	5.02	656	1.6	ANL+•NE+V
399	49.2	50.8	44.6	5.02	656	1.6	ANL+••NE+V
397	57.0	43.0	50.0	5.02	656	1.6	ANL+•AB+V
394	57.0	43.0	50.0	5.02	652	1.6	ANL+V
395	49.2	50.8	50.0	5.02	652	1.6	ANL+•NE+V
299	64.8	35.2	49.0	4.86	661	0.7	GL+AB+V
300	49.2	50.8	41.4	4.86	661	0.7	GL+•NE+V
374	57.0	43.0	44.6	4.45	674	1.6	GL+••NE+V
375	49.2	50.8	38.0	4.45	674	1.6	GL+••NE+V
372	57.0	43.0	46.8	4.45	651	1.6	ANL+V
373	49.2	50.8	38.8	4.45	651	1.6	ANL+•NE+V

TABLE IVc

DATA FOR THE (ANL) AND (L) UNIVARIANT CURVES

RUN	COMPOSITION, Wt% ANHYDROUS		WATER	EXPERIMENTAL CONDITION PRESS	TEMP	TIME	RESULTS (PHASE)
NO.	AB	NE	AMOUNT	KB	°C	DAY	
382	49.2	50.8	34.2	3.24	692	3.0	GL+NE+AB+V
381	49.2	50.8	31.8	3.24	681	3.0	NE+AB+V
19	64.8	35.2	24.1	2.03	750	21.5	GL+AB+V
224	57.0	43.0	34.7	1.99	761	3.9	GL+AB+NE+V
209	84.0	16.0	35.6	1.99	737	13.1	AB+.NE+V
118	64.8	35.2	30.8	1.07	852	24.0	GL+.AB+.NE+V
144	57.0	43.0	19.8	0.97	827	33.0	AB+NE+V
306	64.8	35.2	46.5	4.10	650	1.8	ANL+.AB+V
307	49.2	50.8	36.7	4.10	650	1.8	ANL+.NE+V
304	64.8	35.2	47.0	4.10	631	1.8	ANL+.AB+V
305	49.2	50.8	35.2	4.10	631	1.8	ANL+V
378	49.2	50.8	33.0	3.28	655	2.4	NE+AB+V
376	57.0	43.0	35.1	3.28	645	2.4	ANL+.AB+.NE+V
377	49.2	50.8	32.5	3.28	645	2.4	ANL+.NE+..AB+V
17	64.8	35.2	22.8	2.03	588	21.5	ANL+AB+V
330	64.8	35.2	45.0	2.28	607	8.9	ANL+.AB+V
365	57.0	43.0	43.8	2.01	620	2.7	AB+NE+V
363	57.0	43.0	41.7	2.01	602	2.7	ANL+..AB+V
364	49.2	50.8	34.1	2.01	602	2.7	ANL+.NE+V
585	54.7	45.3	23.7	2.00	605	7.1	NE+AB+V
586	49.2	50.8	29.8	2.00	605	7.1	NE+AB+..ANL+V
211	85.9	14.1	34.5	1.99	612	13.1	AB+.NE+V
661	54.7	45.3	24.6	1.97	594	8.8	ANL+.NE+..AB+V
451	64.8	35.2	35.0	1.01	555	8.8	AB+NE+V
449	64.8	35.2	40.0	1.01	535	8.8	ANL+.AB+V
450	49.2	50.8	31.5	1.01	535	8.8	ANL+.NE+V
393	49.2	50.8	35.2	0.99	544	13.0	ANL+.NE+V
569	54.7	45.3	20.5	0.49	502	14.0	ANL+..NE+..AB+V
568	64.8	35.2	20.5	0.49	502	14.0	ANL+AB+.NE+V
566	64.8	35.2	22.1	0.49	485	14.0	ANL+.AB+V
567	54.7	45.3	19.7	0.49	485	14.0	ANL+V
101	64.8	35.2	31.7	0.40	505	46.0	AB+NE+..ANL+V

CD TOT 0043

TABLE IVd

DATA FOR AN UNIVARIANT CURVE FOR THE REACTION
NEPHELINE HYDRATE I + ANALCITE = NEPHELINE + H_2O (MOSTLY).

RUN	COMPOSITION, Wt % ANHYDROUS		WATER	EXPERIMENTAL CONDITION PRESS	TEMP	TIME	RESULTS (PHASE)
NO.	AB	NE	AMOUNT	KB	°C	DAY	
483	12.7	87.3	30.0	9.79	479	4.9	ANL+N-HI+NE+V
484	0.0	100.0	47.2	9.79	479	4.9	NE+V
480	12.7	87.3	48.1	9.79	467	4.9	ANL+N-HI+V
481	-1.0	101.0	30.0	9.79	467	4.9	N-HI+..ANL+V
466	5.8	94.2	48.3	8.76	467	1.8	ANL+.N-HI+.NE+V
467	0.0	100.0	20.0	8.76	467	1.8	N-HI+NE+V
463	12.7	87.3	50.3	8.76	454	1.8	ANL+N-HI+V
464	5.8	94.2	49.0	8.76	454	1.8	N-HI+ANL+V
465	0.0	100.0	40.0	8.76	454	1.8	N-HI+.ANL+V
424	0.0	100.0	30.0	8.67	472	3.9	NE+V
440	69.1	30.9	38.4	7.72	456	1.4	ANL+.AB+V
441	64.8	35.2	5T80	7.72	456	1.4	ANL+V
437	29.1	70.9	43.0	7.72	445	1.4	ANL+..N-HI+..NE+V
455	5.8	94.2	53.5	5.14	452	2.0	NE+.ANL+V
456	0.0	100.0	53.9	5.14	452	2.0	NE+.N-HI+V
452	12.7	87.3	54.4	5.14	441	2.0	ANL+N-HI+NE+V
453	5.8	94.2	50.4	5.14	441	2.0	N-HI+NE+.ANL+V
454	0.0	100.0	49.3	5.14	441	2.0	N-HI+NE+..ANL+V
427	0.0	100.0	59.5	5.12	429	1.5	N-HI+.ANL+V
242	5.8	94.2	35.6	2.02	403	10.1	N-HI+ANL+V
243	-1.0	101.0	37.7	2.02	403	10.1	N-HI+NE+V
475	5.8	94.2	52.2	1.98	413	12.0	NE+N-HI+V
476	0.0	100.0	42.5	1.95	413	12.0	NE+N-HI+V
564	5.8	94.2	32.6	0.49	402	14.0	NE+V
565	0.0	100.0	29.3	0.49	402	14.0	NE+V
560	21.2	78.8	32.1	0.49	387	14.0	ANL+NE+V
561	5.8	94.2	36.9	0.49	387	14.0	N-HI+NE+V
562	0.0	100.0	32.0	0.49	387	14.0	NE+V
511	5.8	94.2	31.1	0.48	374	20.5	N-HI+NE+V
512	0.0	100.0	29.2	0.48	374	20.5	NE+N-HI+V
508	12.7	87.3	36.6	0.48	355	20.5	N-HI+ANL+V
509	5.8	94.2	33.7	0.48	355	20.5	N-HI+.ANL+V
510	0.0	100.0	37.2	0.48	355	20.5	N-HI+V
538	5.8	94.2	29.4	0.24	345	28.5	N-HI+.ANL+V

CD TOT 0047

TABLE IVe

DATA FOR AN UNIVARIANT CURVE FOR THE REACTION
NEPHELINE HYDRATE I + ANALCITE + H_2O = ZEOLITE SPECIES P.

RUN	COMPOSITION, Wt % ANHYDROUS		WATER	EXPERIMENTAL CONDITION PRESS	TEMP	TIME	RESULTS (PHASE)
NO.	AB	NE	AMOUNT	KB	°C	DAY	
505	89.7	10.3	26.3	7.72	257	5.9	ANL+ZP+V
506	64.8	35.2	26.6	7.72	257	5.9	ANL+V
507	5.8	94.2	26.8	7.72	257	5.9	ZP+.N-HI+V
502	89.7	10.3	27.7	7.72	227	5.7	ZP+V
503	64.8	35.2	26.1	7.72	227	5.9	ANL+V
504	0.0	100.0	30.2	7.72	227	5.9	ZP+V
386	49.2	50.8	45.8	6.25	274	8.0	ANL+V
384	49.2	50.8	45.6	6.25	223	8.0	ZP+V
354	64.8	35.2	47.6	6.25	158	2.8	ANL+V
574	21.2	78.8	30.2	5.14	225	8.6	ZP+.ANL+V
575	12.7	87.3	39.0	5.14	225	8.6	ZP+..N-HI+V
500	64.8	35.2	47.5	5.10	245	7.8	ANL+V
501	0.0	100.0	41.3	5.10	245	7.8	N-HI+ANL+V
497	64.8	35.2	44.8	5.10	227	7.8	ANL+V
498	0.0	100.0	41.7	5.10	227	7.8	ZP+N-HI+V
637	12.7	87.3	33.9	2.04	233	14.8	N-HI+ANL+V
645	21.2	78.8	37.3	2.04	200	14.8	ZP+..ANL+V
617	64.8	35.2	40.0	2.04	169	14.8	ANL+V
618	59.8	40.2	34.5	2.04	169	14.8	ANL+V
619	54.7	45.3	34.9	2.04	169	14.8	ANL+ZP+V
273	64.8	35.2	50.0	2.04	141	24.0	NON-CRYSTAL+V
533	54.7	45.3	46.0	0.24	172	28.5	ANL+.ZP+V

CD TOT 0036

FIG. 5. PHASE EQUILIBRIA ON A P-T (PRESSURE-TEMPERATURE) PROJECTION IN THE SYSTEM $NaAlSi_3O_8$-$NaAlSiO_4$-H_2O UP TO 10Kb

Experimental data (small open circles) are presented in Tables I, II & IV.

The data of reversal runs, denoted by big open circles accompanied by run numbers, are presented in Table III.

Invariant point and singular point are denoted by I and S respectively.

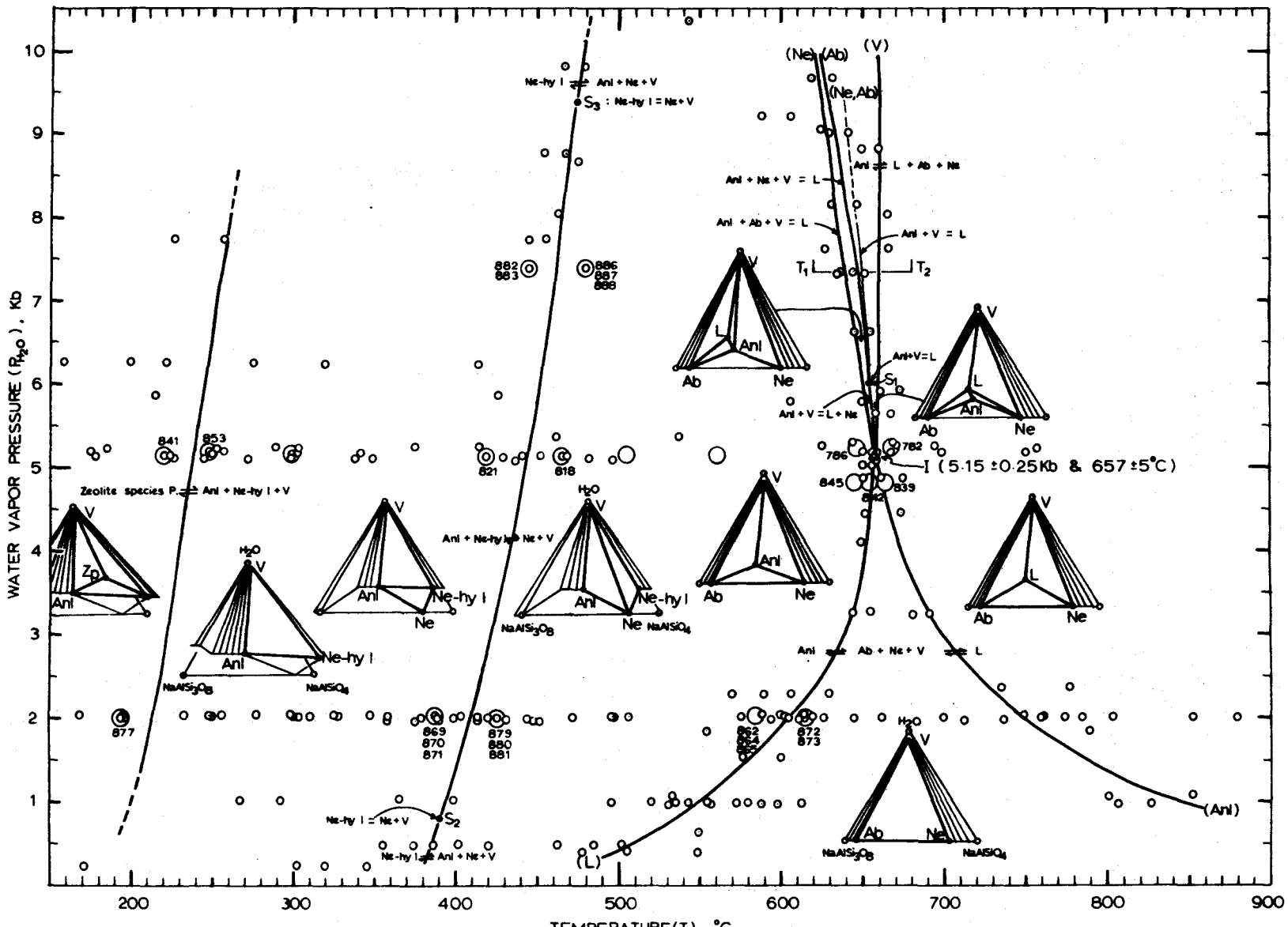
WATER VAPOR PRESSURE (P_{H_2O}), Kb
TEMPERATURE(T), °C
I (5.15 ±0.25Kb & 657±5°C)
(Ne) (Ab) (V)
(Ne,Ab)
(Anl)
(L)
Anl + Ne + V = L
Anl + Ab + V = L
Anl + V = L
Anl = L + Ab + Ne
Anl + V = L + Ne
Ne-hy I = Ne + V
Anl + Ne-hy I = Ne + V
Anl = Ab + Ne + V = L
Zeolite species P = Anl + Ne-hy I + V
Ne-hy I + Anl = Ne + V
Ne-hy I = Ne + V
Ne-hy I = Anl + Ne + V
S_1
S_2
S_3 : Ne-hy I = Ne + V
T_1
T_2
$NaAlSi_3O_8$
$NaAlSiO_4$

FIG. 5

TABLE V. Composition of Invariant Phases

Phases	Present Work at 5.15±0.25 and 657±5°C	Peters, Luth & Tuttle (1966) at 4.75±0.25Kb and 665±5°C
Albite	$Ab_{94.5}Ne_{5.5}$ ± 1	?
Nepheline	$Ab_{19}Ne_{81}$ ± 1	$Ab_{13}.Ne_{87}$ ± 2
Analcite	$Ab_{56}Ne_{44}$ ± 1(8 Wt.% H_2O)	$Ab_{50}.Ne_{50}$(8-9 Wt.% H_2O)
Liquid	$Ab_{57}Ne_{43}$ ± 1(11.5 Wt.% H_2O)	$Ab_{57}.Ne_{43}$ ± 1(12 Wt.% H_2O)
Vapor	- (?)	Dissolved solid 5±2% (Ab ≤ Ne)

The determination of the invariant point and the compositions of the invariant phases were accomplished very precisely by studying the phase-equilibria in a P-T projection (Fig. 5) as well as on a T-X projection (Fig. 2).

A number of runs as well as several reversible runs were made in the immediate vicinity of the invariant point (5.15Kb and 657°C) using powdered gels, synthetic minerals and quenched hydrous glasses, to try and check this point as carefully as possible.

From the results of runs 380, 379, 595 and 398 (Table IVb), the invariant point must be located between 5.08 and 5.17Kb and between 656°C and 658°C. From several reversible runs (run No. 782, 786, 839, 842 and 845 in Table III), made using synthetic minerals, viz. albite, nepheline and analcite as starting materials, it was confirmed that the equilibria around the invariant point are reversible.

Hence it is concluded that the invariant point determined in this study is located at 5.15±0.25Kb and 657±5°C.

2. A Singular Point on the (Ab) Univariant Curve

In the present study, a singular point was found to be located within the range 5.15 - 6.6Kb and 655°±5°C. Thus, the singular point is estimated to be at 6±0.5Kb and 655±5°C on the (Ab) univariant curve, as shown in Fig. 5, which is slightly above the invariant pressure.

It is not impossible experimentally to determine the singular point, but it is a very difficult problem. In this study, the singular point was obtained indirectly from the compositional data of univariant phases (see Fig. 7). At this point, a singular reaction Anl+V = L occurs. Below this pressure, the (Ab) univariant reaction is Anl+V=L+Ne, and above the pressure, the (Ab) reaction is Anl+Ne+V=L, at least, up to 10Kb. Accordingly, the anhydrous compositions of the singular phases, liquid and analcite must be the same, which is estimated to be $Ab_{51}.Ne_{49}$. Theoretically they can be slightly different depending on the anhydrous composition of an equilibrium vapor phase, but the difference is negligible in practice. The phase-equilibrium relations at the singular point are essentially similar to those shown in Figs. 6a,b and 6(4).

From the singular point, a new P-T curve is produced which is separated from the (Ab) univariant curve. In other words, from the singular point toward higher pressure, a thermal divide begins to form along the compositional join of the three singular (colinear) phases, analcite, liquid and vapor, in an isobaric-polythermal ternary diagram. Thus, the system is divided into two subsystems in the excess water region of the system. There exists already another subsystem in the water-deficient region of the system. At pressures above the singular point, therefore, the system $NaAlSi_3O_8$-$NaAlSiO_4$-H_2O is basically divided into three portions.

It is very interesting to note that analcite always melts incongruently in the water-deficient region, but analcite melts congruently in the water-excess region of the system above the singular pressure. Thus, the singular point has a very important meaning for the direct crystallization of analcite from a melt, in addition to the invariant point.

Peters, Luth and Tuttle (1966, p. 744-747) pointed out the possibility of such a singular point on the (Ab) univariant curve and described the possible reaction equations at, below and above the pressure of the singular point. The present data supports their prediction.

3. Univariant Equilibria (L), (Anl), (Ne), (Ab) and (V) and the singular equilibrium (Ab, Ne)

The five univariant P-T curves (L), (Anl), (Ne), (Ab) and (V) reproduced in this study are very close respectively to those of Peters, Luth and Tuttle (1966). The differences between them are mostly within 10°C at any pressure up to 10Kb. Below 1.5Kb, however, the univariant curve (L) is separated from that of Peters et al. and becomes much closer to those of Yoder (1954) and Greenwood (1961).

The univariant curves determined in this study and the experimental data are presented in Fig. 5 and Table IV, (IVa, IVb and IVc) respectively and are also shown in Fig. 10for the comparison with previous works.

The reactions of the six univariant P-T curves including a degenerate one are as follows, within the P-T range up to 10Kb and 900°C:

(L): Anl = Ab + Ne + V

(Anl): Ab + Ne + V = L

(Ne): Anl + Ab + V = L

(Ab): Anl + V = Ne + L ... between invariant point (5.15Kb and 657°C) and singular point (6.0Kb and 657°C)

Anl + V = L ..... at singular point, singular reaction due to the compositional colinearity

Anl + Ne + V = L ... at any pressure above the singular point.

(V): Anl = Ab + Ne + L

(Ne, Ab): Anl + V = L ..... singular univariant reaction occurring at the T and X of the thermal divide at any pressure above the singular point in the presence of excess water.

The two univariant P-T curves,(L) and (Anl), which exist stably below the invariant pressure are based on phase-reactions involving the total system. Their univariant chemographs (i.e. reaction equations) are topologically the same throughout their respective P-T stability ranges.

From the invariant point towards higher pressures, three univariant curves (Ne), (Ab) and (V) radiate. The (V) univariant curve has nearly constant temperature, regardless of the change of pressure. The univariant temperatures of both of the other two curves (Ne) and (Ab) lowers slightly but continuously as pressure increases. Consequently, it is evident

that the maximum temperature of analcite stability is nearly constant ($657^{\circ}\pm5^{\circ}C$) above the pressure of the invariant point, but the temperature minimum of melting is slowly decreasing with increasing pressure. Note that there are two temperature minima of melting above the pressure of the singular point due to the formation of a thermal divide, one of them for the (Ne) univariant P-T curve and the other one for the (Ab) curve.

At P_{H_2O} = 7.32Kb, an isobaric T-X projection (Fig. 6a) was made within a restricted temperature range, across the three univariant curves including one singular P-T curve (see T_1-T_2 section on P-T diagram in Fig. 5). The 7.32Kb T-X diagram was constructed essentially on the basis of the data points shown in the diagram (Fig. 6a). Another $T\text{-}X_{H_2O}$ diagram along the composition join $Ab_{47}Ne_{53}$-H_2O along which the thermal divide lies was constructed (see Fig. 6b). On the basis of these two diagrams, nine isobaric-isothermal sections were schematically constructed (Fig. 6(1)-(9)), which illustrate the phase-equilibria relations above the pressure of the singular point. The univariant chemograms (V), (Ab) and (Ne) are illustrated in Fig. 6-(2), (6) and (8) respectively, and one singular reaction chemogram is given in Fig. 6(4). Thick tie-lines are used between univariant reaction phases.

FIG. 6a. ISOBARIC T-X_{Ab-Ne} PROJECTION AT P_{H_2O} = 7.32Kb.

Based on the experimental data given in the diagram and the data above and below 7.32Kb (see Table IVa).

FIG. 6b. ISOBARIC T-$X_{H_2O-Ab_{47}Ne_{53}}$ SECTION AT P_{H_2O} = 7.32Kb.

Approximately constructed.

FIG. 6(1)-(9) ISOBARIC ISOTHERMAL SECTIONS (Schematic)

AT P_{H_2O} = 7.32Kb

Illustrating the phase relations around the three univariant temperatures and also thermal divide (4).

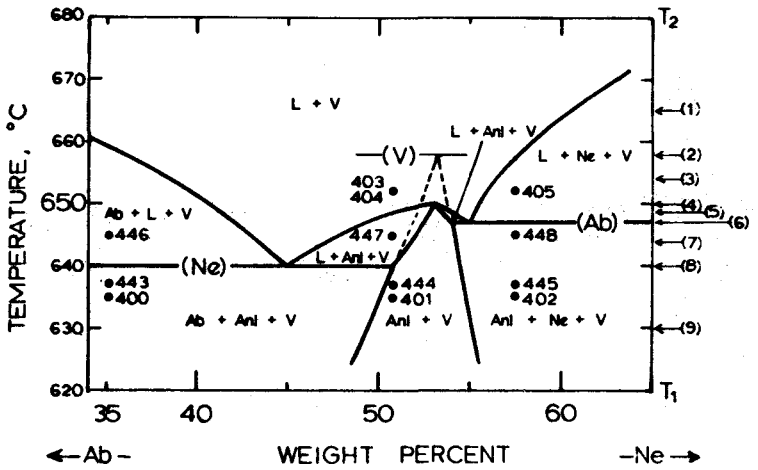

FIG. 6a

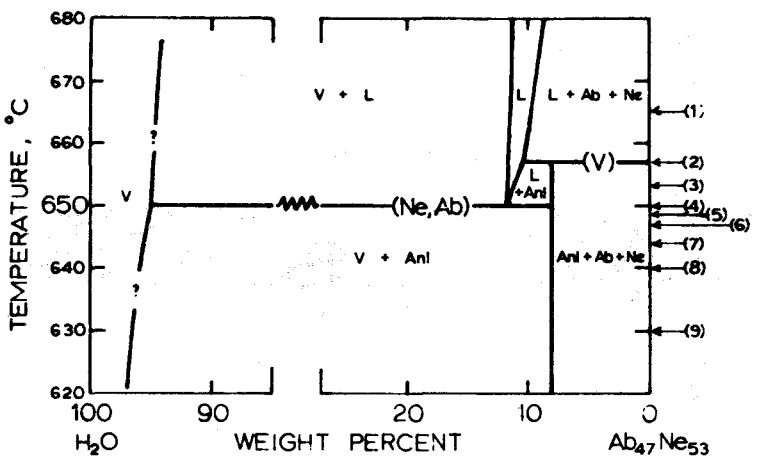

FIG. 6b

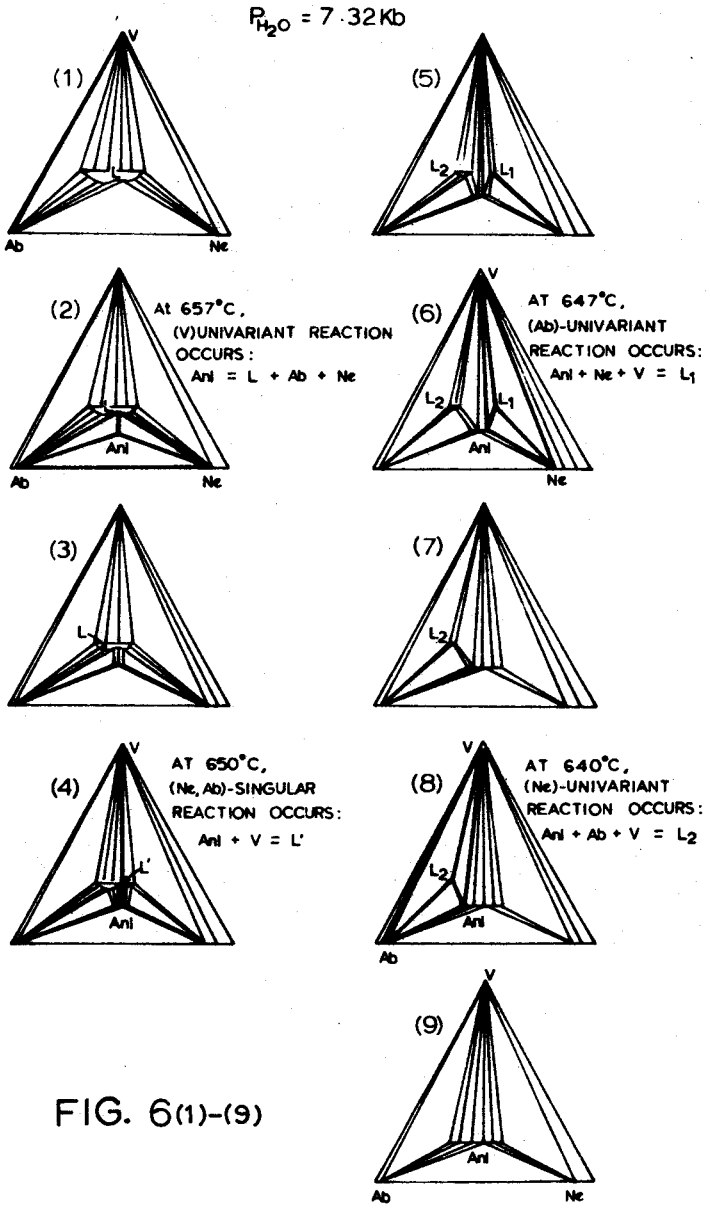

FIG. 6(1)-(9)

The singular univariant P-T curve starts from the singular point (6±0.5Kb/657±5°C) and passes through a point (7.32±0.25Kb/650±5°C). The three singular phases, liquid, analcite and vapor, are colinear along the thermal divide. Accordingly, their equilibrium compositions change according to the change of position of the thermal divide. The compositions of the singular phases, therefore, change in the three component plane and the reaction is ternary, as predicted by Peters, Luth and Tuttle (1966, p. 747).

4. Compositions of Univariant Phases L, Anl, Ne and Ab

The equilibrium compositions of the univariant phases along each of the P-T curves, (L), (Anl), (V), (Ab) and (Ne) were determined or estimated through the method of phase boundary-location in an isobaric T-X diagram (or projection). The data of the phase-compositions determined in this study are presented in Table VI. The H_2O-contents of hydrous phases presented in the table were obtained from the data determined in Part 2. The anhydrous compositions of the phases were based on a number of runs of similar P, T and X, but a representative run is given in Table VI.

TABLE VI. COMPOSITION OF UNIVARIANT LIQUID, ANALCITE, ALBITE AND NEPHELINE

Univariant Phase	Run No. or (Fig. No.)	Run Condition		Composition of Liquid or Analcite		
		Press. Kb	Temp. °C	Anhydrous Wt. % Ab	Ne	H_2O content Wt. %
$L_{(Anl)}$	118	1.07	852	65.0	35.0±2.5	4.5
	(fig. 16)	2.00	750	62.0	38.0±1.0	6.5
L_i	(fig. 17)	5.15	657	57.0	43.0±1.0	11.4
$L_{(Ne)}$	342	5.64	657	56.5	43.5±2.0	11.7
	(fig. 11)	7.32	640	55.0	45.0±5.0	13.0
	489	9.65	632	54.5	45.5±2.5	14.0
$L_{(Ab)}$	409	6.62	655	48.0	52.5±1.0	12.5
	(fig. 11)	7.32	647	44.5	55.5±1.5	13.0
$L_{(V)}$	(fig. 11)	7.32	657	47.0	53.0±2.0	13.0
$Anl_{(L)}$	569	0.49	502	56.0	44.0±1.0	8.0
	(fig. 16)	2.00	600	56.0	44.0±1.0	8.0
Anl_i	(fig. 17)	5.15	657	56.0	44.0±1.0	8.0
$Anl_{(Ne)}$	(fig. 11)	7.32	640	49.0	51.0±1.0	8.0
	458	8.14	632	49.0	51.0±1.0	8.0
$Anl_{(Ab)}$	407	6.62	646	49.5	51.5±1.5	8.0
	(fig. 11)	7.32	647	46.0	54.0±2.0	7.6
$Anl_{(V)}$	(fig. 11)	7.32	657	47.0	53.0±2.0	8.0
Ab_i	(fig. 17)	5.15	657	95.0	5.0±1.0	-
$Ab_{(Anl)}$	(fig. 16)	2.00	750	94.5	5.5±1.0	-
$Ab_{(L)}$	(fig. 16)	2.00	600	98.5	1.5±1.0	-
Ne_i	(fig. 17)	5.15	657	9.0	81.0±1.0	-
$Ne_{(Anl)}$	(fig. 16)	2.00	750	26.0	74.0±1.0	-
$Ne_{(L)}$	(fig. 16)	2.00	600	21.0	79.0±1.0	-

On the basis of the data, two diagrams were constructed. One of them is a polythermal P-X diagram, as shown in Fig. 7, which was constructed plotting the anhydrous compositions of phases against pressure in a rectangular coordinate. The other one is a polybaric-polythermal composition diagram (Fig. 8), constructed plotting the compositions of the phases in the ternary component system.

The polythermal P-X diagram is very useful, especially for the illustration of the equilibrium compositions of univariant phases at a given pressure. A few examples suffice to explain the diagram (Fig. 7). For instance, $Ab_{(L)}$, $Anl_{(L)}$ and $Ne_{(L)}$ are the curves which show the compositions of the equilibrium phases, albite solid solution, analcite solid solution and nepheline solid solution for the (L) univariant reaction Anl = Ab+Ne+V at any pressure up to the invariant point. Similarly, three curves, $Ab_{(Ne)}$, $L_{(Ne)}$ and $Anl_{(Ne)}$, show the compositions of the (Ne) univariant reaction phases albite, liquid and analcite respectively at any pressure above the invariant point, and so on. The compositions of $Ab_{(L)}$, $L_{(Anl)}$ and $Ne_{(Anl)}$ at $P_{H_2O} = 0$ and $P_{total} = 1$ Atm are based on the data after Greig and Barth (1938). Note that $Anl_{(V)}$ and $L_{(V)}$ are presented on the same curve because they have the same anhydrous compositions, and also the compositions of analcite and liquid for the singular reaction are changing along the same curve denoted by $Anl_{(V)}$ and $L_{(V)}$ as pressure changes.

FIG. 7. POLYTHERMAL P-X (PRESSURE-COMPOSITION) DIAGRAM FOR THE EQUILIBRIUM-COMPOSITIONS OF UNIVARIANT PHASES, LIQUID, ANALCITE, ALBITE & NEPHELINE

(Essentially based on Table VI)

The diagram shows the anhydrous composition of each univariant phase with respect to pressure, along each of the five univariant curves radiating from an invariant point (5.15Kb and 657°C) where Ab, Ne, Anl, L, and V coexist.

Ab_i, L_i, Anl_i & Ne_i denote invariant albite, liquid, analcite and nepheline respectively. $Ab_{(Anl)}$, $L_{(Anl)}$, and $Ne_{(Anl)}$ denote respectively univariant albite, liquid and nepheline for the reaction (Anl): Ab+Ne+V = L. $Ab_{(Ne)}$, $L_{(Ne)}$ and $Anl_{(Ne)}$ denote respectively univariant albite, liquid and analcite for the reaction (Ne): Ab+Anl+V = L, and so on.

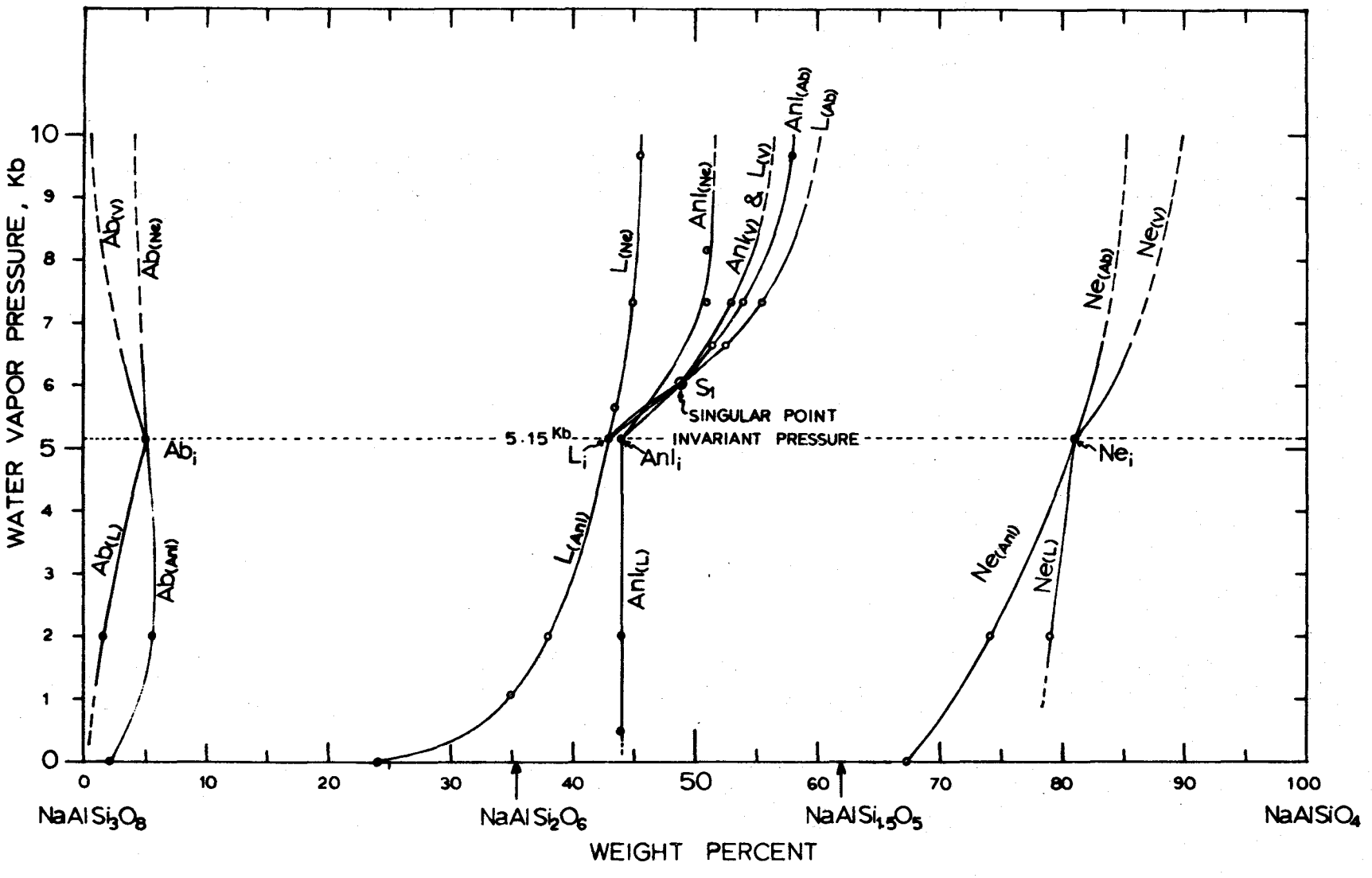
WATER VAPOR PRESSURE, Kb
10
9
8
7
6
5
4
3
2
1
0
Ab(v)
Ab(Ne)
Ab(L)
Ab(Anl)
Abi
5.15 Kb.
INVARIANT PRESSURE
L(Ne)
Anl(Ne)
Anl(v) & L(v)
Anl(Ab)
L(Ab)
S1
SINGULAR POINT
Li
Anli
L(Anl)
Anl(L)
Ne(Ab)
Ne(v)
Ne(Anl)
Ne(L)
Nei
0
10
20
30
40
50
60
70
80
90
100
NaAlSi3O8
NaAlSi2O6
NaAlSi1.5O5
NaAlSiO4
WEIGHT PERCENT

FIG. 7

All the corresponding phases in different univariant reactions, of course, have the same composition at the invariant point. Accordingly, the four curves meet in a point (see Fig. 7). The invariant phases are denoted by Ab_i, Ne_i, Anl_i and L_i. At the singular point S_1, the anhydrous compositions for $Anl_{(Ab)}$, $Anl_{(V)}$, $L_{(Ab)}$ and $L_{(V)}$ are the same. As the water-vapor pressure increases, every equilibrium phase involved in a univariant reaction has a tendency to be enriched in $NaAlSiO_4$-content, with few exceptions ($Anl_{(Ne)}$, $Ab_{(Ne)}$ and $Ab_{(V)}$). There are two important pressures (P_{H_2O} = 0Kb and 5.15Kb) for compositional changes of the univariant phases, especially hydrous phases. As shown in Fig. 7, $L_{(Anl)}$ from P_{H_2O} = 0Kb to about 2Kb, and $Anl_{(Ne)}$, $Anl_{(V)}$, $L_{(V)}$, $Anl_{(Ab)}$ and $L_{(Ab)}$ from P_{H_2O} = 5.15Kb to about 7.5Kb change their compositions rapidly.

On the basis of the polythermal P-X diagram (Fig. 7), it seems to be likely that every univariant phase concerned is approaching a fixed value of its composition above 10Kb H_2O-pressure, and the fixed composition should not be far from that obtained at 10Kb.

The solubility data which will be discussed in Part 2 (Fig. 16a) implies that the solubility of water in the univariant melt $L_{(Ne)}$ also approaches a fixed value which should not be very different from the value at 10Kb. Again, the solubility of water in the melt is nearly constant regardless of the variation of the anhydrous composition of the

melt, at least within the range of $Ab_{80}\cdot Ne_{20}$-$Ab_{40}\cdot Ne_{60}$, in this system (see Figs. 14 and 15 in Part 2).

Thus, it is possible to construct a polybaric-polythermal composition diagram for the univariant phases, L, Anl, Ab and Ne (see Fig. 8). The ternary composition diagram represents the compositions of univariant phases throughout the whole P-T stability range of each of the five univariant curves, including those of invariant and singular phases.

FIG. 8. POLYBARIC-POLYTHERMAL TERNARY COMPOSITION DIAGRAM FOR THE UNIVARIANT AND INVARIANT PHASES

The compositions of invariant phases are denoted by big open circles. The compositions of univariant phases at the terminal point of each univariant curve radiating from the invariant point are denoted by small solid circles. The compositions of liquid (L_s) and analcite (Anl_s) at a singular point are denoted by small open circles. In this study, the vapor phases are not determined.

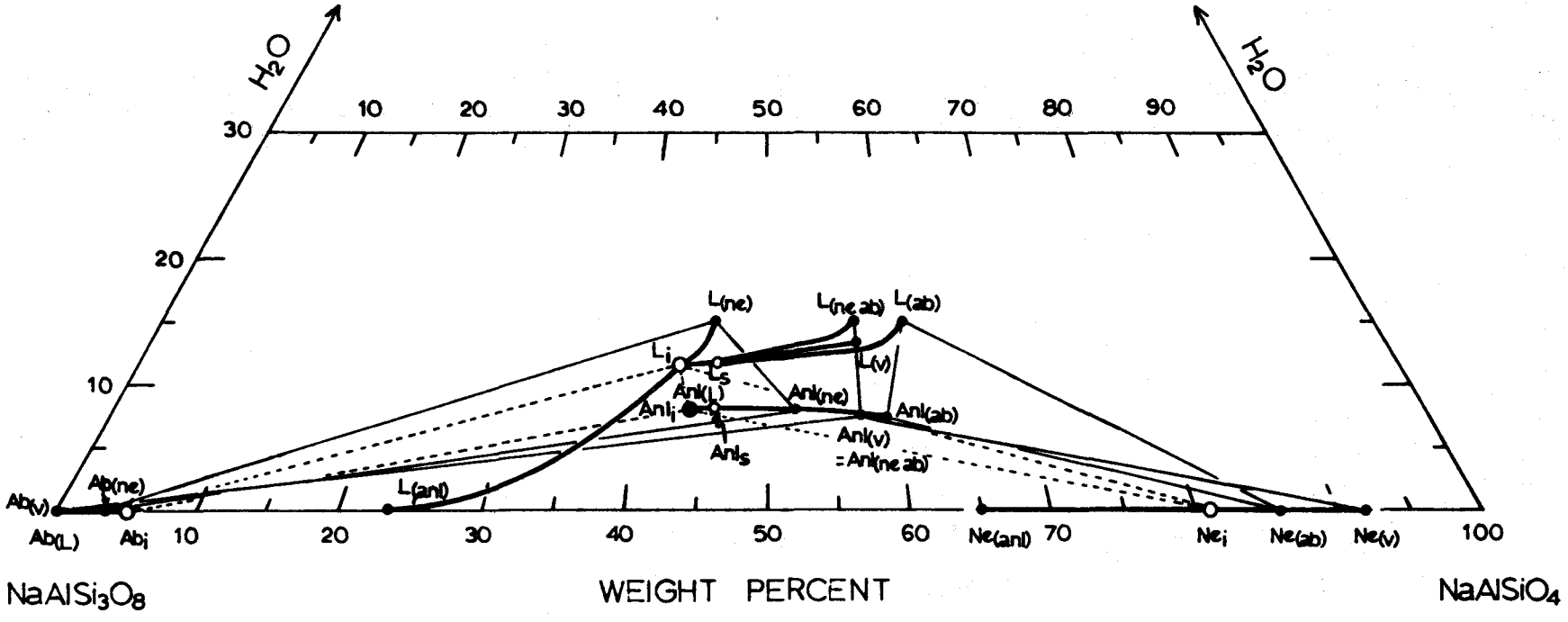
H2O
H2O
10
20
30
40
50
60
70
80
90
30
20
10
L(ne)
L(ne,ab)
L(ab)
Li
Ls
L(v)
Anl(L)
Anli
Anl(ne)
Anl(ab)
Anls
Anl(v)
=Anl(ne,ab)
Ab(v)
Ab(ne)
L(anl)
Ab(L)
Abi
10
20
30
40
50
60
Ne(anl)
70
Nei
Ne(ab)
Ne(v)
100
NaAlSi3O8
WEIGHT PERCENT
NaAlSiO4

FIG. 8

5. Univariant Equilibria, Anl + N-h I ≠ Ne + V

The experimental data for the determination of the univariant curve on P-T projection were given in Table IVd. The reaction equation of the univariant equilibrium is mainly analcite + nepheline-hydrate I = nepheline + water within the P-T range of the present study.

The equilibrium compositions of the univariant phases, nepheline and nepheline-hydrate I do not consist of the pure nepheline composition ($NaAlSiO_4$). Knowing the composition of both mineral solid solutions, it can be understood why Sand et al. (1957, p. 176) and Saha (1961, p. 867) were not able to determine the univariant equilibrium and P-T curve, because there is a transitional 3-phase region due to the non-binary phase relations on the join Ne-H_2O.

The equilibrium phases involved in the univariant reaction concerned herein are analcite, nepheline, nepheline-hydrate I and vapor (Figs. 1, 2 and 3c & g). The equilibrium composition of analcite is nearly natrolitic: its anhydrous composition is $Ab_{40}.Ne_{60}$ with 7.3 weight per cent water at 2Kb water vapor pressure and also the same at the invariant pressure (5.15Kb). The compositions of univariant Ne and N-h I were determined or estimated from .5Kb up to 10Kb and are presented in Table VII and plotted in a polythermal P-X diagram as shown in Fig. 9a.

The composition of the univariant nepheline changes within the range of $Ab_{90}.Ne_{10}$-$Ab_{0}.Ne_{100}$. The anhydrous composition of the univariant nepheline-hydrate I solid solution is also changing within a

TABLE VII. COMPOSITION OF UNIVARIANT NEPHELINE AND NEPHELINE HYDRATE I

(Relevant to Fig. 9a)

Run No. or (Fig. No.)	Univariant Press. & Temp.		Nepheline Solid Solution		Nepheline-hydrate I (S. S.) Anhydrous Wt. %		
	P_{H_2O}	T					H_2O content
	Kb	°C	Ab	Ne	Ab	Ne	Wt. %
483, 484, 480, 481	9.79	480	1	99	2	98	6
424, 466, 467, 463, 464, 465	8.76	467	3	97	1	99	6
(Fig. 17)	5.15	435	4	96	-1	101	6
(Fig. 16)	2.00	400	9	91	4	96	6
564, 565, 561, 562, 511, 512, 508, 509, 510	0.49	388	6	94	9	91	6

FIG. 9a. EQUILIBRIUM COMPOSITIONS OF UNIVARIANT ANALCITE, NEPHELINE HYDRATE I, AND NEPHELINE. Along a univariant curve, where analcite, nepheline, nepheline hydrate I and water vapor phases coexist. Nepheline and nepheline hydrate I have the same anhydrous composition at C_2 and C_3 respectively.

FIG. 9b. UNIVARIANT P-T CURVE, involving four phases Anl, Ne, N-h I and V, in the system $NaAlSi_3O_8$-$NaAlSiO_4$-H_2O. Two singular points S_2 and S_3 are located approximately at 0.8Kb/390°C and 9.4Kb/475 respectively, in which singular reactions nepheline hydrate I = nepheline + H_2O occurs. The zone for the transition N-h I + H_2O = Ne + H_2O is stippled, on composition join $NaAlSiO_4$-H_2O.

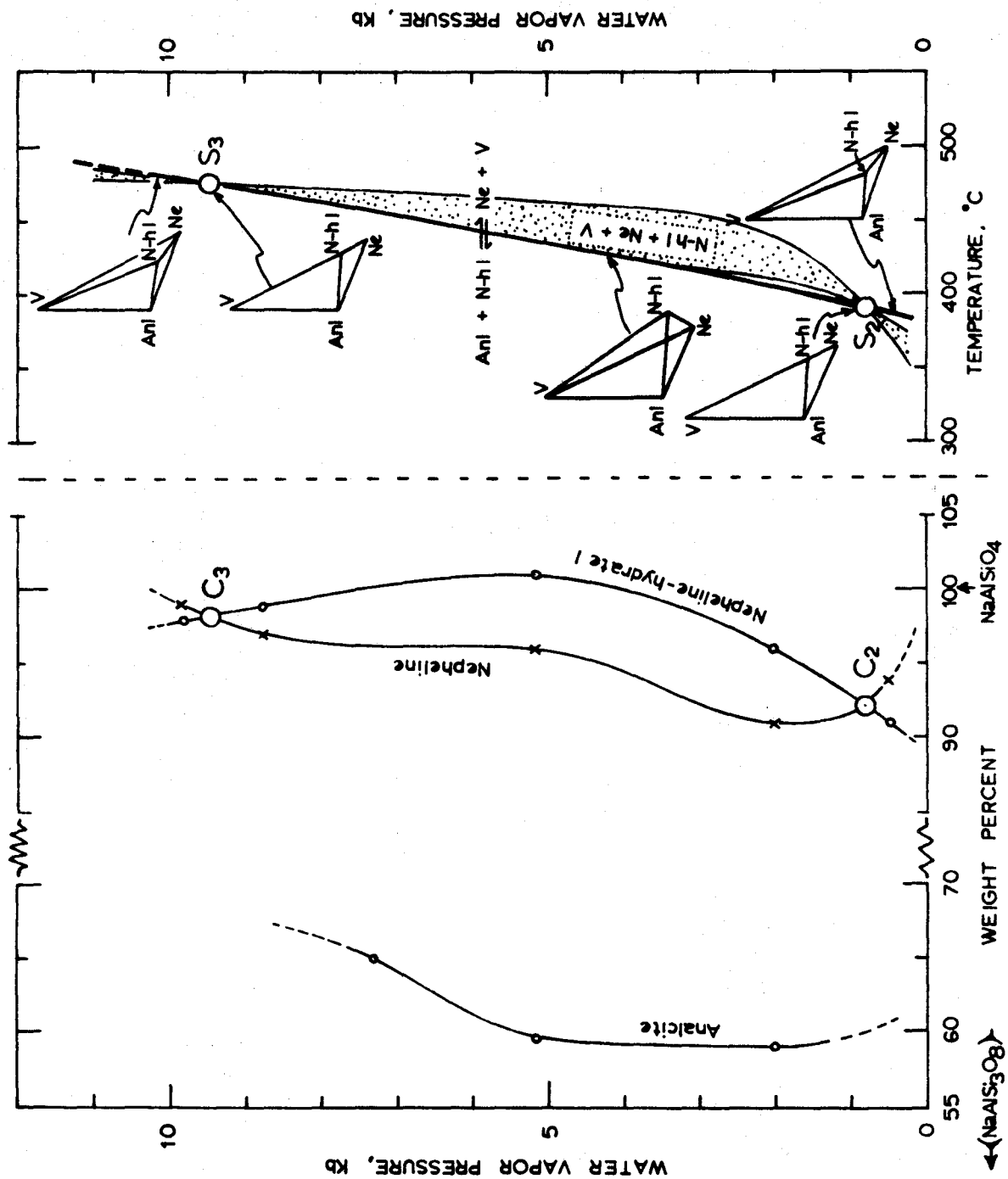
WATER VAPOR PRESSURE, kb
10
5
0
TEMPERATURE, °C
500
400
300
S3
S2
C3
C2
N-hl + Ne + V
Ani + N-hl ⇌ Ne + V
N-hl
Ne
Ani
V
WATER VAPOR PRESSURE, kb
10
5
0
WEIGHT PERCENT
105
100
90
70
60
55
NaAlSiO4
(NaAlSi3O8)
Nepheline-hydrate I
Nepheline
Analcite
C3
C2

FIG 9b

FIG. 9a

similar range: $Ab_{90}.Ne_{10}$-$Ab_{-1}.Ne_{101}$. The Ab-content in the nepheline solid solution is higher than that of the nepheline-hydrate I solid solution within the range of water vapor pressure .8 to 9.4Kb, and the case is reversed above and below this pressure range.

As shown in Fig. 9a, the two composition curves intersect in two points, C_2 (.8Kb, $Ab_8.Ne_{92}$) and C_3 (9.4Kb, $Ab_2.Ne_{98}$), where the two phases have the same composition except for H_2O. Accordingly, a singular reaction N-h I = Ne + V should occur at each of these pressures. Therefore, there exist two singular points, S_2 and S_3 on the univariant P-T curve as shown in Fig. 9b. The two singular points obtained in this way are approximately located at S_2 (.8Kb, 390°C) and S_3 (9.4Kb, 475°C).

These two singular points are both transition points for the univariant reaction equation as summarized below.

[1] N-h I = Anl + Ne + V at any pressure above S_3

[2] N-h I = Ne + V at a singular point S_3 (9.4Kb, 4.75°C)

[3] N-h I + Anl = Ne + V at any pressure between S_3 and S_2.

[4] N-h I = Ne + V at a singular point S_2 (0.8Kb, 390°C)

[5] N-h I = Anl + Ne + V at any pressure below S_2.

The singular reactions allow a new P-T curve to pass through the two singular points S_2 and S_3, but the new P-T curve is related to the phase relation in the system $NaAlO_2$-$NaAlSiO_4$-H_2O. So it will not be further discussed herein.

For comparison of the present data with the previous work, the curve for the transition N-h I + V = Ne + V determined by Saha (1961, p. 868) was drawn in Fig. 10. At 2Kb, the univariant temperature in the present study is 400±5°C for the reaction n-h I + Anl = Ne + V, but Saha's temperature of transition is 455°C at the same pressure. This discrepancy between them seems to be mainly due to the different properties of the reaction concerned. As shown in the isobaric (2Kb) T-X projection (Fig. 1) determined in this study, the system $NaAlSiO_4$-H_2O is not binary but ternary. Accordingly, there is a temperature zone 405-440°C, in which Ne, N-h I and V are coexisting. The upper limit of the temperature zone (440°C) is very close to the transition temperature (455°C) of Saha (see Figs. 9b and 10 herein).

Many reversible runs were made, essentially for the reversibility Nepheline-hydrate I ⇌ Nepheline + Water, using synthetic nepheline and nepheline hydrate I. It was made certain that the reversibility held true perfectly. Consequently, there is no doubt about the stability of the univariant P-T curve determined herein. As long as it is a stable P-T curve, it may probably extend above 10Kb.

FIG. 10. P-T PROJECTION GIVING A COMPARISON WITH PREVIOUS WORK IN THE SYSTEM $NaAlSi_3O_8$-$NaAlSiO_4$-H_2O

All the P-T curves shown in this diagram are univariant except two curves. One of them is the curve for the transition nepheline hydrate I + H_2O = nepheline + H_2O determined by Saha (1961). The other one is the P-T zone (stippled area) for the same transition in the system $NaAlSiO_4$-H_2O, determined in the present study.

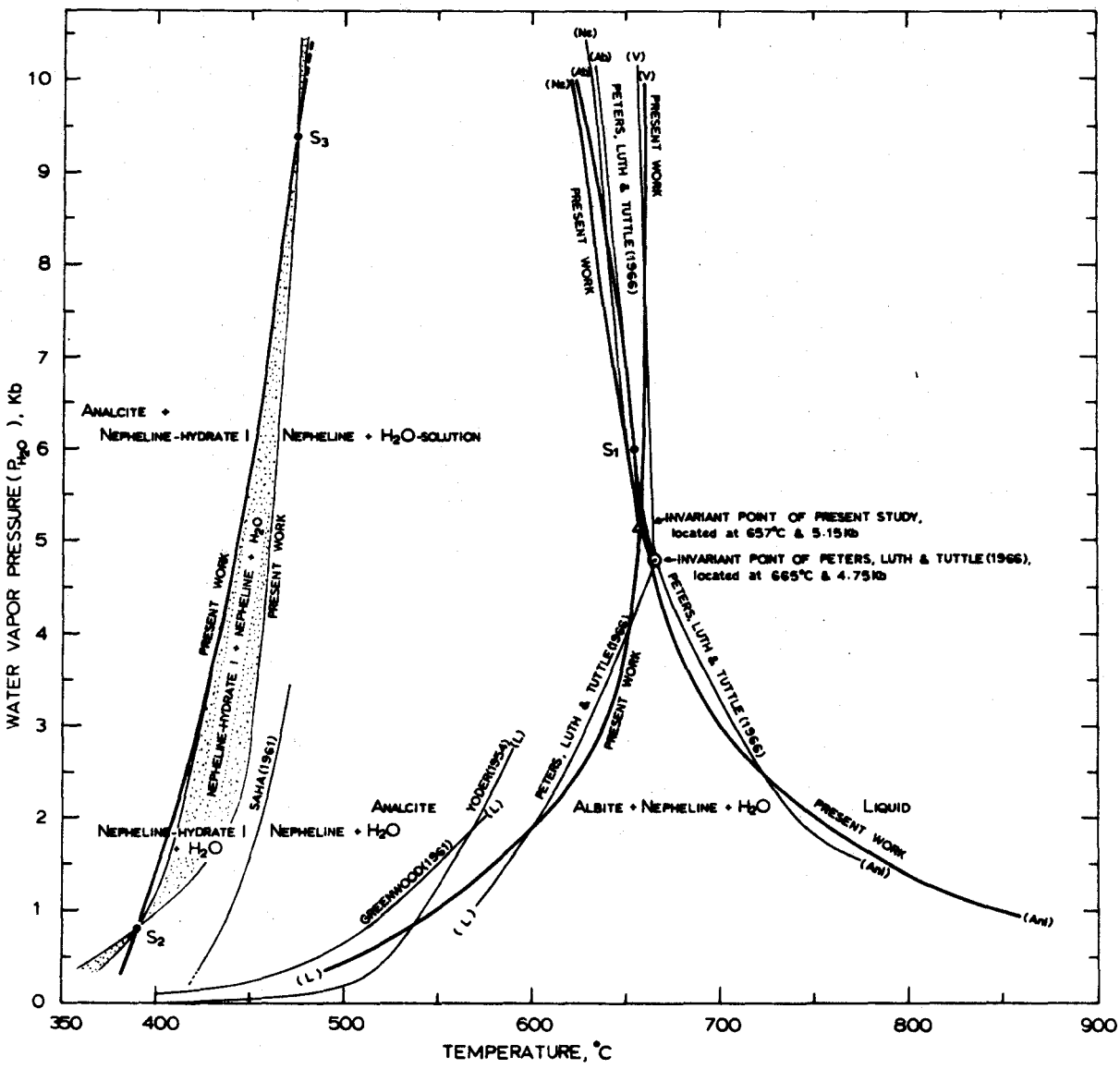
WATER VAPOR PRESSURE (P_{H_2O}), Kb
TEMPERATURE, °C
ANALCITE + NEPHELINE-HYDRATE I
NEPHELINE + H_2O-SOLUTION
NEPHELINE-HYDRATE I + H_2O
NEPHELINE + H_2O
ANALCITE
ALBITE + NEPHELINE + H_2O
LIQUID
S_1
S_2
S_3
INVARIANT POINT OF PRESENT STUDY, located at 657°C & 5.15 Kb
INVARIANT POINT OF PETERS, LUTH & TUTTLE (1966), located at 665°C & 4.75 Kb
PRESENT WORK
PETERS, LUTH & TUTTLE (1966)
SAHA (1961)
GREENWOOD (1961)
YODER (1954)
(Ne)
(Ab)
(V)
(Ani)
(L)

FIG. 10

6. Univariant Equilibrium for the Reaction:

(Zeolite P. = Analcite + Nepheline-Hydrate I + Water)

In this univariant reaction, a zeolite species P. (cubic form) is involved. The zeolite species P. was reported to be hydrothermally synthesized at low temperature (60-110°C) in the presence of excess NaOH (200-300%) by Barrer et al. (1959, p. 200). The zeolite encountered in this study was identified to be zeolite species P. (cubic form) by 15 X-ray patterns. Saha (1961, p. 868) reported a zeolite "B" synthesized at low temperature (~300°C at P_{H_2O} = 1Kb etc.) in his study of the system $NaAlSiO_4$-H_2O. Saha's zeolite "B" is very similar to zeolite P. The univariant P-T curve involving zeolite species P. as a reaction phase was determined.

The univariant P-T curve passes through the P-T points (2Kb, 215°C), (5.15Kb, 235°C) and (8Kb, 260°C), and the P-T curve is nearly a straight line, as shown in Fig. 5. The univariant reaction along the P-T curve is zeolite species P. ⇌ Analcite + Nepheline hydrate I + Water (see Fig. 3e & d). The experimental data are given in Table IVe.

The equilibrium compositions of the univariant phases were estimated from the phase relations on the isobaric T-X projections determined at 2Kb and 5.15Kb (Figs. 1 and 2); these are, therefore, only approximate compositions. The univariant zeolite has an anhydrous composition of $Ab_{16}.Ne_{84}$ with 11.5 weight percent water at 2Kb and 5.15Kb. The univariant analcite has an anhydrous composition of $Ab_{44}Ne_{56}$ with 7.3 weight percent water at 2Kb and 5.15Kb. The univariant nepheline hydrate I has an anhydrous composition of $Ab_{-4}.Ne_{104}$ at 2Kb and $Ab_{-8}.Ne_{108}$ at 5.15Kb with 5.9 weight percent water respectively. The univariant analcite and zeolite P. have nearly constant compositions in the pressure range between 2Kb and 5.15Kb, but the nepheline hydrate I becomes richer in $NaAlO_2$-component as the pressure increases.

V. DISCUSSION AND PETROGENETIC CONSIDERATION

When discussing petrological implications, the CaO-component cannot of course be neglected but for the sake of simplification, the present discussion is restricted to alkali rocks in the quaternary system $NaAlSiO_4$-$KAlSiO_4$-SiO_2-H_2O, with special emphasis on the analcite problem.

Direct crystallization of analcite from a melt was demonstrated by Peters et al. (1966) in their experimental study in the system $NaAlSi_3O_8$-$NaAlSiO_4$-H_2O. The liquidus analcite solid solution was shown by them to crystallize in a narrow temperature range and to be compositionally limited (Peters et al., 1966, p. 752). According to their study(p. 751),the maximum content of K_2O in analcite solid solution is about 2 weight percent (at the P-T range: 2.2 - 6.4Kb and 630-650°C).

Fudali (1963, p. 1120) found the maximum substitution of Na_2O by K_2O to be about 1.7 weight percent (8 Wt.% $KAlSi_2O_6$) in analcite crystallized on the join $NaAlSi_2O_6$-$KAlSi_2O_6$ at 4Kb water vapor pressure. Wilkinson (1968, p. 252) confirmed his earlier conclusion (Wilkinson & Whetten, 1964) that analcite solid solution contains up to approximately 2 Wt.% K_2O. Such very limited analcite solid solutions with respect to K_2O may be interpreted as probably applying most typically to liquidus analcites.

According to the analyses of primary analcites reported by MacKenzie (1914), Larson & Buie (1938, p. 839), Wilkinson (1965, p. 429) and Pearce (1970, p. 53), the compositional range of analcites is approximately from $NaAlSi_2O_6 . H_2O$ to $NaAlSi_{1.5}O_5 . 0.75\ H_2O$. Wilkinson (1965, p. 429) reported in his study of the Square Top intrusion that the three analcites he analysed depart in their chemistry from the ideal stoichiometric ratio $Na_2O:SiO_2$ of 1:4 and demonstrated in his diagram (Fig. 5, p. 438) that the compositional trend of liquidus analcites is from an approximately natrolitic composition ($Ne_{79.6}Ks_{30}Qz_{17.4}$) toward a silica-rich one ($Ne_{73.1}Ks_{1.8}Qz_{25.1}$) with progressive differentiation (from analcite-olivine theralite to analcite tinguaite).

He concluded that the replacement of Si by NaAl in the analcites decreased with progressive differentiation. The present experimental study in the system $NaAlSi_3O_8$-$NaAlSiO_4$-H_2O agrees fairly well with this trend, namely that the range of liquidus analcite solid solutions is from nearly natrolitic analcite ($Ne_{58} . Ab_{42} = Ne_{81}Qz_{19}$) to $Ne_{44} . Ab_{56}$ ($= Ne_{74} . Qz_{26}$) in the pressure range of 5.15 - 10Kb and the compositional change of liquidus analcite with progressive differentiation also corresponds to Wilkinson's results.

On the basis of the present experimental study, it was expected that all the mineral phases except the silica-phases form a considerable range of solid solutions in the system $NaAlSiO_4$-$KAlSiO_4$-SiO_2-H_2O. A

ternary composition diagram (projected to the dry base, $NaAlSiO_4$-$KAlSiO_4$-SiO_2) was constructed using some of the analysed chemical data of alkali feldspars, analcites, nephelines, kalsilites, and leucites, reported in the literature (Fig. 11).

The compositions of alkali feldspar, analcite and leucite were mostly recalculated on the basis of three components, $NaAlSiO_4$, $KAlSiO_4$ and SiO_2, and presented in Tables VIII and IX. For nepheline and kalsilite, the chemical data compiled by Deer, Howie & Zussman (1963, v. 4, p. 242-244, p. 253-254) were used.

Indeed, every natural mineral considered here has a wide range of solid solutions as shown in Fig. 11. It is noteworthy that the wide ranges of analcite solid solution, alkali feldspar s.s., and leucite s.s. have been generally overlooked or neglected inspite of several investigations reported by Larsen & Buie (1938), Barrer (1950, p. 2342), Barrer et al. (1953) and Barrer & Baynham (1956, p. 2888), etc. On the basis of the experimental data (in Figs. 1, 2, 4 and 7) and also the chemical data for the natural minerals (in Fig. 11), the maximum stability boundaries of the mineral solid solutions were sketched in. The writer's experimental information is, of course, limited only to the system albite-nepheline-H_2O.

TABLE VIII. CHEMICAL COMPOSITION OF NATURAL ALKALI FELDSPAR
Recalculated in the terms of three components $NaAlSi0_4$(Ne), $KAlSi0_4$(Ks) and $Si0_2$(Qz) using the analytical data compiled by Deer, Howie & Zussman (1963, v. 4, pp. 36-110, tables 4-8, and 12-13).

* Relevant to Fig. 11.

No.	Ne	Ks	Qz	Total, Wt %
4001	42.09902	12.02420	45.87678	100.00000
4002	36.19809	19.18435	44.61756	100.00000
4003	29.15886	26.10082	44.74032	100.00000
4004	26.86394	28.85007	44.28599	100.00000
4005	24.86567	30.66338	44.47095	100.00000
4006	22.54770	33.60179	43.85051	100.00000
4007	21.34637	34.64267	44.01096	100.00000
4008	20.00332	35.34213	44.65455	100.00000
4009	17.42363	38.51205	44.06432	100.00000
4010	16.08938	40.39909	43.51153	100.00000
4011	14.33802	42.16146	43.50053	100.00000
4012	13.20957	41.68224	45.10819	100.00000
4013	11.38319	44.19092	44.42589	100.00000
4014	7.54694	48.40197	44.05109	100.00000
4015	7.18589	50.66405	42.15006	100.00000
4016	3.77270	53.90359	42.32371	100.00000
5001	33.87560	21.61372	44.51067	100.00000
5002	28.03343	27.43350	44.53307	100.00000
5003	25.96507	31.11278	42.92215	100.00000
5004	20.15707	35.74788	44.09505	100.00000
5005	17.49117	39.50985	42.99898	100.00000
5006	12.00922	46.97840	41.01238	100.00000
5007	12.29552	44.21350	43.49099	100.00000
5008	10.71013	46.18948	43.10039	100.00000
5009	9.14228	47.59723	43.26049	100.00000
5010	7.42440	49.55206	43.02354	100.00000
5011	6.95626	49.31599	43.72776	100.00000
5013	5.04868	51.78889	43.16243	100.00000
5014	1.79443	54.04497	44.16060	100.00000
5015	2.27182	54.59151	43.13667	100.00000
5016	0.00000	55.35829	44.64171	100.00000
6001	31.07515	23.59371	45.33114	100.00000
6002	29.95568	23.99050	46.05382	100.00000
6003	30.31134	26.68794	43.00072	100.00000
6004	28.15703	26.89504	44.94793	100.00000
6005	23.61602	30.23384	46.15014	100.00000
6006	20.80786	34.20363	44.98851	100.00000
6007	22.33660	33.98873	43.67467	100.00000
6008	21.80055	35.12758	43.07187	100.00000
6009	19.55226	35.99341	44.45433	100.00000
6010	19.06694	37.44775	43.48531	100.00000
6011	17.62253	38.17963	44.19784	100.00000
6012	13.45866	42.57787	43.96347	100.00000
6013	12.90109	42.96373	44.13518	100.00000
6014	11.70138	43.24272	45.05589	100.00000
6015	11.66372	44.18959	44.14669	100.00000
6016	8.72086	45.68736	45.59178	100.00000
7001	42.56992	7.57180	49.85828	100.00000
7002	41.91439	12.45153	45.63408	100.00000
7003	41.09517	13.63348	45.27135	100.00000
7004	42.51752	11.10047	46.38201	100.00000
7005	40.84392	12.99307	46.16301	100.00000
7006	40.43491	14.71539	44.84970	100.00000
7007	40.59773	14.12675	45.27552	100.00000
7008	41.95887	13.59879	44.44234	100.00000
7009	38.22297	16.40992	45.36710	100.00000
7010	37.21387	17.78769	44.99844	100.00000
7011	37.32680	17.96939	44.70381	100.00000
7012	36.57940	18.04250	45.37810	100.00000
7013	36.75547	18.42109	44.82343	100.00000

TABLE VIII. NATURAL ALKALI FELDSPAR (continued)

No.	Ne	Ks	Qz	Total, Wt %
7014	34.73382	19.28900	45.97719	100.00000
8001	9.48538	45.68151	44.83311	100.00000
8002	8.74801	48.27980	42.97219	100.00000
8003	7.58484	48.25681	44.15835	100.00000
8004	6.96323	47.87504	45.16173	100.00000
8005	4.48786	51.85120	43.66094	100.00000
8006	4.29168	52.29518	43.41314	100.00000
8007	3.83962	52.21802	43.94236	100.00000
8008	3.41065	53.28969	43.29966	100.00000
12001	53.81990	.27079	45.90930	100.00000
12002	53.99322	.60916	45.39762	100.00000
12003	54.25744	.82110	44.92146	100.00000
12004	54.09769	.10146	45.80085	100.00000
12005	54.87796	.34874	44.77330	100.00000
12006	52.22420	2.19670	45.57911	100.00000
12007	52.68448	1.26680	46.04872	100.00000
12008	51.48901	.38893	48.12205	100.00000
12009	50.07898	3.74127	46.17975	100.00000
12010	46.74436	7.69097	45.56467	100.00000
12011	51.60655	2.32023	46.07322	100.00000
12012	49.94678	2.13183	47.92139	100.00000
12013	53.06909	1.25433	45.67659	100.00000
12014	49.84930	4.01738	46.13332	100.00000
13001	53.38179	1.44119	45.17702	100.00000
13002	53.58213	.68457	45.73330	100.00000
13003	50.16843	2.40641	47.42516	100.00000
13004	52.43665	.95455	46.60880	100.00000
13005	53.68929	.38159	45.92912	100.00000
13006	53.53961	1.51012	44.95027	100.00000
13007	51.92132	.99661	47.08206	100.00000
13008	53.53163	.94758	45.52079	100.00000

TABLE IX. CHEMICAL COMPOSITION OF NATURAL ANALCITE AND NATURAL LEUCITE

Recalculated on the basis of three components, $NaAlSiO_4$(Ne), $KAlSiO_4$(Ks) and SiO_2(Qz), using the analytical data compiled by Deer, Howie & Zussman (1963, v. 4, table 44 in p. 343 for analcite, and table 33 in p. 280 for leucite) and the other data of analcites reported by Larsen & Buie (1938), Wilkinson (1962, 1963, 1965 and 1968), Coombs & Whetten (1967) and Pearce (1970).

* Relevant to Fig. 11.

No.	Ne	Ks	Qz	Total, Wt %
44001	68.70332	2.76092	28.53576	100.00000
44002	65.68412	0.00000	34.31588	100.00000
44003	69.12254	.66109	30.21637	100.00000
44004	69.74729	0.00000	30.25271	100.00000
44005	68.35734	.74201	30.90065	100.00000
44006	69.54258	1.29287	29.16455	100.00000
44007	70.03259	0.00000	29.96741	100.00000
44008	67.10222	.36582	32.53196	100.00000
44009	63.27057	6.77810	29.95134	100.00000
44010	49.78832	19.27261	30.93907	100.00000
38001	49.78832	19.27261	30.93907	100.00000
38002	61.43321	6.92501	31.64178	100.00000
62001	53.16188	25.54361	21.29451	100.00000
62002	49.75592	32.10225	18.14183	100.00000
63001	82.54495	3.00349	14.45156	100.00000
63002	74.31782	2.87414	22.80804	100.00000
63003	73.10289	1.88337	25.01374	100.00000
63004	59.28855	25.23785	15.47360	100.00000
65005	58.99021	18.46245	22.54734	100.00000
65006	59.81738	16.47285	23.70977	100.00000
65007	57.80865	17.48425	24.70710	100.00000
65008	55.08198	18.43950	26.47852	100.00000
65009	68.28683	18.13743	13.57574	100.00000
65011	48.30323	22.06371	29.63307	100.00000
68001	67.91682	2.50357	29.57961	100.00000
68002	67.44529	4.28093	28.27378	100.00000
68003	68.40457	2.76224	28.83320	100.00000
68004	70.29808	.99513	28.70679	100.00000
68005	49.78832	19.27261	30.93907	100.00000
68006	82.54495	3.00349	14.45156	100.00000
68007	73.10289	1.88337	25.01374	100.00000
68008	70.94960	.40671	28.64369	100.00000
68009	70.44138	1.53106	28.02755	100.00000
68010	62.84758	7.21349	29.93893	100.00000
68011	67.21845	1.08864	31.69291	100.00000
68012	54.32130	8.80036	36.87834	100.00000
70001	72.44576	1.67411	25.88013	100.00000
70002	66.75372	.52673	32.71955	100.00000
70003	68.97347	1.28229	29.74424	100.00000
70004	66.68388	2.30803	31.00809	100.00000
70005	68.83830	3.15721	28.00448	100.00000
70007	68.70749	.61021	30.68230	100.00000
67008	63.08467	0.00000	36.91533	100.00000
67009	60.27978	.18312	39.53710	100.00000
67011	62.51860	.12292	37.35849	100.00000
67012	61.69882	.19536	38.10582	100.00000
67013	54.93997	3.73953	41.32050	100.00000
33001	3.03127	70.73668	26.23205	100.00000
33002	9.46983	70.19814	20.33203	100.00000
33003	1.43836	72.68366	25.87798	100.00000
33004	8.81862	65.69167	25.48971	100.00000
33005	2.95897	68.96497	28.07606	100.00000
33006	5.19140	68.65454	26.15405	100.00000
33007	10.09140	61.50348	28.40512	100.00000

FIG. 11. TERNARY COMPOSITION DIAGRAM OF NATURAL MINERALS in the terms of three components $NaAlSiO_4$, $KAlSiO_4$ and SiO_2
showing the solid solution range of natural minerals, alkali-feldspar, analcite, leucite, nepheline, and kalsilite.

- Natural minerals*; chemical analysis data were collected from the literature. Most of the mineral compositions were recalculated on the basis of three components, $NaAlSiO_4$, $KAlSiO_4$ and SiO_2.

- Equilibrium compositions of invariant phases, analcite = Anl_i, Albite = Ab_i and Nepheline = Ne_i at 5.15Kb and 657°C (invariant point) in the system $NaAlSi_3O_8$-$NaAlSiO_4$-H_2O (Synthetic) experimentally determined by writers.

  Ab'=Albite is the albite at 5.15Kb and 657°C in the system $NaAlSi_3O_8$-SiO_2-H_2O, which contains 5 weight percent of silica (maximum) in solid solution at the given P and T.

- Equilibrium compositions of univariant phases, analcite, albite and nepheline, at P_{H_2O} = 10Kb. in the system $NaAlSi_3O_8$-$NaAlSiO_4$-H_2O (synthetic), experimentally determined by the writers.

  $Ab_{(Ne)}$ and $Anl_{(Ne)}$ are the equilibrium compositions of albite and analcite for the reaction (Ne):Ab+Anl+V=I
  $Ne_{(Ab)}$ and $Anl_{(Ab)}$ are the equilibrium compositions of nepheline and analcite " (Ab):Ne+Anl+V=I
  $Ab_{(V)}$, $Ne_{(V)}$ and $Anl_{(V)}$ are the equilibrium compositions of albite, nepheline and analcite for the reaction (V):Anl=L+Ab+Ne.

* For details, see Tables VIII and IX.

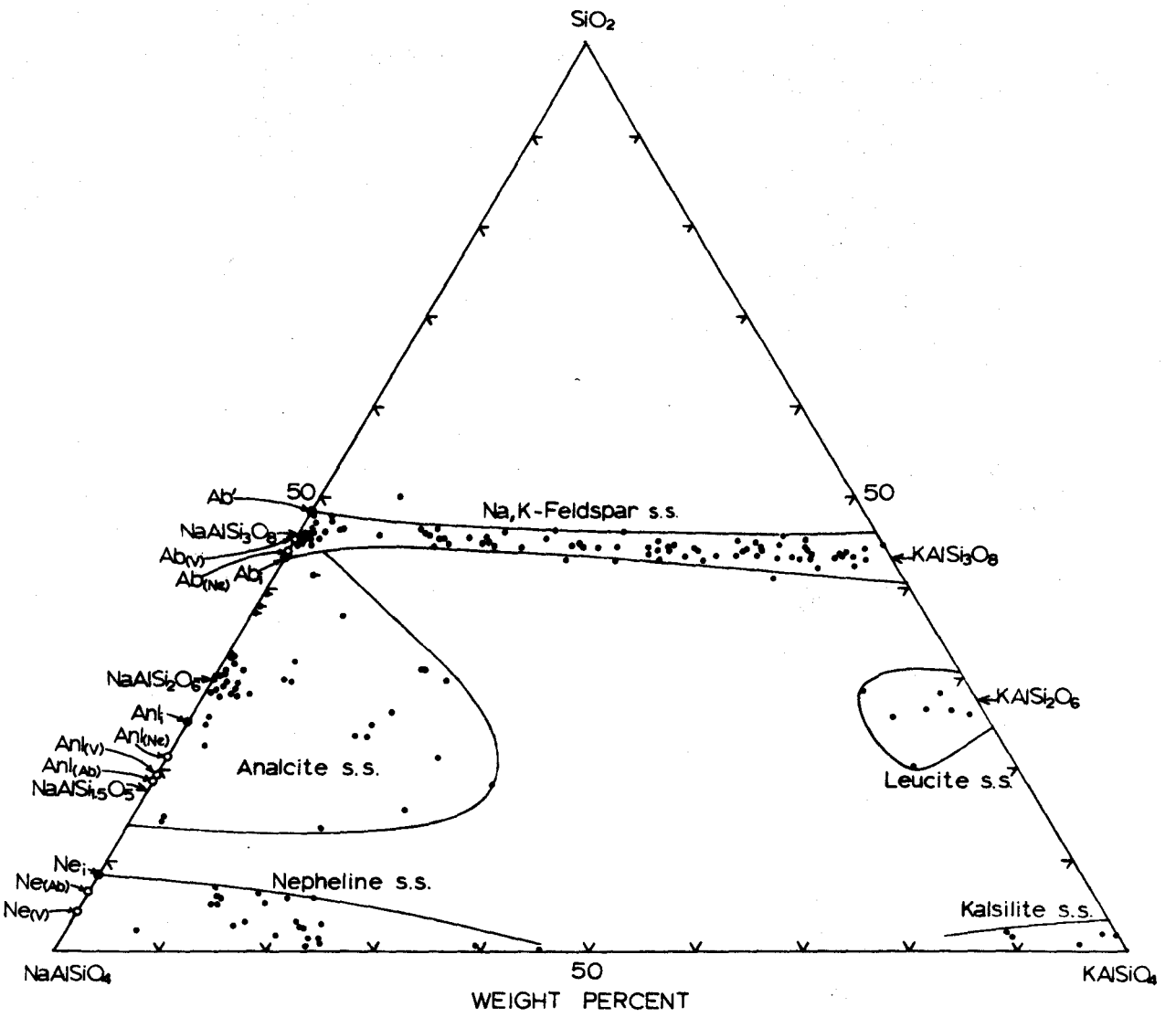
SiO2
50
50
Ab'
NaAlSi3O8
Ab(v)
Ab(Ne)
Abi
Na,K-Feldspar s.s.
KAlSi3O8
NaAlSi2O6
Ani
Ani(Ne)
Ani(v)
Ani(Ab)
NaAlSi1.5O5
Analcite s.s.
KAlSi2O6
Leucite s.s.
Nei
Ne(Ab)
Ne(v)
Nepheline s.s.
Kalsilite s.s.
NaAlSiO4
50
KAlSiO4
WEIGHT PERCENT

FIG. 11

The ranges of nepheline and kalsilite are generally concordant with the experimental results reported by Tuttle & Smith (1958, p. 583, and p. 586), and Hamilton & MacKenzie (1960, p. 61; 1965, p. 222). Leucite compositions have been known not to depart significantly from the ideal formula, $KAlSi_2O_6$, through the investigations reported by Bowen & Schairer (1929), Chirvinsky (1953), Sahama (1952), Schairer & Bowen (1955), Tilley (1958), etc. But the chemical data for leucite suggest a possible enlargement of its stability range.

Alkali feldspars form a narrow zone of solid solutions along the join $NaAlSi_3O_8$-$KAlSi_3O_8$, approximately defined by two boundary lines which depart from the join by ±2.5 Wt.% silica. These analyses seem to be in good support of the present experimental results.

For the analcite solid solutions, an idealized diagram to illustrate petrologic trends was constructed as shown in Fig. 12. The diagram shows a general idea for the compositional trend of analcites in regard to the petrogenesis of analcite-bearing rocks. In Fig. 12, the solid triangle denotes the quaternary invariant analcite composition in the system $NaAlSiO_4$-$KAlSiO_4$-SiO_2-H_2O. Consequently, it is a thermal peak of the analcite stability field. On the basis of the results investigated by Peters et al. (1966, p. 741), Wilkinson (1965 and 1968) and the results in this study, it was reasonably inferred that the invariant analcite

has an anhydrous composition $Ne_{73}Ks_2Qz_{25}$ (approximately). The X-mark denotes the thermal trough of the analcite stability field. Since the analcite of the thermal trough was estimated to be of the ideal formula, $NaAlSi_2O_6 . H_2O$, in the system $NaAlSi_3O_8$-$NaAlSiO_4$-H_2O (see Figs. 1 and 2), the analcite composition of the quaternary thermal trough was reasonably assumed to be $Ne_{68}Ks_2Qz_{30}$ (anhydrous).

As shown in the diagram (fig. 12), the liquidus analcite changes from near the natrolitic composition toward the invariant analcite composition, during the progressive differentiation of a magma (marked as a thick solid arrow; the solid arrow on the Ab-Ne join is the one for the Na-analcite). The invariant analcite (at about 5Kb) is the silica-richest terminal composition for the liquidus analcite.

The subsolidus compositional readjustment of the primary analcite in equilibrium with coexisting phases is interpreted to be accomplished along each of the fine lines radiating from the invariant analcite. And then the composition of the analcites reversely converges toward the ideal formula (X), with or without the aid of a residual aqueous fluid. This is the idealized situation. But it is hard to expect the completion of the compositional readjustment down to the thermal trough. In most cases, the compositional readjustment of analcite might stop at a temperature above about 400°C. On the basis of this idea combined with the fact of bulk-compositional frequency near the

FIG. 12. IDEALIZED PETROGENETIC DIAGRAM FOR ANALCITE SOLID SOLUTIONS (PROJECTED TO THE DRY BASE) I N THE SYSTEM $NaAlSiO_4$-$KAlSiO_4$-SiO_2-H_2O

constructed approximately on the basis of data in Figs. 1, 2, 4 and 11, and the data reported by Wilkinson (1965, p. 438, Fig. 5). The thick solid arrow indicates the trend of compositional change for the liquidus analcite during progressive differentiation. The solid triangle is the thermal peak of analcite stability field at an invariant pressure and temperature ($\sim$ 5 Kb and 635+°C). X-mark indicates the thermal trough of analcite stability field (150±50°C at 2-5Kb).

For the details, see text.

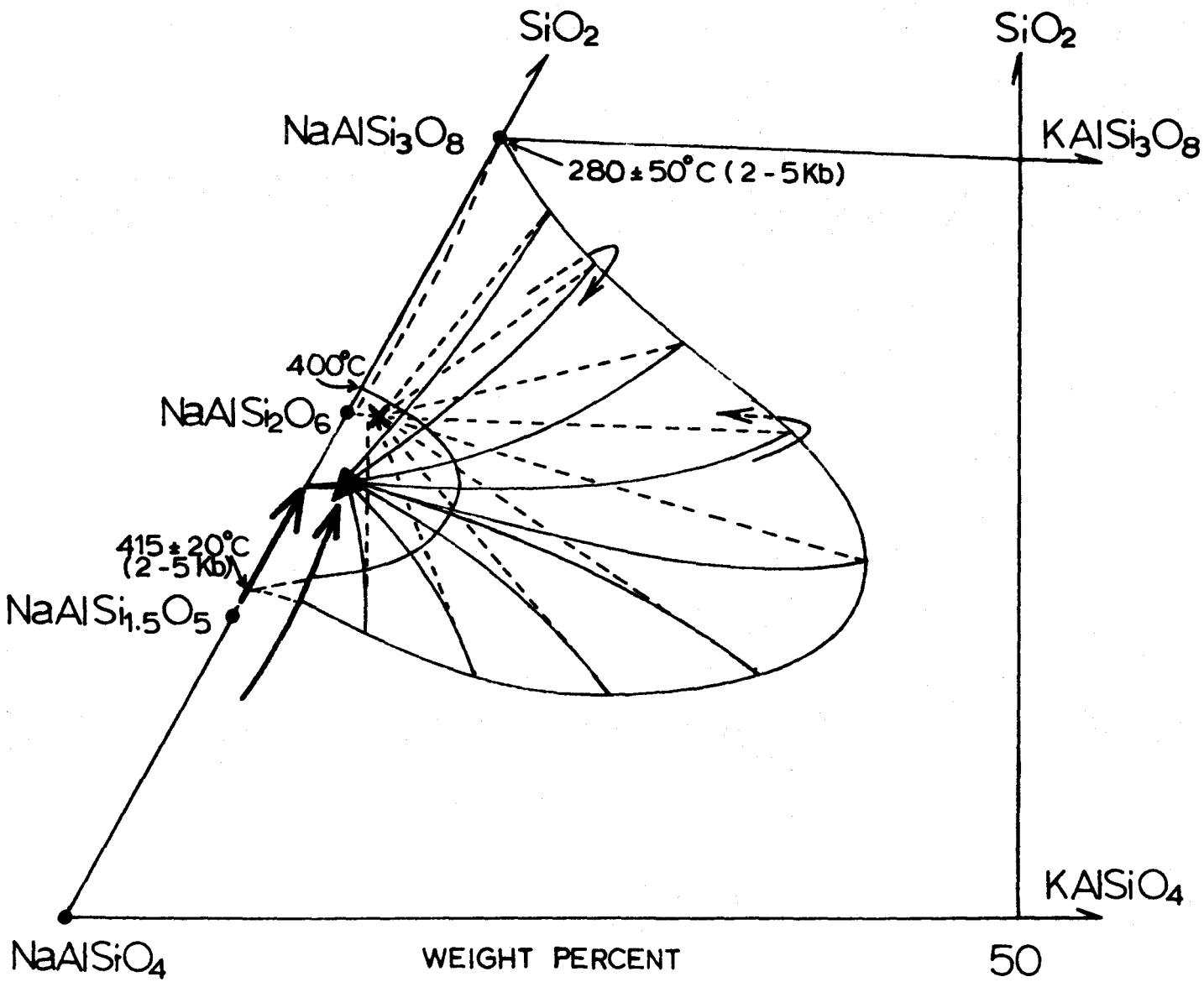
SiO2
SiO2
NaAlSi3O8
KAlSi3O8
280 ± 50°C (2 - 5Kb)
400°C
NaAlSi2O6
415 ± 20°C
(2 - 5Kb)
NaAlSi1.5O5
KAlSiO4
NaAlSiO4
WEIGHT PERCENT
50

FIG. 12

saturated syenitic and slightly undersaturated syenitic compositions (that of temperature minimum of melting), the abundant occurrence of nearly ideal compositional analcites can be explained. The compositional variance of analcite can also be expected, when either pressure or temperature decreases relatively rapidly from the liquidus region. It is to be noted that the thermal divide formed due to the thermal peak of the analcite stability field generates another minor trend of a primary analcite composition which changes toward a nepheline-rich one on cooling. But the change of the thermal divide with pressure makes the situation complicated.

Sedimentary analcites including low-grade metamorphic ones show a wide range of compositions according to the data reported by Wilkinson & Whetten (1964), Whetten & Coombs (1965), and Coombs & Whetten (1967).

Coombs & Whetten (1967) further specified the compositional range of sedimentary analcites into three groups, silica-rich sedimentary analcites (approximately $Na_{13}Al_{13}Si_{35}O_{96}$-$Na_{14}Al_{14}Si_{34}O_{96}\cdot n\,H_2O$), burial-metamorphic analcites (close to $Na_{14}Al_{14}Si_{34}O_{96}\cdot n\,H_2O$), and silica-poor sedimentary analcites (approximately $Na_{15}Al_{15}Si_{33}O_{96}\cdot n\,H_2O$ to $NaAlSi_2O_6\cdot H_2O$). It was concluded that the compositional range of sedimentary analcites including burial-metamorphic ones is approximately from $NaAlSi_3O_8\cdot 1.5\,H_2O$ to $NaAlSi_2O_6\cdot H_2O$.

This agrees very well with the present experimental data (see Figs. 1, 2 and 4). In the light of the experimental study in the system $NaAlSi_3O_8$-$NaAlSiO_4$-H_2O, it is interpreted as follows:

(i) If the bulk-composition (mostly local ?) of analcite-bearing sedimentary rock is richer in silica than that of $NaAlSi_2O_6$, then the analcite belongs compositionally to the range of $NaAlSi_3O_8 . 1.5\ H_2O$ to $NaAlSi_2O_6 . H_2O$. If it is less in silica than that of $NaAlSi_2O_6$, then its analcite will belong to the range from $NaAlSi_2O_6 . H_2O$ to $NaAlSi_{1.5}O_5 . .75\ H_2O$. The thermal trough of the analcite-stability field was experimentally estimated to be at ideal composition analcite. Thus, most of the sedimentary analcites including low-grade metamorphic ones have compositions within $NaAlSi_3O_8 . 1.5H_2O$ and $NaAlSi_2O_6 . H_2O$, since the sedimentary rocks are mostly silica-rich.

(ii) The composition of a sedimentary analcite seems to depend essentially on the local bulk-composition of starting materials (rock) including aqueous fluid phase and temperature (at a given pressure).

In the petrogenetic diagram (Fig. 12), assuming the attainment of chemical equilibrium, the compositional change of equilibrium analcite during progressive metamorphism including diagenesis is interpreted to be accomplished along the dashed line starting from the nearly ideal analcitic composition (the thermal trough) outwardly, and then from

the boundary rim toward the thermal peak of analcite stability field. However, the situation is complicated by the possible effect of a_{Na^+} and a_{SiO_2} in the aqueous phase and the general difficulties in attaining equilibrium at low temperatures, as pointed out by Coombs & Whetten (1967, p. 277) in their comment on the use of analcite as a possible geothermometer which was suggested by Saha (1961).

On the basis of the present experimental results (Figs. 1, 2, 4 and 7), it is pointed out again that the analcites of very albitic composition are found within a limited temperature interval, which is not very dependent on pressure ($280^{\circ}\pm50^{\circ}C$ in the pressure range of 2-7.3Kb). This would seem to be a possible use of analcite as a geothermometer.

Liquidus analcite (e.g. primary phenocryst of analcite) seems to be useful as a geobarometer to define the lower limit of pressures (about 5Kb), since analcite cannot crystallize from a melt below about 5Kb.

PART 2

A METHOD FOR THE DETERMINATION OF THE SOLUBILITY OF WATER IN SILICATE MELTS, WITH APPLICATION TO H_2O-SOLUBILITY IN THE SYSTEM $NaAlSi_3O_8$-$NaAlSiO_4$-H_2O

I. GENERAL STATEMENT

Generally, the determination of the solubility of water in a silicate melt is one of the most difficult problems encountered in experimental investigations of a silicate system, as pointed out by Tuttle & Bowen (1958, p. 14). In many cases, therefore, solubility data have not been reported in spite of the fact that data to determine the solubilities were available as by-products of the determination of P-T curves or T-X phase diagrams, if the present method were used. A new method used in this study is especially suitable to such cases. This method was developed in order to obtain the solubility values directly from the experimental runs made to study the phase equilibria.

In this study, the solubility of water in melts of various compositions were determined at P_{H_2O} = 2Kb & 5.15Kb respectively, and also the solubility of H_2O in the (Anl) and (Ne) univariant melts in the system $NaAlSi_3O_8$-$NaAlSiO_4$-H_2O were determined, using the present method. The H_2O-contents in hydrous mineral phases were also determined.

It should be noted that the writer does not assert the superiority of the present method over the previous ones but he does wish to stress the simplicity of the method.

II. PREVIOUS METHODS

1. Goranson's Method (1931): weight-loss-on-ignition method.

His pioneer work to determine water-solubility in reconstituted granite magma prepared by melting mica-granite from Stone Mountain, Georgia, has greatly contributed to petrological research. His method is essentially as follows:

i) A charge was prepared using a sealed-tube technique (with excess water.

ii) Quenched after equilibrium attained at a desired P-T condition.

iii) Glass dried at 100-106^{o}C until attaining to constant weight, and then weighed.

iv) Ignited over a gas burner for 30 minutes and finally reweighed.

The weight differences before and after ignition is considered as the amount of dissolved water in the melt.

2. The Method of Yoder (1954) and Yoder, Stewart & Smith (1957):

Weight-loss-on-crystallization method combined with phase boundary-location

Instead of using the final step (iv) of Goranson's method, hydrous glass (run product) was retreated such as to be completely crystallized,and then dried and weighed. The weight difference before and

after the crystallization is taken as the amount of water dissolved in the melt. This method was devised by Yoder (1954) in his study of the system diopside-anorthite-H_2O. Subsequently, the method was improved using the known amount of water in an original charge by Yoder, Stewart & Smith (1957, p. 209; Fig. 39 and 40) in their study of ternary feldspars (personal communication with Yoder, July, 1970). In fact, their method was combined with phase boundary-location on the $T\text{-}X_{H_2O}$ sections.

Note that neither of Yoder's methods have been published but have been mentioned by Burnham & Jahns (1962, p. 723) through personal communication with Yoder (1960). For information, see Yoder (1965).

3. The Method of Khitarov et al. (1959): Water-loss-on-ignition method

Their modification was to specify the amount of water-loss from the total ignition loss, during the final step of Goranson's method. For this purpose, an apparatus was specially designed such that the dissolved water in a quenched glass was expelled from the glass on ignition and absorbed in anhydrone in a "Pregl tube". The amount of weight increased in the Pregl tube was considered as that of the dissolved water in the melt.

4. The Method of Burnham & Jahns (1962):

Liquidus boundary-location method with the aid of excess water-criteria

The solubility value is essentially obtained by locating the liquidus boundary (or boundaries) on an isobaric $T\text{-}X_{H_2O}$ section. The solubility value

is corrected through the examination of the quenched glass for evidence of excess water and by the amount of water trapped as internal bubbles. The latter quantity is measured by means of point-counting on a specially prepared thin section.

III. THE PRESENT METHOD

1. Sealing of known amounts of water and starting material (20-50mg in this study) in a capsule.
2. Quenching after the required period to attain equilibrium at a desired P-T condition.
3. The capsule (run product) is dried in an oven (80°-110°C) for 30 minutes or longer, and then weighed, in order to eliminate any possible water and/or other volatile materials on the surface wall of the capsule, and also to equalize the physical condition of the capsule for weighing.
4. A number of pinholes are made on the capsule, and then the pinholed capsule is dried again in an oven (80°-110°C) for several hours (usually overnight) so that all possible excess water inside the capsule is driven off through the pinholes.
5. The capsule is finally reweighed and then opened for phase-identification.

The value of the H_2O-content in a melt or in a hydrous mineral may be obtained through a simple calculation and correction as described below.

6. The weight difference between the total amount of water (originally put into the capsule) and that of free water (driven off during drying) after the run is the essential value for the H_2O-content in a hydrous phase. If there is no other source of water available, then it becomes directly the amount of H_2O in the hydrous phase. Note that the amount of free water after the run is the weight-difference before and after drying the pinholed capsule.

7. There is a source of error due to the moisture content in the starting material, which is related to the hygroscopic properties of powdered gels. Therefore, it is necessary to know how much moisture has been obsorbed in a powdered gel before making a charge. For this, the amount of water released from a powdered gel when the gel is completely crystallized and no hydrated minerals occur is considered as the amount of the moisture originally contained in the gel. This is basically a similar idea to that of Yoder (1954, p. 106-107).

In order to minimize the error connected with moisture content, in gels, the starting materials were heated (e.g., at a temperature slightly above 300°C in over night in the present system) such as to be moisture-free and kept in a moisture-free condition (e.g. in an

oven at 115°C) before being used. In this study, the H_2O-contents in various hydrous phases determined are believed to be correct within ±0.5 weight percent except for those in quenched glasses at pressures above ~8Kb (see statement 9).

8. The method for determining the H_2O-content in a hydrous phase is summarized in the following equation:

$$H_2O\text{-content in a hydrous phase} = \frac{H_2O \text{ (step 6)} + \text{moisture (step 7)}}{\text{starting gel} + H_2O \text{ (step 6)}} \times 100 \text{ Wt.\%}$$

Note that the weight of a starting gel equals that of an ideally moisture-free gel plus moisture (7) which is originally absorbed in the gel.

9. There is another source of error, which is related to the vesiculation in a quenched glass of water-bubbles. Accordingly, the origin of water-bubbles in a quenched hydrous glass is important and has to be determined, in order to correct the solubility value obtained. If water bubbles are inclusions of excess vapour phase, then the amount (wt.) of the bubble-water should be subtracted respectively from the numerator and the denominator of the above equation. When the amount of the bubble water is sufficiently small, then its effect on the

solubility value may be negligible. If water bubbles in a glass are due to the exsolution of some of the dissolved water in a melt upon quenching, then the above equation can be directly used, regardless of the amount of water bubbles, for the determination of H_2O-solubility. In this case, however, the solubility value obtained is probably slightly less than the real value, because some of the dissolved water in a melt may be lost by exsolution from the H_2O-saturated melt during quenching. The amount of the water lost in this way would be proportional to the degree of vesiculation in the quenched glass. The degree of vesiculation, therefore, may be a crude measure of the amount of water driven off into the vapor phase.

In this study of solubility in the system $NaAlSi_3O_8$-$NaAlSiO_4$-H_2O, the vesiculation of water-bubbles in a hydrous glass is essentially attributed to the exsolution of some of the dissolved water in the melt upon quenching. This feature will be fully discussed later.

10. The present method is generally applicable to the determination of H_2O-content in a hydrous phase (e.g., analcite).

IV. EXPERIMENTAL RESULTS AND THEIR INTERPRETATION IN THE SYSTEM $NaAlSi_3O_8$-$NaAlSiO_4$-H_2O

The data used below in determining the solubility of water in a melt and the H_2O-content in a hydrous mineral were collected from the run products used in the investigation of phase-equilibria in the system $NaAlSi_3O_8$-$NaAlSiO_4$-H_2O (Part 1). Note that the starting materials used were oxide gels for the experiments. All the experiments were carried out in the manner described in the previous sections.

1. Correction Factor for H_2O-contents in Melts and Hydrous Minerals

The amounts of moisture initially absorbed in the gels of various composition were determined from suitable run products (see step 7), and plotted against the compositions of the dry gels (see Fig. 13). In this particular system, any run product which crystallized to a mixture of Ab+V, Ab+Ne+V or Ne+V, is suitable for the determination of moisture, because they are neither hydrated minerals nor hydrous glasses.

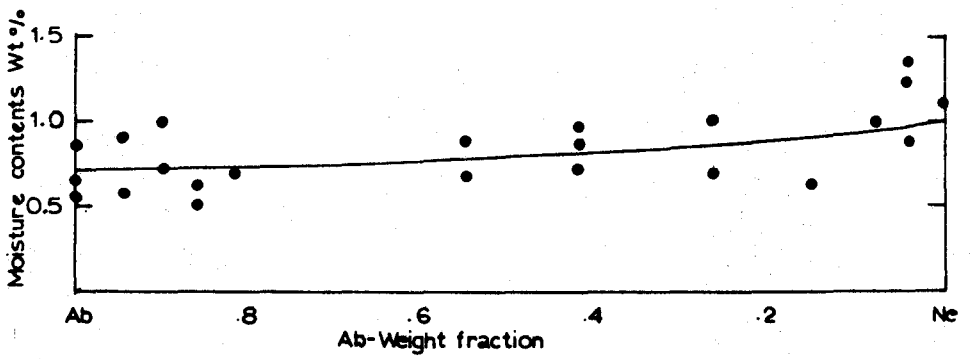

Fig.13 The correction curve of H_2O-contents in hydrous phases, showing the amounts of moistures initially absorbed in the gels of various composition.

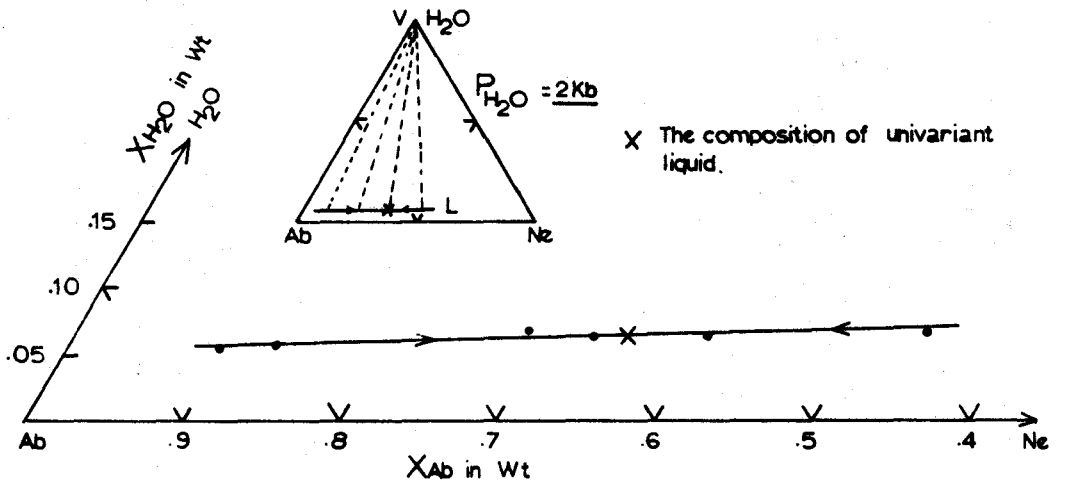

Fig.14 The solubility of water in melt of various composition, at the minimum temperature of water-saturated melt of each composition, at P_{H_2O} = 2 Kb. Shown in isobaric polythermal diagram, projected to the system Ab-Ne-H_2O.

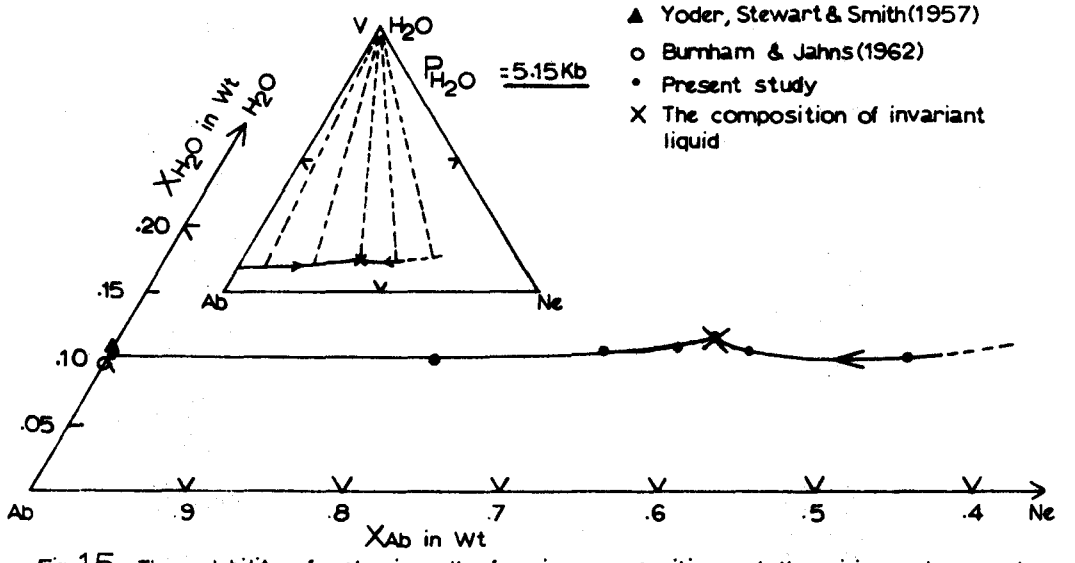

Fig.15 The solubility of water in melt of various composition, at the minimum temperature of water-saturated melt of each composition, at the invariant water vapor pressure 5.15 Kb. Shown in isobaric-polythermal diagram, projected to the plane of the system Ab-Ne-H_2O.

TABLE X

H_2O-contents in water-saturated melts of various composition in the system Ab-Ne-H_2O, at temperature slightly above the minimum temperature of water-saturated melt as a function of each composition, & at the given pressures 2Kb & 5.15Kb respectively, in the presence of excess water. The data shown graphically in fig.14 &15.

Run No.	Composition of melt			Run condition (excess water)		
	Anhydrous, in Wt%		H_2O-content	Pressure	Temp.	Time
	Ab	Ne	Wt.%	Kb	°C	Hour
235	89.7	10.3	5.5	2.00	880	22
236	85.9	14.1	5.8	2.00	880	22
192	69.1	30.9	6.9	2.02	853	91
201	64.8	35.2	6.2	2.00	804	91
193	57.0	43.0	6.2	2.02	853	91
237	42.3	57.7	6.4	2.00	880	22
691	76.7	23.3	9.9	5.17	754	22
695	64.8	35.2	10.4	5.17	699	22
600	59.8	40.2	10.8	5.23	672	53
361	57.0	43.0	11.5	5.29	669	19
696	54.7	45.3	10.5	5.17	699	22
692	43.5	56.5	9.9	5.17	751	22

The moisture-contents in the gels of different compositions are nearly the same as one another, but the content increases slightly from the albitic composition (~0.7 Wt.%) toward the nepheline-composition (~1 Wt.%). The accuracy limits for the H_2O-contents in hydrous phases are largely dependent on the variation of moisture-content in the gel of individual charge, when the generalized moisture curve (Fig. 13) is used as the correction factor. Because the variation of moisture-content is within the range of ±0.5 weight percent (see Fig. 13), the values of H_2O-contents presented in Tables X, XI and XII are believed to be correct within ±0.5 Wt.%, assuming no other source of error.

There is another source of error due to the vesiculation in quenched glasses at pressures above~5Kb, which may be serious at pressures above ~8Kb and is discussed later.

2. The Solubility of Water in Melts of Various Compositions at P_{H_2O} = 2Kb and 5.15Kb

Suitable quenched glasses which were run at a temperature slightly above the liquidus temperature were selected from the run products for the determination of water-saturated liquidus boundaries

on a T-X phase diagram (projected to the dry base), at P_{H_2O} = 2Kb and 5.15Kb respectively (for the detail refer to Figs. 1 and 2 in Part 1). The solubility values determined using the present method are presented in Table X and plotted in the diagrams shown in Figs. 14 and 15.

The water-solubility values of various compositional melts along the liquidus boundaries are similar, but slightly increasing toward the nepheline-rich composition. Thus, it appears that the solubility values are not sensitive to the compositional variation of melts within the considerable range of composition in the system.

3. The Solubility of Water in Univariant Melts at the temperature minimum of melting up to 10Kb

The solubility of water in melts occurring along two univariant P-T curves, (Anl) and (Ne), was determined and is presented in Table XI and plotted against water-vapor pressure (see Fig. 16a). In order to get a water-saturated glass completely free from any crystal phase, the run product which was selected for the determination of the water-solubility in the melt was that which was run at a temperature slightly above the univariant temperature (generally 10°C above) at a given pressure. The solubility curve shown in Fig. 16a was drawn so as to represent the mean values of the data, except for those above 8Kb.

TABLE XI

The solubility of water in univariant melt in the system Ab-Ne-H_2O up to water-vapor pressure 10 Kb. The solubility values were determined using the present method. (The size of water bubble given in parenthesis is the most frequently observed.)

Run No.	Composition of melt: Anhydrous composition, in Wt. %: Ab	Ne	(Solubility of water) H_2O-contents, in Wt. %	Run condition (excess H_2O): Pressure Kb	Temp. °C	Time hour	Water bubbles in glass: Volume % of bubble	Size of bubble, in micron	Wt. % of bubble water	H_2O-contents in melt, obtained assuming water bubbles in a quenched glass as those of external origin, in Wt. %
117	69.1	30.9	4.7	1.07	852	566	nil	-	-	
201	64.8	35.2	6.2	2.00	804	91	nil	-	-	
600	57.0	43.0	10.8	5.23	672	53	trace	.5-2.5	-	
361	57.0	43.0	11.5	5.29	699	19	tr.	.5-2.5	-	
409	49.2	50.8	12.2	6.62	655	19	4	.5-10.0 (6.0)	1.5	10.9
404	49.2	50.8	13.2	7.31	652	21	6	.5-5.0 (2.5)	2.6	10.9
473	49.2	50.8	12.5?	9.00	642	40	10	.5-5.0 (2.5)	4.8	8.1
489	54.7	45.3	12.2?	9.65	632	20	12	.5-5.0 (2.0)	5.8	6.8

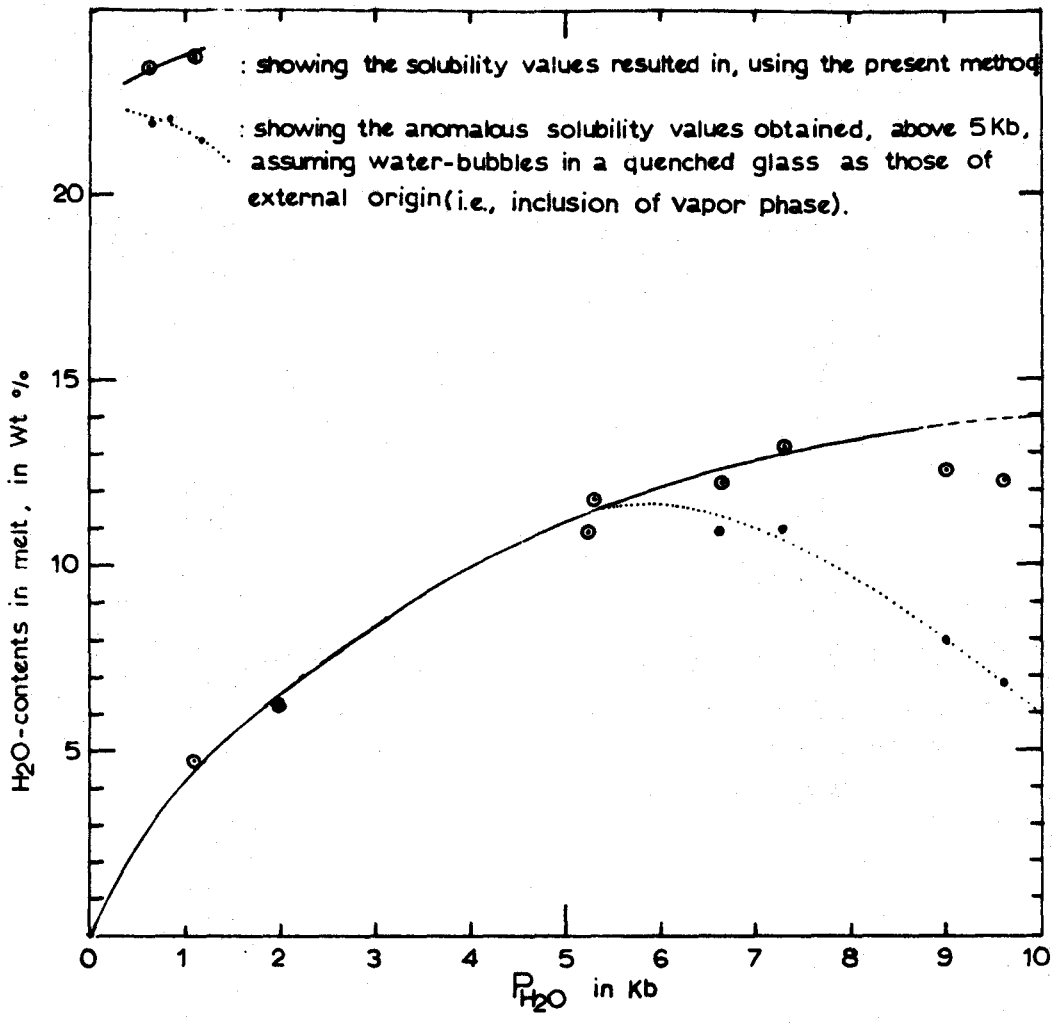

Fig.16a. The solubility of water in univariant melt, in the system Ab-Ne-H_2O. Showing the amounts of dissolved water in the melt as a function of each of the given pressures. The minimum temperature of a melt is definite at a given pressure. The diagram is based on the solubility data presented in table XI.

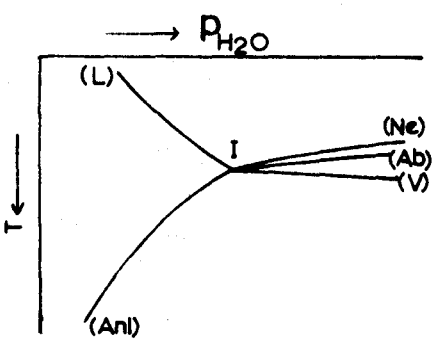

Fig.16b. P-T diagram(schematic) in the same system, presented for better understanding the concept of univariant melt.

The univariant melt concerned herein occurs along the curve (Anl)-I-(Ne) which consists of two univariant curves (Anl) & (Ne) and an invariant point I,

where (Anl): Ab + Ne + V = L

(Ne) : Ab + Anl + V = L ,

The invariant point I located at 5·15Kb & 657°C.

In the present study, it was noted that the quenched glasses were completely free from water bubbles up to 5Kb, and above 5Kb water-bubbles began to appear in the glasses. At pressures slightly above 5Kb, the water-bubbles observed in a quenched glass were just a few in number and as small as 0.5μ (micron) in diameter. As pressure increases, the number as well as the size of bubbles increases. The size of bubbles observed were mostly within the range 0.5-5.0μ, and the most frequently observed size is about 2.5μ. All intermediate sizes within the range were observed in each glass. If the water-bubbles in the quenched glass were initially trapped in the starting material and preserved in the quenched glass, then such bubbles should have also formed in glass at pressures below 5Kb. But this was not the case. Thus it appears that the bubbles were formed during the quenching of high pressure runs, which is compatible with the results reported by Burnham & Jahns (1962, p. 728).

An attempt was made to check the origin of the bubbles in the following fashion. The weight percent of the bubble-water in each of the quenched glasses was approximately calculated on the basis of available P-V-T data (Kennedy & Holser, 1966) from the volume percent of the water-bubbles which were measured by a point-counting method. The specific gravity of glass was assumed to be about 2.2,

in order to compute the weight percent of the bubble-water. The supposed water-solubility values were recalculated and plotted in Fig. 16a as small solid circles, using the method described by Burnham & Jahns (1962) assuming that the water-bubbles are inclusions of excess water phase. As shown in Fig. 16a, the solubility values decrease at pressures above about 5.5Kb, which is unlikely. Therefore, it appears that the assumption is incorrect.

Hence it is believed that the water-bubbles were formed by segregation of the dissolved water from the melt upon quenching. Accordingly, it may also be expected that some of the dissolved water in a melt of high pressure is possibly driven off from the melt into the aqueous phase during quenching. The solubility values determined at pressures above 5.5Kb by this method are therefore probably slightly lower than the real values. The discrepancy may be significant at pressures above 8Kb (more than 1 Wt.% deviation ?).

The solubility values in the univariant melts are nearly the same as those reported for the Harding pegmatite melt (Burnham & Jahns, 1962), up to about 5.5Kb. As pressure increases above this, they are different (see Fig. 17). The solubility of water in the melt is estimated to be equal to or slightly greater than 14 Wt.% H_2O at 10Kb. Note that the solubility curve of Peters et al. approximately obtained

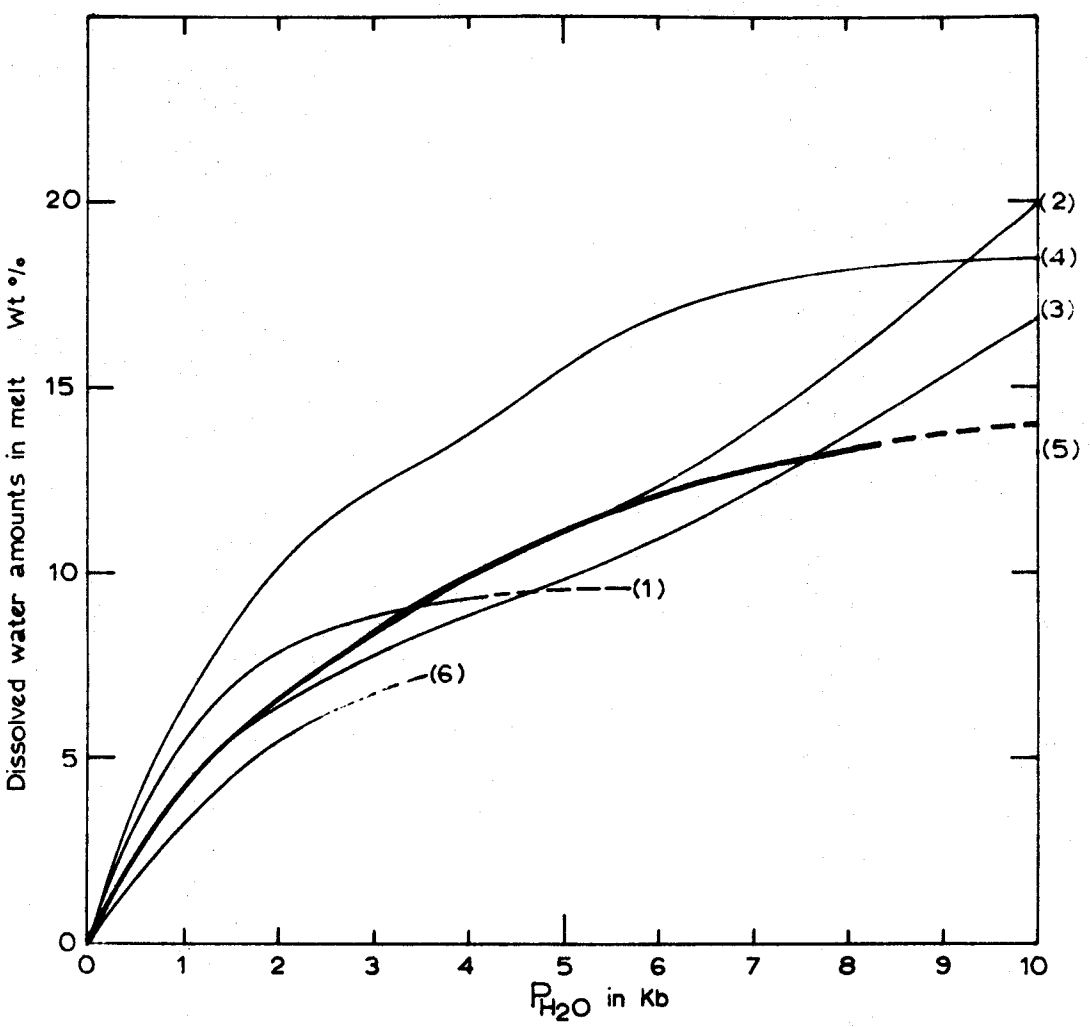

Fig.17. The comparison of the water-solubility in melt with the results of previous work.

(1): Goranson(1931), the water-solubility curve of Stone Mountain granite melt

(2): Burnham & Jahns(1962), the water-solubility curve of Harding pegmatite melt

(3): Burnham & Jahns(1962), the water-solubility curve of albite melt

(4): Peters, Luth, & Tuttle(1966), the water-solubility curve of univariant melt in the system Ab-Ne-H_2O. The solubility values were approximately obtained from their fig.3 a in p.745.

(5): Present work, the water-solubility curve of univariant melt in the system Ab-Ne-H_2O

(6): Khitarov et al(1959), the water-solubility curve of El'dzurtinskii granite melt.

from their diagram (1966, Fig. 3a, p. 745) is very much different from the present one (see Fig. 17).

4. H_2O-content in Hydrous Minerals

The hydrous minerals encountered in this study were analcite, nepheline-hydrate I and zeolite species P. They all form a wide range of solid solutions respectively (see Figs. 1 & 2, Part 1). The H_2O-contents in these hydrous minerals were determined using the present method and are presented in Table XII and are also plotted against composition as a weight fraction as shown in Fig. 18. The data for the H_2O-contents in analcite solid solutions are also presented with respect to the mole ratio of SiO_2 of analcite in Table XIIa and Fig. 18 (upper part), in order to compare the present data with that determined by Saha (1959, p. 305 and 310) using the method of ignition-loss.

The present results agree closely with those of Saha. It was found that the H_2O-contents of analcites of various compositions within the range from $Ab_{90}Ne_{10}$ to $Ab_{50}Ne_{50}$ are very similar (8 Wt.%) (for details, see Table XIIa and Fig. 18). The approximate chemical formulae for the analcites are presented in the last column of the table.

TABLE XII

H_2O-contents in hydrous minerals, analcite, nepheline-hydrate I, & zeolite species P., encounted in this study of the system Ab-Ne-H_2O.
Showing the variation of H_2O-contents according to the anhydrous-compositional change in a given phase

TABLE XIIa H_2O-contents in analcite (various composition)

Composition of analcite			Mol. ratios of SiO_2 & H_2O with respect to 1 mol. of Na_2O or Al_2O_3 in Na-analcite		Approximate chemical formula of analcite, in the form $NaAlSi_pO_q \cdot rH_2O$
Anhydrous, Wt °/o		H_2O-content in Wt. °/o			
Ab	Ne		SiO_2	H_2O	
100.0	0.0	9.3	6.0	3.0	$NaAlSi_3O_8 \cdot 1.5H_2O$
87.7	12.3	8.1	5.2	2.3	$NaAlSi_{2.6}O_{7.2} \cdot 1.2H_2O$
76.7	23.3	7.9	4.6	2.1	$NaAlSi_{2.3}O_{6.6} \cdot 1.1H_2O$
70.7	29.3	7.8	4.3	2.0	$NaAlSi_{2.15}O_{6.3} \cdot 1.0H_2O$
64.8	35.2	8.1	4.0	2.0	$NaAlSi_2O_6 \cdot 1.0H_2O$
59.8	40.2	8.1	3.8	1.9	$NaAlSi_{1.9}O_{5.8} \cdot 1.0H_2O$
57.0	43.0	7.9	3.7	1.8	$NaAlSi_{1.85}O_{5.7} \cdot .9H_2O$
54.7	45.3	8.0	3.6	1.8	$NaAlSi_{1.8}O_{5.6} \cdot .9H_2O$
49.2	50.8	7.9	3.4	1.7	$NaAlSi_{1.7}O_{5.4} \cdot .9H_2O$
43.5	56.5	7.3	3.2	1.5	$NaAlSi_{1.6}O_{5.2} \cdot .8H_2O$

TABLE XIIb H_2O-contents in nepheline-hydate I

Anhydous composition in Wt °/o		H_2O-contents in Wt °/o
Ab	Ne	
-1.0	101.0	6.2
-5.2	105.2	5.9
-9.3	109.3	5.9

TABLE XIIc H_2O-contents in zeolite species P.

Anhydrous composition in Wt °/o		H_2O-contents in Wt °/o
Ab	Ne	
112.3	-12.3	12.4
29.1	70.9	12.0
21.2	78.8	11.9
5.8	94.2	10.6

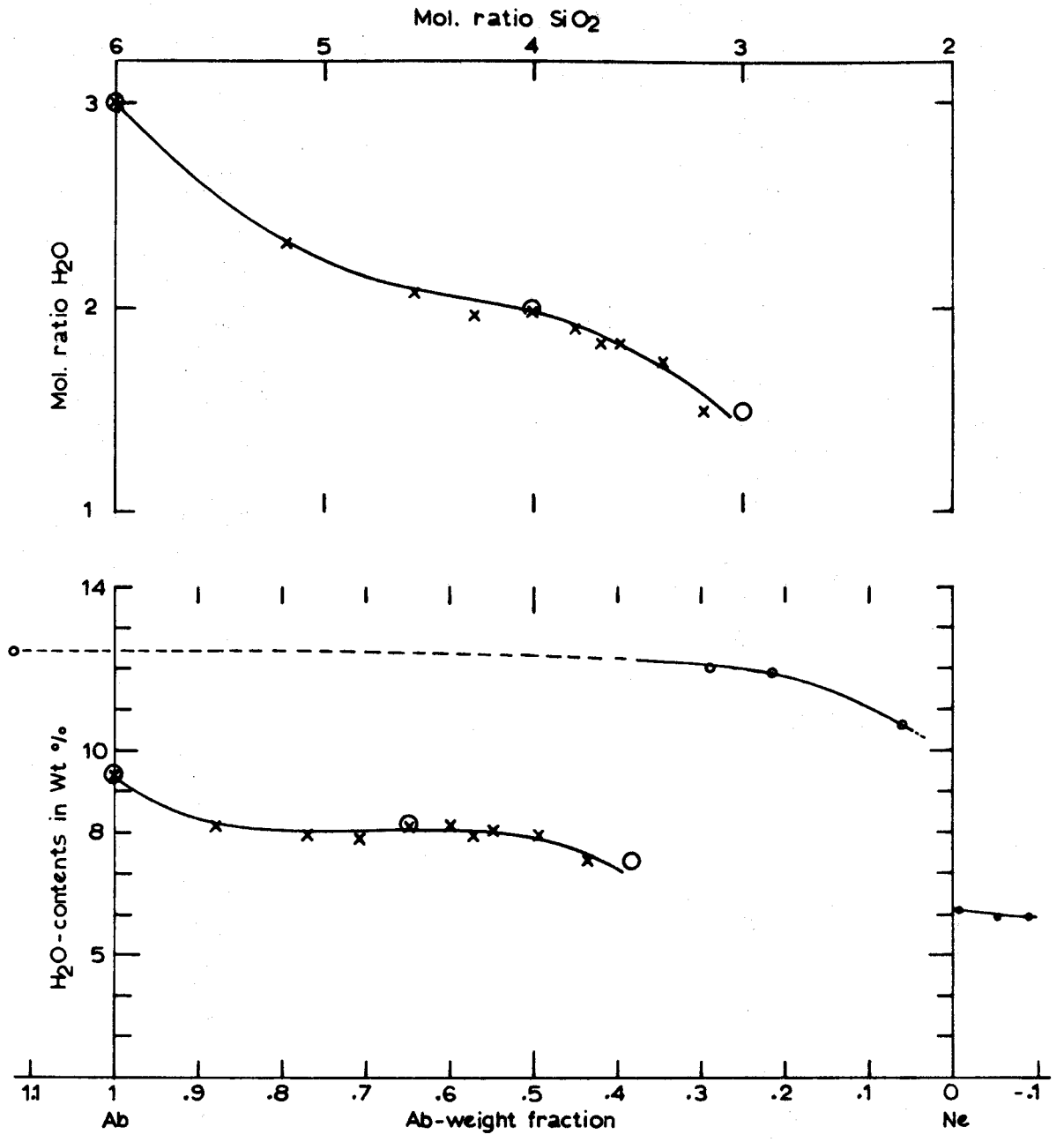

Fig.18. H_2O-contents in hydrous minerals, at various composition in the system Ab-Ne-H_2O.

Saha (1959) : H_2O-contents in analcite ..... O

Present work : H_2O-contents in { analcite x
nepheline-hydrate I .....•
zeolite species P .....o }

On the basis of the data presented in Table XIIa, b and c, it appears to the writer that the H_2O-contents in these hydrous minerals are generally proportional to their SiO_2-contents, in the system $NaAlO_2$-SiO_2-H_2O, and this may be related to their cell dimensions.

V. DISCUSSION AND SOME NOTES

1. The Accuracy of the Present Method

There are two main sources of error in the present method. One of these is caused by the hygroscopic properties of the powdered gels (starting materials). The other is due to the vesiculation in glasses quenched from high pressure runs.

1-1. Hygroscopic Properties of Powdered Gels

The hygroscopic properties of three gels were tested over a period of time. The compositions of the gels used and the results are given in Fig. 19. All the gels were nearly saturated with moisture after exposure for 10 days under the laboratory conditions (25°C, 1 atm.). The saturated moisture amounts in the gels, 1, 2 and 3, were 2.85, 4.43 and 5.30 in weight percents respectively. This indicates that the larger the content of K_2O-component, the larger the amount of moisture absorbed in a gel. More than half the amount of the total moisture was absorbed by a gel in a day; one fifth in 20 minutes.

Fig. 19. Hygroscopic properties of powdered gels in laboratory condition. Showing the amount of moisture in each of the gels as a function of time. The compositions of three gels used are given in below

Gel No.	Composition of dry gel (Wt %)		
	$KAlSiO_4$	$NaAlSiO_4$	SiO_2
1	-	94.2	5.8
2	20.4	73.2	6.4
3	33.5	60.1	6.4

$\longrightarrow$ ($Ab_{12.7}Ne_{87.3}$ in Wt. %)

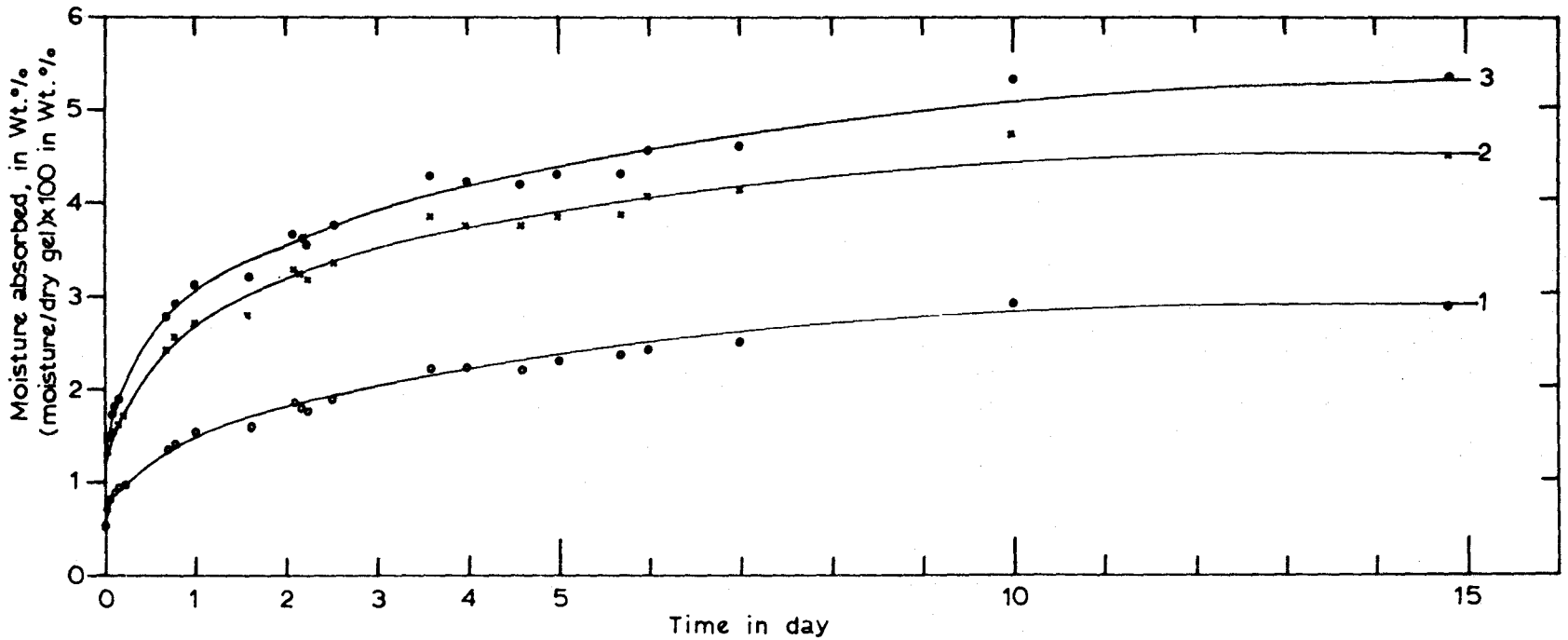

The absorbed moisture consists essentially of H_2O and a very small amount of CO_2. By heat treatment (110°C/overnight), the moisture contents in the gels were reduced down to about 1 Wt.%, and again by further heat-treatment of the gels (higher than 300°C/overnight), the moisture was nearly completely driven off from the gels.

Thus, it is advisable that the starting materials should be heat-treated at temperatures slightly above 300°C overnight before being used and kept under moisture-free conditions. Because the smaller the amount of moisture originally absorbed in a gel, the smaller the error range of the solubility values. When the powdered gel is completely free from moisture as a limiting case, then it is evident that the solubility value can be obtained directly from the weight difference between the total amount of water and the water remaining after saturating the melt, assuming no other source of error.

Note that there is, of course, an alternative method, i.e. to use a moisture-saturated gel as a starting material instead of moisture-free gel. The moisture-content in a gel is nearly unique if the gel is once saturated with respect to moisture (see Fig. 19). But the CO_2-content in the moisture can be sometimes a difficult problem to evaluate.

1-2. Origin of Water-Bubbles in the Quenched Glasses

Bowen & Tuttle (1950, p. 498) concluded that the vesicles in a quenched glass represent the water trapped initially in the powdered glass at the beginning of the run, or conversely in a powdered gel if that is used. Tuttle & Bowen (1958, p. 14) demonstrated experimentally that the water content of the final hydrous glass depends on the initial grain size of the starting glass powder. They used these experiments to confirm their earlier conclusion. Burnham & Jahns (1962, p. 730) also concluded that the vesiculation in a quenched glass is essentially due to the capture of water of external origin whether it was trapped invapour phase in the melt during quenching or initially trapped in the powdered glass. In the present study, however, it is interpreted that the vesiculation is essentially due to the segregation of dissolved water in the melt upon quenching. However, notice that the solubility values reported by Burnham & Jahns (1962) are larger than those given in this study and this is, presumably, because of their method of choosing the phase boundary between L+V and L.

If the water initially trapped in powdered glass is still preserved in the quenched glass after a run, and if a variation in the grain size of glass particles used initially influences the final water content, it seems unlikely that phase-equilibrium in such a run was attained.

Note that "initially trapped water" may include, in a broad sense, any water trapped in the starting material before equilibrium attained. If the H_2O-saturated melt is in equilibrium with the water vapor phase in a charge, then the water initially trapped in the starting powder is hardly expected to be preserved, and the grain size of glass particles should not influence the H_2O-content in a melt either. In other words, the situation in the charge (closed system) is controlled by the P-T conditions applied and not by the physical condition of starting material as long as equilibrium is attained.

The present experimental data (i.e. the absence of water-bubbles in quenched hydrous glasses at pressures below 5Kb; see Chapter IV, § 3) support the above reasoning. Thus it is concluded that the vesiculation in the quenched glasses studied is due to the segregation of some of the dissolved water in the melt and/or the inclusion of the water vapor phase in the melt upon quenching.

In the previous chapter (VI, § 3) it was shown that the water bubbles in quenched glasses at pressures above 5Kb were originated essentially by the exsolution of some of the dissolved water in the melts upon quenching.

Burnham & Jahns (1962, p. 729) reported in their solubility study that some aqueous bubbles nearly always are trapped and preserved within the charge, whether or not the melt becomes saturated. Let us study carefully their report. As concluded above, first of all, the water bubbles cannot be the initially trapped ones in the starting glass powder, as long as equilibrium attained. Accordingly, the vesiculation is either due to inclusion or exsolution upon quenching. According to their report, however, there exist water-bubbles even in the water-undersaturated melt (glass). Consequently, it is obvious that the water bubbles were formed by exsolution of the dissolved water in the melt during quenching. Thus, we may use their data as confirming evidence for the present conclusion.

It should be noted that the amount of starting powder used by Burnham & Jahns was 200-400mg which is 10 times greater than that of the present study. Accordingly, the chance that the water-bubbles are trapped and preserved in a hydrous glass upon quenching may be much greater than that of this study. It appears to the writer that the quantity used as starting materials may be (partly) responsible for which one predominates over the other.

2. Effect of Temperature and Composition on Solubility Values at Constant Pressure (P_{H_2O})—

In an isobaric T-X_{H_2O} section, the water-saturated liquidus boundary is very steep (i.e. nearly parallel to temperature axis) in most silicate systems. Therefore, the change of the water-solubility value in an H_2O-saturated melt is probably negligible within a small interval of temperature above the minimum temperature of complete melting of a solid phase or phases. Thus, the solubility value is not sensitive to temperature at a fixed P_{H_2O} and a fixed composition. This is one of the important properties of a silicate melt used in the determination of solubility value because most of the solubility determinations are made at temperatures slightly above those of the H_2O-saturated liquidus.

Yoder, Stewart & Smith (1957, p. 208) reported that the water-solubility of an albite melt is ~11 Wt.% at P_{H_2O} = 5Kb. Burnham & Jahns (1962, p. 744) reported that the water-solubility value at P_{H_2O} = 5Kb is 9.9 Wt.% in albite-melt and 11.2 Wt.% in Harding pegmatite-melt. The H_2O-content in the (Anl) univariant melt determined in this study is ~11 Wt.% P_{H_2O} = 5Kb. They are very different compositional melts, but they contain nearly the same amounts of dissolved water. In this study, it is demonstrated that the solubility values

in various compositional melts are very similar; $\sim 6 \pm 1$ Wt.% H_2O in the melts from $Ab_{90} \cdot Ne_{10}$ - $Ab_{40} \cdot Ab_{60}$ at P_{H_2O} = 2Kb; $\sim 11 \pm 1$ Wt.% H_2O in the melts from $Ab_{80} \cdot Ne_{20}$ - $Ab_{40} \cdot Ne_{60}$ composition at $P_{H_2O} \simeq 5$Kb (for details, see Figs. 13 and 14, and Table X). Thus it is concluded that the H_2O-solubility in a melt is not too sensitive to the variations in composition of the melt in the system Ab-Ne-H_2O.

In an isobaric T-X_{H_2O} section, the amount of excess water vapor phase in equilibrium with a liquid phase (melt) does not generally affect the solubility value either, except in cases of a very high pressure run.

Therefore, one can infer the approximate solubility values in silicate melts around a melt whose solubility value is known.

3. Relationship between the Univariant Melting Curve and the Solubility of Water in the Melt

It is well known that the depression of the melting point of anhydrous solids by water pressure is due to the solution of water in the melt (e.g. compare Fig. 16a and b).

Yoder (1958, p. 190) presented a P-T diagram showing various univariant liquidus curves (albite, nepheline, sanidine, quartz, anorthite and diopside) in his study of the effect of water on the melting of silicates. As shown in his diagram, the (univariant) temperature of the melting of each crystal phase falls drastically at low water pressure, but the slope ($dT_{univariant}/dP_{H_2O}$) of each liquidus P-T curve is nearly constant above about 2Kb. Such a common tendency of each univariant P-T curve seems to be related to a certain restricted capacity of the melt to dissolve water.

Therefore, it is likely that the slope of the solubility curve approaches some finite limiting value as P_{H_2O} increases, instead of a sudden change of curvature at about 6Kb as reported by Burnham & Jahns (1962)(see Fig. 17).

PART 3

THE SEQUENCE OF P-T CURVES AROUND A QUATERNARY INVARIANT POINT IN THE SYSTEM $NaAlSiO_4$-$KAlSiO_4$-SiO_2-H_2O.

THEORETICAL DISCUSSION

I. GENERAL STATEMENTS

This study was undertaken as a guide to the experimental determinations in the silica-undersaturated region of the system $NaAlSiO_4$-$KAlSiO_4$-SiO_2-H_2O. The sequence of P-T curves has been theoretically deduced on the basis of experimentally known data, using Schreinemakers' method.

It is necessary to know the compositions of the six invariant phases, in order to construct an invariant chemogram. The most probable invariant chemogram was constructed using estimated compositions of the invariant phases and the P-T diagram type was then deduced using the method of Schreinemakers'.

By allowing the compositions of the invariant phases to move within reasonable ranges on the basis of available data reported by various authors, eighteen possible P-T diagram types were deduced.

Finally, the most probable four of the eighteen possible P-T diagram types are proposed.

II. THE SEQUENCE OF P-T CURVES AROUND THE INVARIANT POINT

Morse (1969a) determined a liquidus diagram and several isobaric-isothermal sections at P_{H_2O} = 5Kb in the silica-undersaturated region of the system $NaAlSiO_4$-$KAlSiO_4$-SiO_2-H_2O. He estimated the invariant point to be located at some pressure not far below 5Kb and at a temperature not far above 635°C.

At the supposed invariant point (approximately 5^-Kb and 635^+°C), the compositions of the six invariant phases, albite, orthoclase, nepheline, analcite, liquid and water-vapor, are reasonably estimated by the writer to be shown as in Table XIII, largely on the basis of Morse's data (1969a, p. 116-118; 1969b, p. 121). Assuming these phase-compositions to be approximately correct (at least their topological relation is acceptable), an invariant chemogram was constructed in a regular tetrahedron defined by the four components, $NaAlSiO_4$, $KAlSiO_4$, SiO_2 and H_2O. As shown in Fig. 20, the chemogram is a monoconcave octahedron, according to the definition made by Schreinemakers (1916, p. 824). It can be also defined as a "hexahedron" with one interior phase point, in a similar fashion as Zen (1966, p. 24) described a monoconcave pentagon as "Four phase compositions define a quadrilateral and the fifth composition point is inside the quadrilateral".

TABLE XIII. THE COMPOSITIONS OF THE INVARIANT PHASES AT A QUATERNARY INVARIANT POINT (5^{-}Kb and 635^{+o}C) IN THE SYSTEM $NaAlSiO_4$-$KAlSiO_4$-SiO_2-H_2O, APPROXIMATELY ESTIMATED FROM THE DATA OF MORSE (1969a, p. 116-118; 1969b, P. 121).

Equilibrium phases	Composition Wt. %	
	Anhydrous Composition	H_2O-Content
Ab(Albite s. s.)	$Ne_{50}.Ks_5.Qz_{45}$	-
Or(Orthoclase s. s.)	$Ne_{17}.Ks_{39}.Qz_{44}$	-
Ne(Nepheline s. s.)	$Ne_{83}Ks_{13}Qz_4$	-
Anl(Analcite s. s.)	$Ne_{67}Ks_3Qz_{30}$	8
L(Liquid)	$Ne_{53}Ks_{19}Qz_{28}$	11*
V(Vapor)	Dissolved solid 5%**	95

* The H_2O-solubility in the melt is estimated from the present data (Fig. 16a in Part 2) on the theoretical basis given in Chap. V, §2 (Part 2).

** The dissolved solid in the ternary invariant vapor phase in the system Ab-Ne-H_2O reported by Peters, Luth & Tuttle (1966, p. 741) is used.

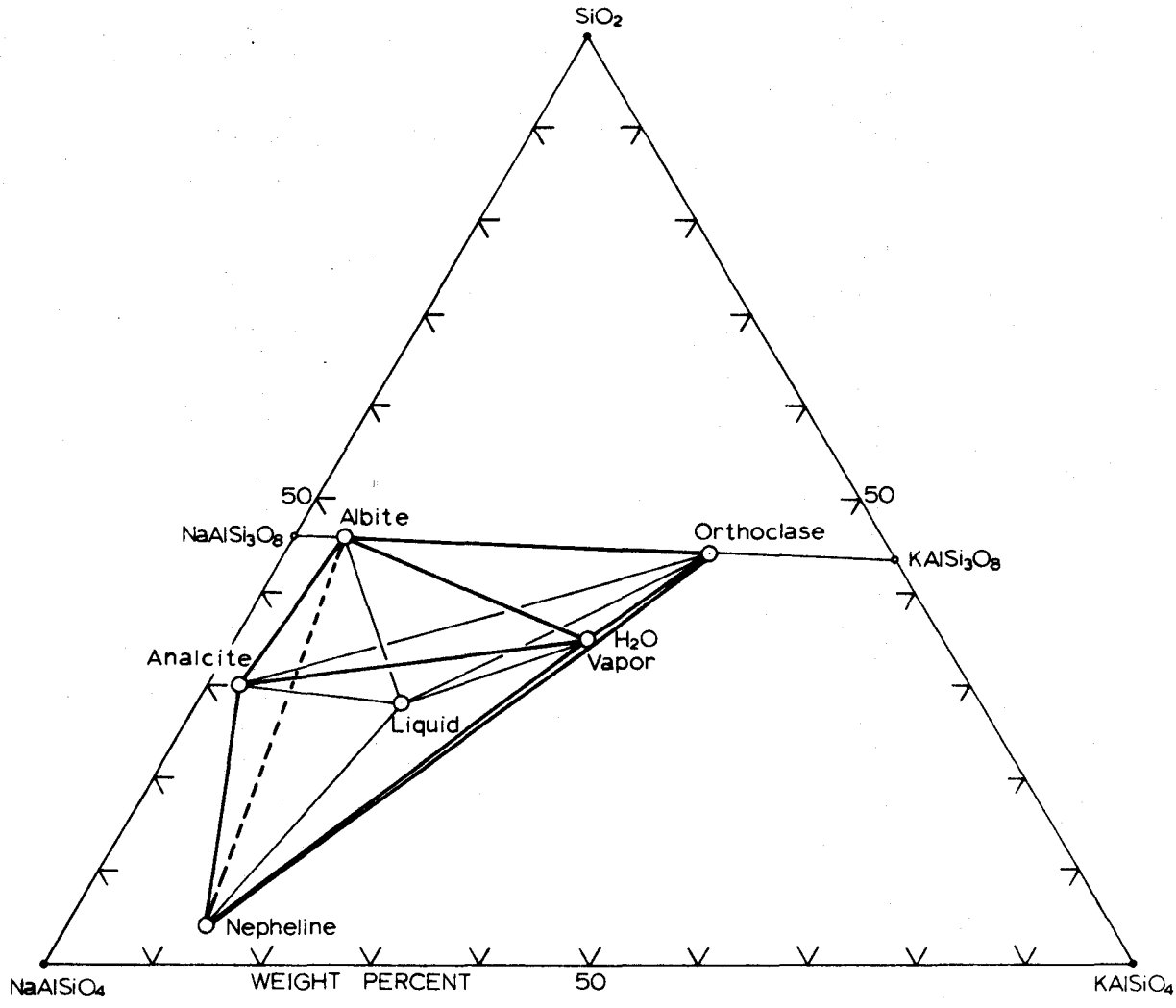

FIG.20. A QUATERNARY INVARIANT CHEMOGRAM IN THE SYSTEM $NaAlSiO_4$-$KAlSiO_4$-SiO_2-H_2O. The compositions of the invariant phases are those most probably assumed on the basis of data reported by Morse(1969a&b). H_2O is towards the reader. The chemogram is a monoconcave octahedron(or a hexahedron with an interior phase).

Since there is no compositional degeneracy in the chemogram, the six univariant reactions must be unique as presented below

(L) : Anl+Or = Ab+Ne+V

(Anl) : Ab+Or+Ne+V = L

(V) : Anl+Or = Ab+Ne+L

(Ab) : Anl+Or+Ne+V = L

(Or) : Ab+Ne+V = Anl+L

(Ne) : Anl+Or+V = Ab+L

where the phase in parentheses is the missing phase in the univariant reaction.

The sequence of P-T curves in the immediate vicinity of the invariant point was deduced using Schreinemakers' method (1916, p. 824) on the basis of these univariant reactions.

By using Morse's experimental data, the following relations of the P-T curves were deduced.

i) Two univariant curves (Ab) and (Ne) are situated between 600°C and 640°C at 5Kb.

ii) A univariant curve (L) extends towards the region of lower temperature and lower pressure from the invariant point.

iii) Two univariant curves (Anl) and (Or) exist at the higher temperature side from the invariant point.

Then the P-T curves were reasonably rearranged on a P-T projection so as to agree with the data deduced above. As shown in Fig. 21, the P-T diagram type consists of one one-curvical bundle (only one (L) univariant curve), one two-curvical bundle (two univariant curves (Or) and (Anl)) and one three-curvical bundle (three curves (Ab), (Ne) and (V)).

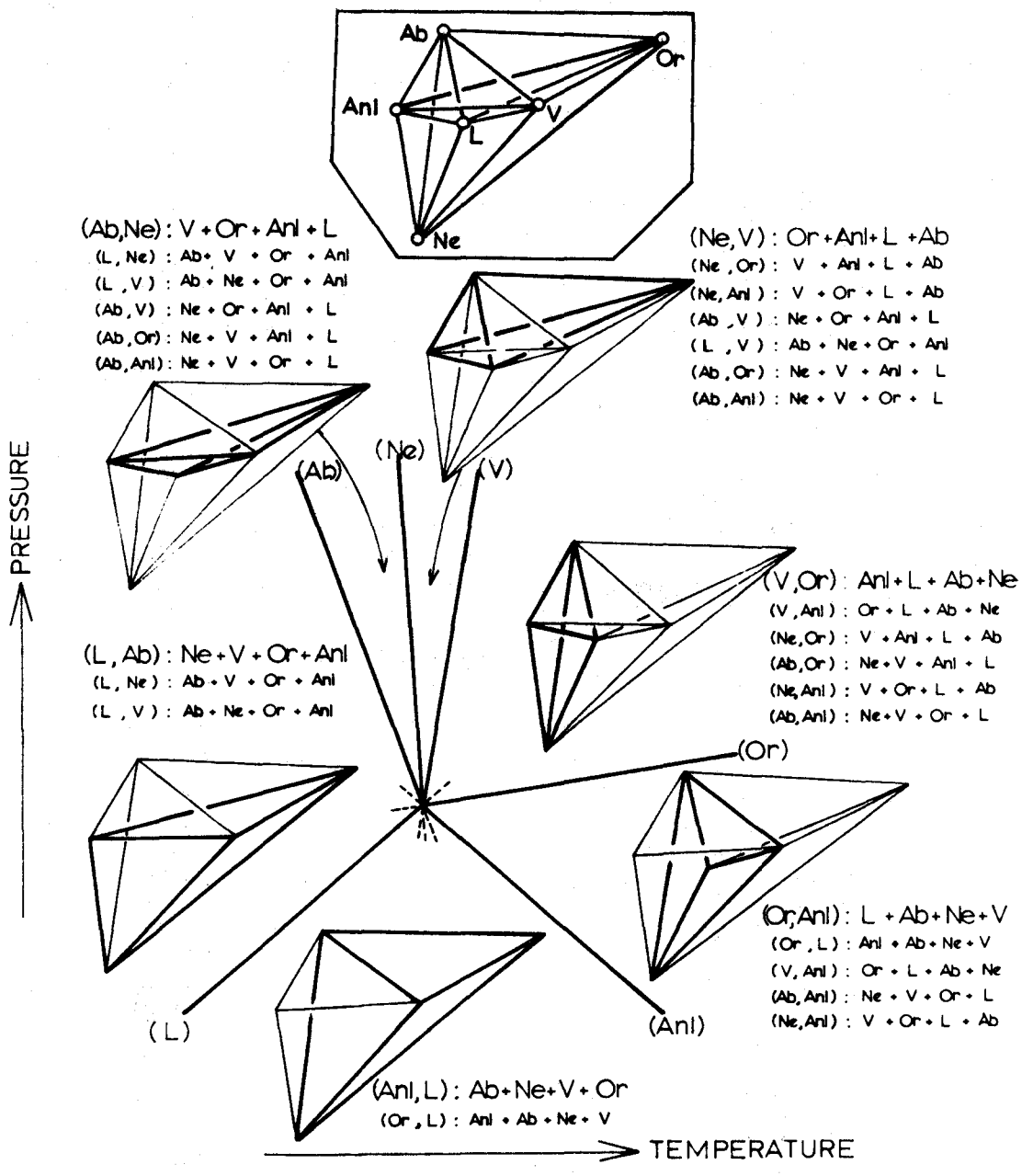

FIG.21. THE SEQUENCE OF P-T CURVES AROUND THE INVARIANT POINT(5 Kb & 635°C) IN THE SYSTEM $NaAlSiO_4$-$KAlSiO_4$-SiO_2-H_2O.

The sequence is deduced on the basis of the invariant chemogram shown in Fig. 20. Tie-tetrahedra represent divariant phase-assemblages in the immediate vicinity of the supposed invariant point.
The tetrahedron drawn with thick solid lines is a representative divariant phase-assemblage among several divariant ones given in the diagram

III. EIGHTEEN POSSIBLE P-T DIAGRAM TYPES

In the previous section, the sequence of P-T curves around an invariant point was deduced on the basis of a reasonably assumed chemogram. Now the available data are reviewed further.

According to Morse's liquidus diagram (1969a, p. 116) the temperature minimum of melting in the ternary system without potash component is located at about the composition $NaAlSi_2O_6$. The peritectic boundary curve is situated in the albite field instead of in the nepheline field. In the ternary system $NaAlSi_3O_8$-$NaAlSiO_4$-H_2O, however, invariant analcite and the liquid compositions are much richer in the nepheline-component (Peters, Luth and Tuttle, 1966, p. 741; the writer, Part 1, Table V) than those of Morse. The peritectic point is located in the nepheline-stability field, on the contrary to that of Morse. The compositional trend of liquidus analcites during progressive differentiation of the Square Top intrusive rocks (Wilkinson, 1965, p. 438, Fig. 5) is in good agreement with the experimental results in the system $NaAlSi_3O_8$-$NaAlSiO_4$-H_2O.

Thus, it is probable that the true analcite composition at the quaternary invariant point is expected to be richer in the nepheline-component than that estimated on the basis of Morse's results. The invariant albite and K-feldspar may also be slightly richer.

in the two components $NaAlSiO_4$ and $KAlSiO_4$ instead of being on the $NaAlSi_3O_8$ -$KAlSi_3O_8$ join (see Fig. 11 in Part 1) and so on.

In order to approach the real invariant chemogram (at least topologically the same one,) it is necessary to move some or all of the six invariant phases within reasonably restricted compositional regions in the four component space. For the sake of simplicity, we may move only the analcite phase point within a somewhat enlarged area instead of moving all the phase points.

For this operation, the compositional area of the invariant analcite is allowed to vary as described below.

a) The analcite of various compositions is assumed to contain 8 weight percent H_2O. In Fig. 22, therefore, the plane defined by points a, b, c and 1 is an isohydrous plane on which analcite points are allowed to lie.

b) The analcite-phase point is restricted to lie in a hexagon defined by six points d, e, 12, f, g, and 1 (stippled area).

Since the possibility of the analcite being located on either of the two edges d-e and f-g of the hexagon is very small, the two edges are excluded from the present consideration. Inother words, the hexagon is an open set with respect to these two edges, but closed with respect to the other four edges. The two edges (d-e and f-g) are both closed sets. This elimination is apparently meaningless. By this, however, it is possible to reduce the compositional area of the analcite to an extremely

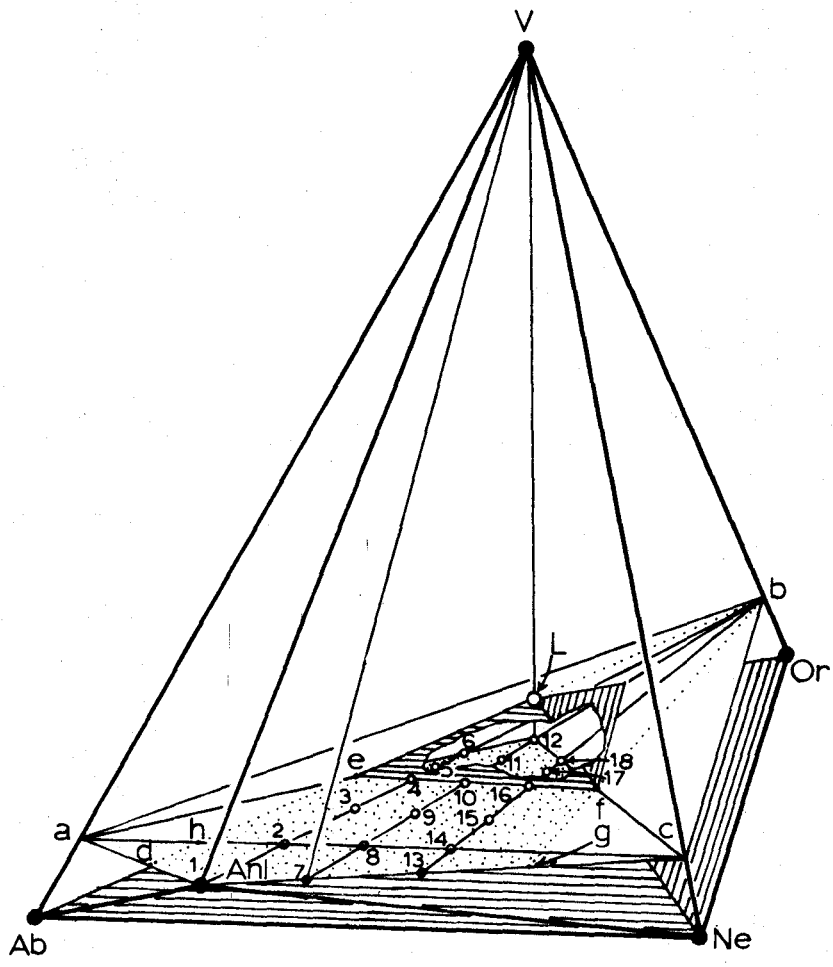

FIG.22 EIGHTEEN DISTINCT CHEMOGRAPHIC RELATIONS OF INVARIANT PHASES.

When the composition point of analcite is allowed to move in a hexagon(stippled area) defined by six points d,e,12,f,g, &1, an infinite number of invariant chemograms are produced, but they are topologically classified into eighteen distinct chemogram types. Each of the eighteen analcite points denoted by small circles with numbers is responsible for a distinct type of chemograms. Note that the quadrilateral defined by four points, a,b,c & 1 is an isohydrous plane (8 Wt % H_2O) on which the hexagon lies, and t he hexagon is an open set with respect to two edges d-e & f-g.

narrow zone (area) along a line defined by two points 7 and 12 without losing any possible number of invariant chemogram types.

There are, of course, an infinitive number of analcite points in the hexagonal area (stippled area). But only 18 phase points of analcites represent distinct invariant chemogram types. Accordingly, there are 18 possible P-T diagram types. For example, any arbitrary analcite point (e.g. No. 3) which belongs to an open quadrilateral defined by four points, h, 8, 10 and e, produces uniquely one and only one invariant chemogram type, as long as the respective position of the six invariant phase-points is concerned. Likewise, any analcite point (e.g. No. 4) on an open line-segment defined by two points, e and 10, also defines one and only one invariant chemogram type. In this way, 18 distinct analcite phase-points were deduced and are presented as small open circles accompanied with numbers in Fig. 22.

There are two most critical planes with respect to the position of the analcite composition; one of them is the plane defined by the three phase points Or, V and L, and the other one is the one defined by Ab, Ne and V.

With respect to the former reference plane Or-V-L, the eighteen possible chemogram types are grouped into three principal categories. The six analcite points from number 7 to 12 are located

on the reference plane. Accordingly, any invariant chemogram which has an analcite with such a composition must be degenerate due to the compositional coplanarity of the four phases, Or, Anl, L and V. These types may be called a "degenerate group". The six analcite points from number 1 to 6 are located in the albite-rich region, and constitute an albite-rich group. The remaining six analcite points from number 13 to 18 are located in the nepheline-rich region, and form a nepheline-rich group.

Depending on the composition of analcite relative to the latter reference plane Ab-Ne-V, the eighteen chemograms are also grouped into three principal shapes, monoconcave octahedron (points 1, 7 and13 in Fig. 22), monoconcave hexahedron (points 2, 8 and14), and biconcave octahedron (the remaining twelve analcite points).

However, the former reference plane (Or-V-L) is more convenient than the latter, for the diagrammatic summarization of the eighteen possible P-T diagram types by three groups as shown in Fig. 23. In each of three P-T diagrams in Fig. 23, the five P-T curves (Anl), (L), (Ab), (Ne) and (V) are fixed and the remaining one (Or) is variable. The relative position of the (Or) univariant P-T curve is defined in the P-T diagram by the position of the analcite phase

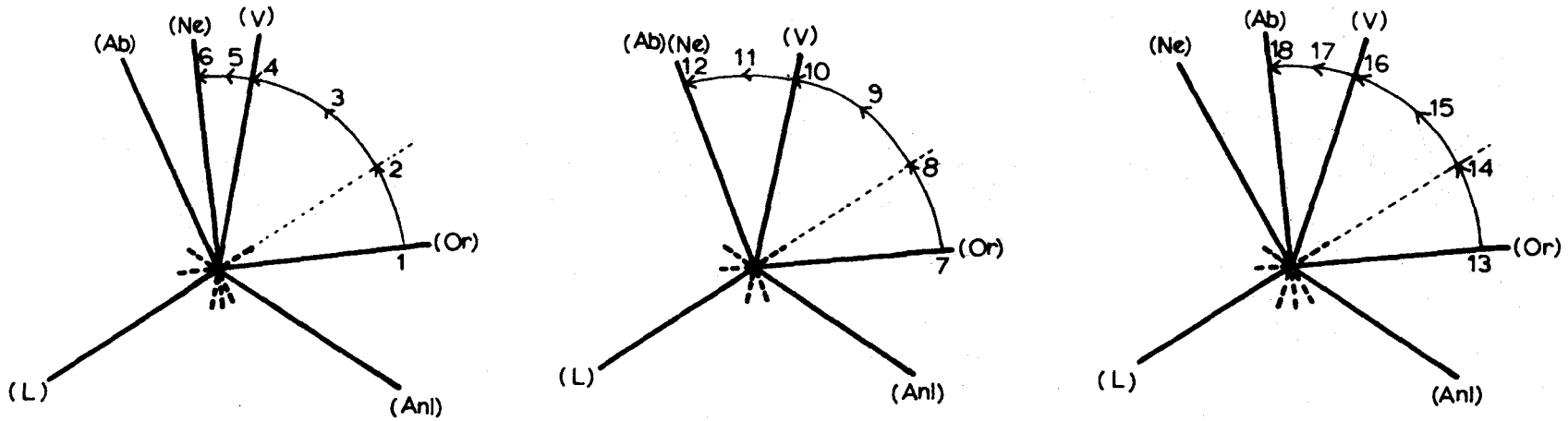

FIG.23 THREE PRINCIPAL GROUPS OF P-T DIAGRAM TYPES.

The 18 possible P-T diagram types are diagramatically summarized by three principal groups, each of which contains 6 distinct P-T diagram types. In each diagram, the relative positions of (Anl), (L), (Ab), (Ne) & (V) are fixed, and the remaining P-T curve(the (Or)univariant) is variable in its position. The position in the P-T diagram is defined by the relative position of analcite in the chemogram(See FIG.22).

in the invariant chemogram. A few examples suffice to explain it. In Fig. 23a, the P-T diagram with the (Or) univariant curve at a position 1 is formed by an invariant chemogram which has its analcite composition at a point 1, in Fig. 22. The P-T diagram with the (Or) curve at a position 2 is produced by an invariant chemogram with its analcite composition at a point 2, and so on.

Six of the eighteen possible invariant chemograms are non-degenerate systems. Consequently, each of the corresponding P-T diagrams consists of six distinct P-T curves. The chemograms which have the analcite positions of odd numbers (1, 3, 5, 13, 15 & 17) belong to this category. The remaining twelve invariant chemograms are degenerate systems.

Accordingly, at least two univariant curves of each P-T diagram are either coincident to each other or one of them corresponds to the metastable prolongation of the other.

1. Albite-rich Group:

Six analcite positions (1, 2, 3, 4, 5 & 6) located in the albite-rich zone from the reference plane Or-V-L (Fig. 22) belong to this group. An invariant chemogram which has each of these analcites derives a distinct P-T diagram type. If the position of analcite composition is moved from 1 to 6 through the positions 2, 3, 4 and 5, then six

P-T diagrams which are distinct from one another with respect to the position of the (Or) univariant curve will be derived successively, shown as arrow marks in Fig. 23a.

2. Degenerate Group:

The six possible analcite positions (7, 8, 9, 10, 11 and 12) are located on the reference plane Or-L-V in the chemogram (Fig. 22). Therefore, each of the six chemograms has at least a compositional coplanarity of four phases, Anl, Or, L and V. Accordingly, in each of the P-T diagrams which belong to this group, it is prerequisite that the (Ab) univariant curve is coincident to the (Ne) one (Fig. 23b). The chemogram having the position of analcite at 12 has the highest degree of compositional degeneracy; one colinearity (Anl, L and V) and three coplanarities (Ab, Anl, L&V; Ne, Anl, L&V; Or, Anl, L&V). In this case, the three unvariant curves, (Ab), (Ne) and (Or), coincide with one another.

3. Nepheline-rich Group:

The remaining six analcite points (13-18) are located in the nepheline-richer zone relative to the reference plane Or-L-V. The sequences of P-T curves characterized by such chemograms is determined by the analcite position from 13 to 18 (see Figs. 22 and 23C).

In this way, the eighteen possible P-T diagram types are summarized by three principal groups.

IV. THE MOST PROBABLE FOUR P-T DIAGRAM TYPES

The six non-degenerate P-T diagram types are the most probable ones among the eighteen possible types, because the remaining twelve degenerate types are very special cases.

According to present knowledge, it is not to be expected that the invariant analcite contains large amounts of $KAlSiO_4$-component in solid solution (for the details, see Chapter V in Part 1). The four invariant chemograms which have the analcite positions at 1, 3, 13, and 15 respectively are therefore most probable.

Thus it is concluded that one of the most probable four P-T diagram types[1] shown in Fig. 24 is expected to be the real one.

---

1. Note that the invariant chemogram which has an analcite position at 1 and its corresponding P-T diagram type given in Fig. 24a correspond to those deduced on the basis of invariant phases estimated from data reported by Morse (1969a & b).

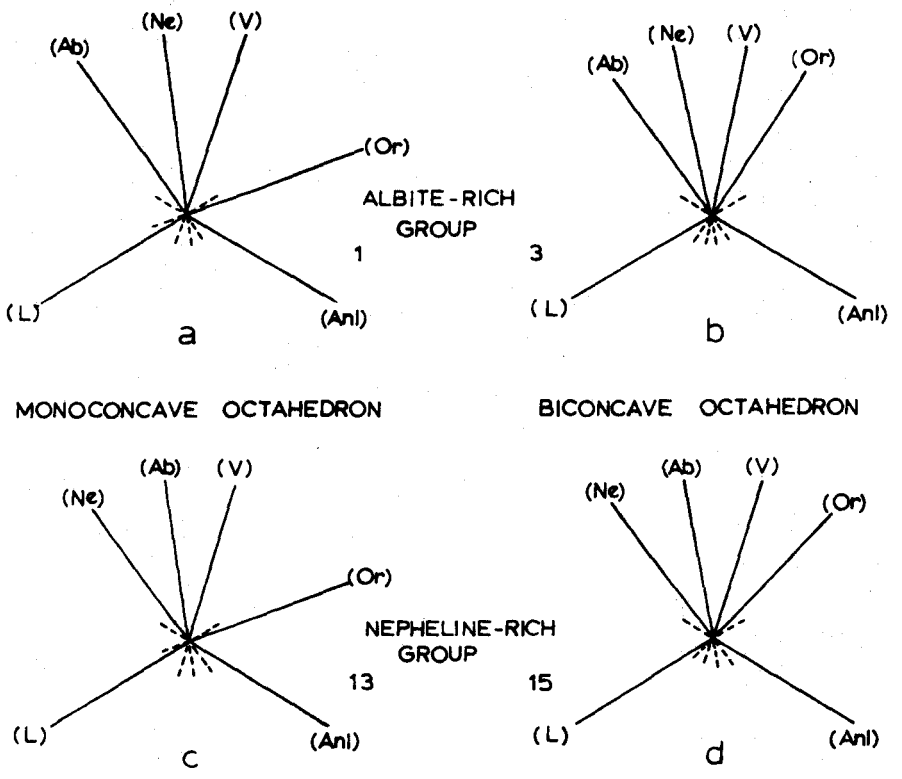

FIG. 24

THE MOST PROBABLE FOUR P-T DIAGRAM TYPES.

The upper two P-T diagram types, a & b, belong to the albite-rich group, and the lower two, c & d, belong to the nepheline-rich group. a,b,c & d were deduced on the basis of the possible invariant chemogram types which have analcite compositions 1,3,13 & 15(in Fig.22) respectively. The invariant chemogram types of a & c are monoconcave octahedrons(or hexahedrons with an interior phase-point), and the ones of b & d are both biconcave octahedrons(or tetrahedrons with two interior phase-points).

PART 4

PHASE EQUILIBRIA IN THE SYSTEM $NaAlSi_3O_8$-$NaAlSiO_4$-H_2O UP TO 15Kb.

THEORETICAL DISCUSSION

I. GENERAL STATEMENT

For a theoretical study of phase relations in a P-T projection, it is essential to configurate invariant phase relations. To do so, it is necessary to know at least the approximate chemical compositions of invariant phases.

A great deal of experimental data for phase equilibria in the system $NaAlSiO_4$-SiO_2-H_2O and its subsystems has been accumulated. However, the compositions of equilibrium phases at various P-T conditions have been mostly assumed to be stoichiometric.

In Part 1 of the thesis, the compositions of the univariant phases were determined or estimated including H_2O-contents in hydrous phases (see Part 2) up to 10Kb water pressure. It is further possible to predict the trend of compositional changes for each univariant phase above 10Kb. The purpose of the present study is to examine the phase relations above 10Kb reported by various authors, using the compositional data of phases obtained from Parts 1 and 2 with the aid of Schreinemakers' rule.

In this study, six invariant points are discussed. Two of them are newly predicted; the other four which are well known invariant points, are partly modified. The four invariant points, I_5, I_3, I_6 & I_7 termed by Boettcher and Wyllie (1969), are denoted by B & W I_5, B & W I_3, B & W I_6 and B & W I_7 which correspond to I_1, I_2, I_3 and I_4 respectively in this study.

II. INVARIANT EQUILBRIA

The invariant chemograms at the invariant points I_1, I_2, I_3, I_4, I_5 and I_6 are schematically constructed on the basis of the compositional data of the invariant phases given in Table XIV (see the second column "b" in Fig. 25). These compositions are approximately obtained through graphical extrapolation from the data presented in Figs. 7 and 9a (in Part 1) and Fig. 16a (in Part 2). In order to clarify the invariant phase relations, an idealized isobaric T-X phase diagram (projection) is given at each invariant pressure (Fig. 25a). The invariant phase relations are emphasized by drawing with thick solid line (or lines) on these diagrams.

The five univariant reaction equations and the sequence of P-T curves at each invariant point are also presented in the same diagram (Fig. 25c and d).

1. Invariant Equilibrium I_1

This point has been experimentally determined at 5.15±0.25 Kb and 657±5°C (see Fig. 5 and Table V in Part 1, for details), and five P-T curves (L), (Ne), (Ab), (V) and (Anl) radiate from the point.

Four of the univariant P-T curves (V), (Ne), (Ab) and (L) meet other P-T curve in a point and then generate four invariant points I_2, I_3, I_4 and I_6, respectively.

2. Invariant Equilibrium I_2

The (V) univariant P-T curve (from I_1) for the reaction Anl = Ab+Ne+L is based on the water-deficient part of the system $NaAlSi_3O_8$-$NaAlSiO_4$-H_2O (see Fig. 6(2) in Part 1). As pressure increases, the (V) curve extends toward the stability region of jadeite phase. This curve meets another univariant curve for the reaction Ab+Ne = Jd in a P-T point (about 11Kb and 650°C). At the P-T point, jadeite begins to appear as a stable phase in the (V) univariant chemographic region. Consequently, the univariant equilibrium becomes an invariant equilibrium as shown in Fig. 25(2), from which five univariant curves, (L), (Ne), (Ab), (Anl) and (Jd) radiate. Note that the invariant liquid phase is undersaturated with respect to H_2O.

The invariant point I_2 was approximately determined at about 11Kb and 615°C by Robertson, Birch and MacDonald (1957, p. 126) in their study of jadeite stability up to 25Kb. Boettcher & Wyllie (1969, p. 895-7) deduced the sequence of the five P-T curves around the point I_2 on the basis of available data. According to their experimental

TABLE XIV. ASSUMED COMPOSITION OF PHASES AT EACH OF FIVE INVARIANT POINTS

The compositions were obtained by extrapolation of the compositional data of univariant phases determined below P_{H_2O} = 10 Kb (see Figs. 7 and 9a in Part 1 and Fig. 16a in Part 2). The compositions of invariant phases at I_1 are given in Table V in Part 1.

Invariant Phase	I_2			I_3			I_4			I_5			I_6		
	Anhydrous		H_2O	Anhydrous		H_2O	Anhydrous		H_2O	Anhydrous		H_2O	Anhydrous		H_2O
	Ab	Ne	Content	Ab	Ne	Content	Ab	Ne	Content	Ab	Ne	Content	Ab	Ne	Content
Liquid	43	57	11	55	45	15	37	63	15	-	-	-	-	-	-
Jadeite	65	35	-	65	35	-	65	35	-	65	35	-	-	-	-
Nepheline	10	90	-	-	-	-	13	87	-	0	100	-	2	98	-
Albite	99	1	-	96	4	-	-	-	-	-	-	-	100	0	-
Analcite	43	57	8	48	52	8	40	60	8	45	55	8	50	50	8
Nepheline hydrate I	-	-	-	-	-	-	-	-	-	5	95	6	10	90	6
Vapor	-	-	-	5-10?		95-90?	5-10?		95-90?	5-10?		95-90?	2?		98?

Note that the composition of jadeite is assumed to be ideal stoichiometric ($NaAlSi_2O_6$).
The compositions given are in Wt. %.

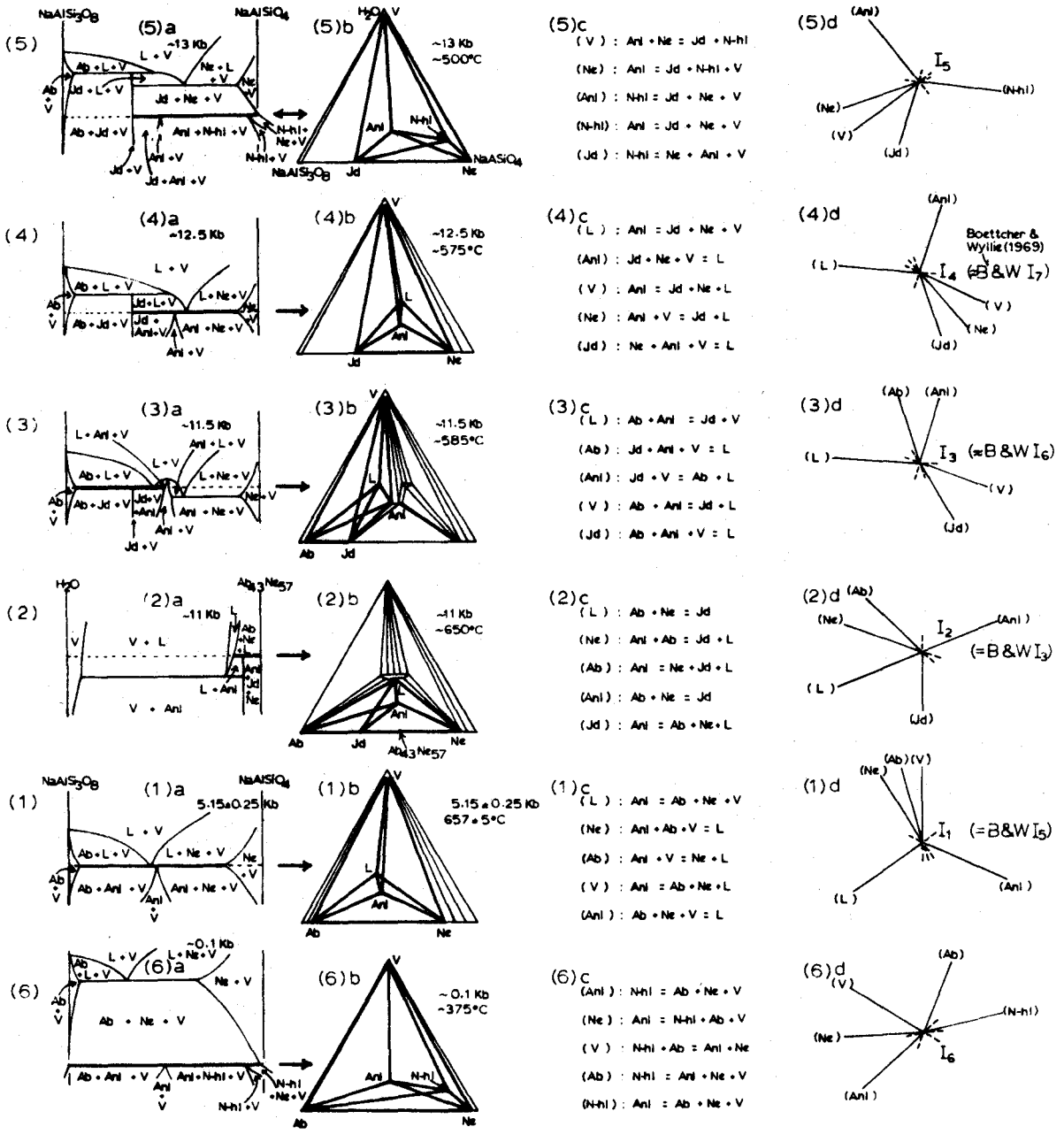

FIG. 25 **INVARIANT PHASE-RELATION AND THE SEQUENCE OF P-T CURVES AROUND EACH OF SIX INVARIANT POINTS, IN THE SYSTEM $NaAlSi_3O_8$-$NaAlSiO_4$-H_2O.**

The invariant chemograms were constructed on the basis of approximately estimated or inferred compositions of invariant phases (see Table XIV). Thick solid line (or lines) denotes an invariant phase relation. Ab=Albite, Ne = Nepheline, Jd = Jadeite, N-h I = nepheline hydrate I, L = Liquid & V = Vapor.

data (1969, p. 1004, Run No. 420), the invariant temperature is expected higher than 620°C at 11Kb.

The inspection of Fig. 5 in Part 1 (see the slope of (V)-curve) indicates that I_2 may be located at about 650°C and 11Kb. The sequence of P-T curves around I_2 deduced in this study is the same as that of Boettcher & Wyllie (1969; B & W I_3).

3. Invariant Equilibrium I_3

The invariant equilibrium I_3 is chemographically related to that of the (Ne) univariant P-T curve radiating from an invariant point I_1 (see Fig. 6(8) in Part 1). As shown in Fig. 6(8), there is a zone of two-phase (analcite and albite) tie lines across a region between the point of jadeite composition and the (Ne) univariant chemogram of I_1. This two-phase tie zone is not broken even in the jadeite stability field until the (Ne) curve meets another P-T curve for the reaction Ab+Anl = Jd+L in a point I_3. At a pressure slightly above this point the tie-line between Ab and Anl is broken and a new tie line forms simultaneously between two phases, jadeite and vapor. Hence, the invariant equilibrium I_3 is generated at the intersecting point (around 580°C and 11.5Kb), where five phases Jd, L, Ab, Anl and V occur.

On the basis of such consideration combined with the data of the expected compositions of the I_3 invariant phases, the invariant chemogram I_3 was constructed as shown in Fig. 25(3)b. From the invariant chemogram, the five equations of univariant reactions and the sequence of the P-T curves were deduced, and are also shown in the same diagram.

Boettcher and Wyllie (1969, p. 895, Fig. 7) estimated the P-T curve for the reaction Ab+Anl = Jd + V, which radiates from the invariant point I_3 (580°C/11.5Kb). Griggs, Fyfe and Kennedy (1955, p. 1569) reported that the jadeite-analcite boundary extends from the triple point[1] at about 600°C and 12Kb, to about 300°C and 18Kb, and its equilibrium was checked by forming jadeite from analcite and forming analcite from jadeite + water. Fyfe & Valpy (1959, p. 318) calculated the jadeite-analcite boundary using thermochemical data available. According to their calculations, the boundary for the reaction analcite = jadeite + H_2O is located approximately at about 600°C/11Kb, 200°C/10Kb and 25°C/7Kb. They also represented an approximately corrected boundary from the data of Robertson, Birch and MacDonald (1957). These previous works may be interpreted as the studies on a ternary univariant P-T curve for the reaction: Ab+Anl = Jd+V, because the equilibrium composition of the analcite (anhydrous) should not be the same as that of the jadeite. However, it was probably unknown at the time of the studies.

---

[1] The point must be a quintuple point instead of a triple point, because the point I_3 is a ternary invariant point.

The present I_3 corresponds to B & W I_6 (Boettcher & Wyllie, 1969). The sequence of P-T curves around I_3 deduced in this study agrees with those around B & W I_6. But the reaction equations of two univariant curves, (Jd) and (Ab) (see Fig. 25-(3)c and d) are different from those of Boettcher and Wyllie (1969, p. 892) respectively.

4. Invariant Equilibrium I_4

When two (Ab) univariant P-T curves emanating respectively from I_1 and I_2 intersect in a point, an invariant equilibrium takes place at the P-T point (I_4). In other words, the two univariant reactions occur simultaneously at the point I_4. It is prerequisite, therefore, that the analcite should have a unique single composition and no range of solid solution. Such phase relations are sketched in an isobaric T-X projection (see Fig. 25-(4)a).

As shown in the diagram, the thermal divide related to the analcite stability peak does not exist any more at this pressure. Note that the invariant pressure (12.5Kb) is an upper limit for analcite to crystallize directly from a melt.

I_4 is equal to B & W I_7. This invariant point was inferred (but not determined) by Boettcher and Wyllie (1969, p. 894). According to their diagram (Fig. 7, p. 895), the point is approximately located at about 12.5Kb and 575°C. The sequence of the P-T curves around I_4

and the equations of five univariant reactions (see Fig. 25(4)c and d) deduced in this study are the same as those reported by Boettcher & Wyllie.

5. Invariant Point I_5

When the univariant P-T curve for the reaction N-h I = Anl+Ne+V intersects another (L) univariant curve radiating from I_4 in a point, an invariant equilbrium takes place as long as the nepheline hydrate I is a stable phase (see Fig. 25-(5)a and b).

The invariant point[1] I_5 is inferred to be located at about 13Kb/500°C where five phases, Jd, Ne, Anl, N-h I and V coexist (for details, see Fig. 25-(5)a, b, c and d). It is newly predicted to exist in this study but its existence does essentially depend on the stability of nepheline hydrate I in the P-T region around the supposed invariant point I_5.

6. Invariant Equilibrium I_6

Another invariant equilibrium I_6 may be expected to occur at about 0.1±0.05Kb and 375°C (or slightly less than 375°C) by intersecting two univariant P-T curves for thereactions N-h I = Anl+Ne+V and Anl = Ab+Ne+V. The former is the (Jd) univariant P-T curve extended from I_5 towards very low P-T region, and the latter is the (L) univariant curve extended from I_1 toward low P-T region.

1. The position of invariant point I_5 essentially depends on two univariant curves, Anl-Jd+Ne+V& N-h I= Anl + Ne + V.

The two P-T curves probably intersect in a point. But it may be difficult to determine the point experimentally.

If and only if they intersect in a point on the P-T projection, then the invariant equilibrium will occur involving five reaction phases, N-h I, Anl, Ab, Ne and V. The T-X phase diagram, the chemogram, its five univariant equilibria and the sequence of P-T curves are presented in Fig. 25(6)a, b, c and d).

III. PHASE RELATIONS UP TO 15Kb

P-T diagrams around the six invariant points were used to make a schematic composite P-T diagram (see Fig. 26).

The (V) univariant P-T curve of I_1 and the (Jd) curve of I_2 have the same equation of univariant reaction, i.e. Anl+Ab+Ne=L, which are denoted by $I_1(V) = (Jd)I_2$ for the reaction Anl+Ab+Ne=L. Accordingly, they compose a single P-T curve between I_1 and I_2. Similarly, several other pairs of P-T curves are related to each other in such a way as follows:

$I_1(Ne) = (Jd)I_3$	for Anl+Ab+V=L
$I_1(Ab) = (Jd)I_4$	through S_1
$I_1(L) = (N\text{-h }I)I_6$	for Anl = Ab+Ne+V
$I_2(Ne) = (V)I_3$	for Anl+Ab = Nd+L
$I_2(Ab) = (V)I_4$	for Anl = Jd+Ne+L
$I_3(Ab) = (Ne)I_4$	through S_4
$I_4(L) = (N\text{-h }I)I_5$	for Anl = Jd+Ne+V
$I_5(Jd) = (Ab)I_6$	through S_2 and S_3

The invariant points as well as the P-T curves were re-arranged, as shown in Fig. 27, using the available experimental data reported by the various authors. In the P-T diagram (Fig. 27),

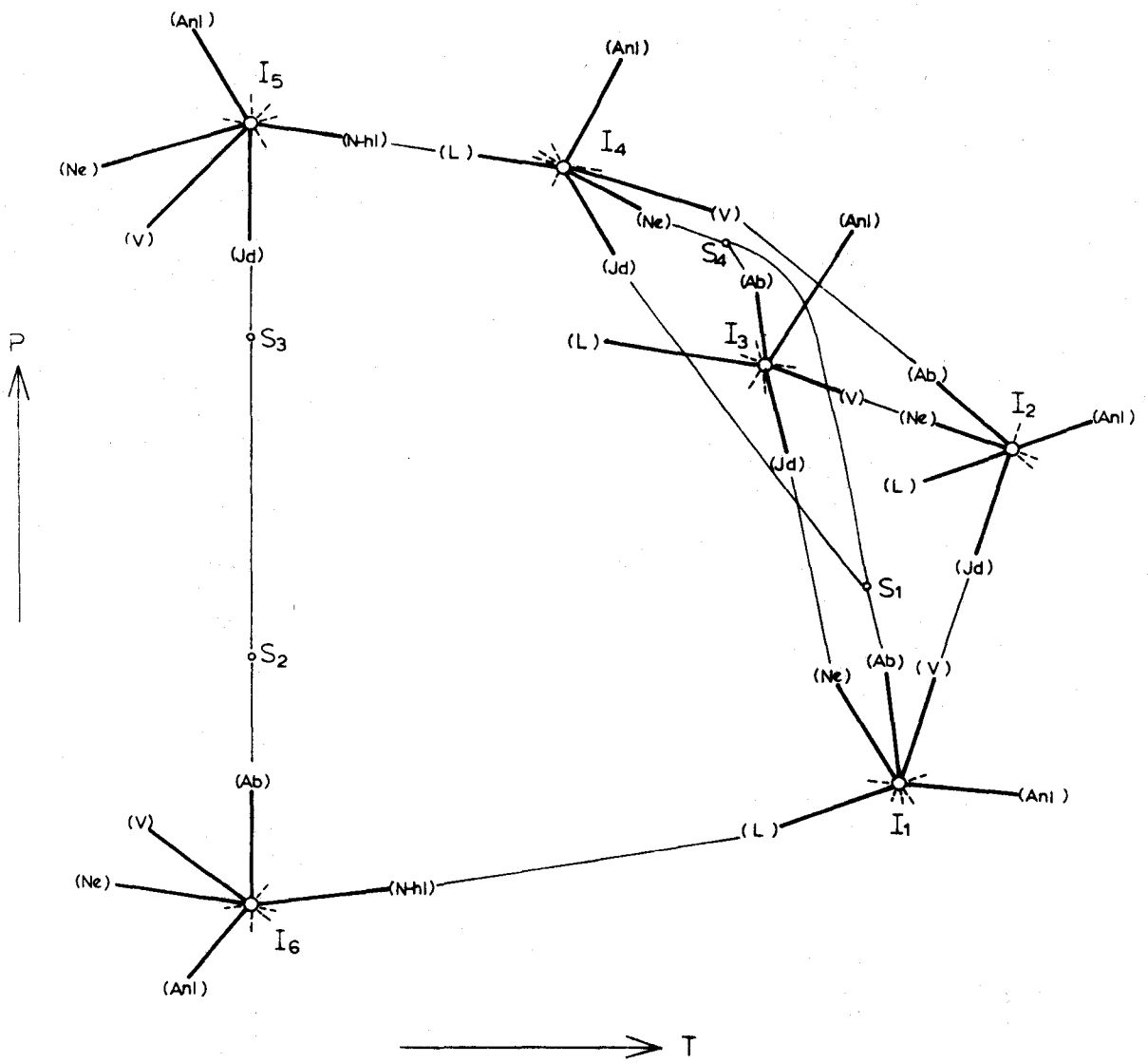

FIG. 26 COMPOSITE P-T DIAGRAM AROUND SIX INVARIANT POINTS(SCHEMATIC)

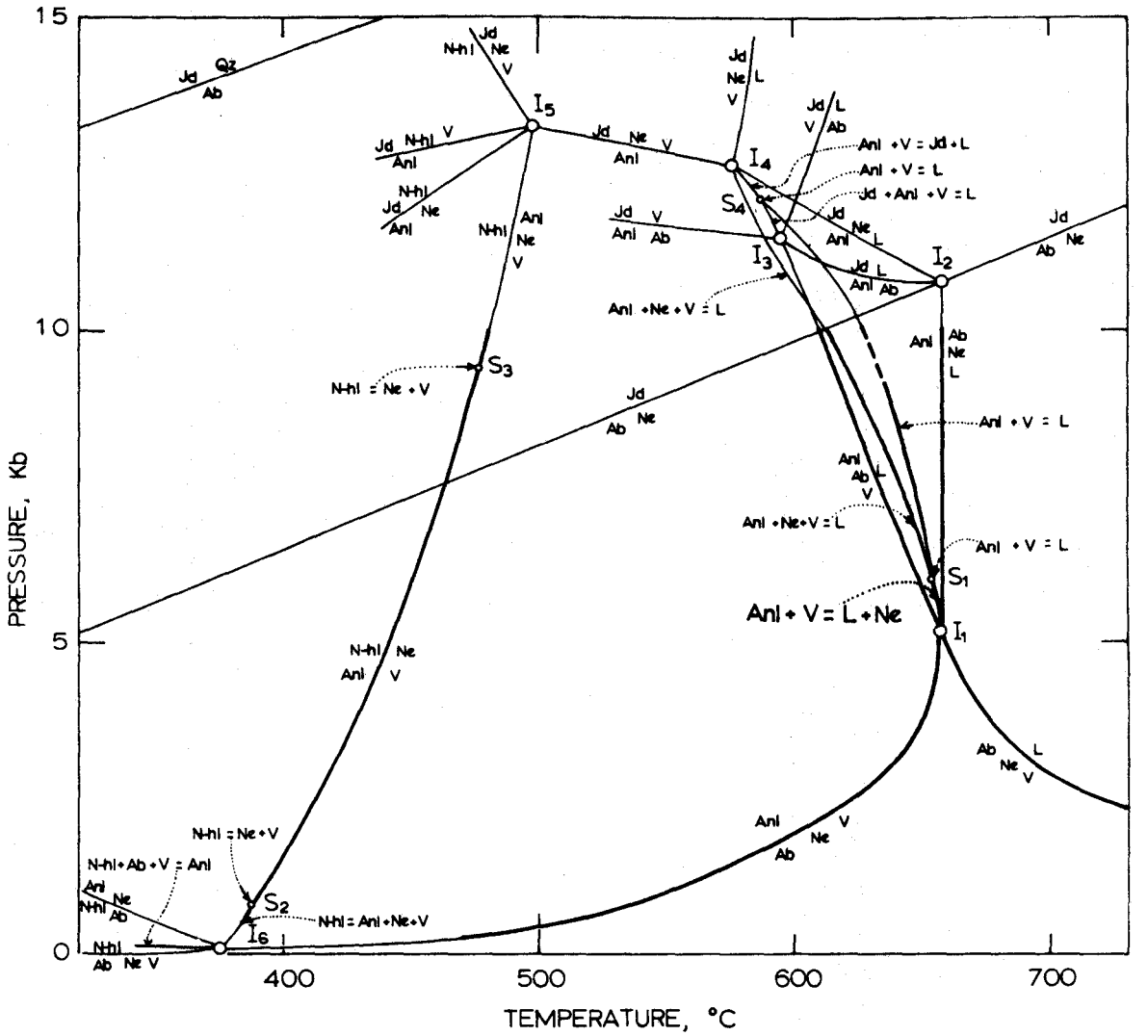

FIG. 27 PHASE RELATIONS ON P-T PROJECTION IN THE SYSTEM $NaAlSi_3O_8$-$NaAlSiO_4$-H_2O UP TO 15 Kb.

The thick solid lines were determined in this study. The fine solid lines were approximately drawn partly on the basis of the previous works reported by various authors and partly on the basis of the present work. The phase relationships between I_1 & I_3 and I_3 & I_4 were partly modified. Two invariant points I_5 & I_6 were predicted probably to exist.

thick lines were determined in this study (see Part 1, especially Fig. 5), and the fine lines are the univariant P-T curves either determined and/or estimated in previous works or expected in this study.

The two P-T curves for the reactions Ab+Ne = Jd and Ab = Jd + Qz in this diagram are the average of the previous results reported by Boettcher & Wyllie (1968, 1969), Hlabse & Kleppa (1968), Newton & Kennedy (1968), Newton & Smith (1967), Bell & Roseboom (1965), Birch & LeComte (1960), Fyfe & Valpy (1959), and Robertson, Birch & MacDonald (1957). Among these authors, Boettcher & Wyllie (1968, p. 1002) and Hlabse & Kleppa (1968, p. 1288) well summarized all previous work pertinent to the two P-T curves in a comparison diagram.

The P-T curve for the reaction Anl+Ab = Jd+V was experimentally determined by Griggs, Fyfe & Kennedy (1955) and thermochemically calculated by Fyfe & Valpy (1959) in the term of Anl= Jd+V. But their results are too different from each other to take a useful average as described in the previous section. So their curves[1] are not shown in diagram (Fig. 27). The correct reaction equation for the jadeite-analcite boundary was proposed firstly by Boettcher & Wyllie (1969, p. 890), which was deduced using Schreinemakers' rule. In the present study, their proposition for the univariant reaction Anl+Ab = Jd+V was confirmed on the basis of estimated compositional data of the invariant phases of I_3 and Schreinemakers' rule (1915).

---

1. Note that the equilibrium curve for the reaction: Anl = Jd+V reported by Newton & Kennedy (1968, p. 733) has a positive slope.

Boettcher & Wyllie (1969, p. 894) deduced the sequence of P-T curves around B & W I_6 (I_3 herein) and had to place a singular point B & W S_4 ($\simeq S_4$ herein) in order to connect B & W I_6 to B & W I_5 (= I_1 herein) as shown in their diagram (Fig. 6). But it is found that it is not necessary in this study (see Fig. 25-(1)c & d and (3)c & d). The invariant point I_3 is directly connected with I_1 by the univariant P-T curve for the reaction Anl+Ab+V = L.

Hamilton (D. L., August 1970; personal communication) suggested that the singular point may be located between the two invariant points I_3 & I_4. This appears very reasonable and his suggestion is adopted in this study. Firstly, the inspection of two isobaric T-X phase diagrams (see Figs. 25(3)a and (4)a) requires the termination of the thermal divide (formed due to the intrusion of analcite stability peak above liquidus curve) at some P-T point between I_3 and I_4. The terminal must be a singular point. Secondly, in order to connect I_3 with I_4, the phase relations require a singular point between I_3 and I_4. Thus, a singular point, S_4, is assumed to be located on a univariant curve between I_3 and I_4.

If the singular point is assumed to be at a higher P-T field than that of I_4, then neither I_4 nor I_5 can be an invariant point. But the two (Ab) univariant P-T curves respectively emanating

from I_1 and I_6 pass through I_4 and I_5 respectively and intersect in a point (~515°C,~17Kb), say I_7. At the invariant point I_7, five phases Anl, Ne, N-h I, L & V may coexist. The invariant chemogram may be a triangle defined by three phases Anl, Ne & V, with two interior phases L & N-h I.

If this point (I_7) exists, then it is important because nepheline hydrate I can crystallize directly from a liquid (magma ?).

However, the invariant point I_7 is hardly expected to occur. Some of the reasons are given below.

i) It is questionable whether nepheline hydrate I is a stable phase at such high pressure (P_{H_2O}).

ii) If phases Jd, Ne and V coexist stably, then I_7 cannot occur. Little is known about the stability of Jd+Ne+V assemblage. Boettcher & Wyllie (1969, p. 884 and 895) reported the occurrence of the three phase assemblage, Jd, Ne and V, and also located the univariant P-T curve Jd+Ne+V = L. As a result, their experimental data suggest the impossibility of the I_7 occurrence. Since their interpretation was based only on a few run products, however, further detailed experimental investigation is needed.

IV. P-T STABILITY FIELD OF ANALCITE IN THE SYSTEM $NaAlSi_3O_4$-$NaAlSiO_4$-H_2O

Fyfe & Turner (1958, p. 177) illustrated an idealized P-T stability field of analcite on the basis of data reported by Griggs, Fyfe and Kennedy (1955, p. 1569). Since then, numerous experimental data have been accumulated as discussed in the previous chapter (for further information, refer to Boettcher & Wyllie, 1969). Now, it becomes possible to improve their idealized diagram, although data in low temperature regions are incomplete mainly due to the difficulty of equilibrium-attainment of coexisting phase assemblage.

The inspection of the P-T diagram (Fig. 27) indicates a very interesting feature of the stability of analcite, especially liquidus analcite. The P-T stability field of analcite is only illustrated in Fig. 28. In most cases, of course, various kinds of phases coexist with analcite in the analcite-stability region. For the sake of simplicity, the other phases are not shown in this diagram (Fig. 28; for details see Fig. 27).

Analcite is classified into two principal categories, subsolidus analcite and liquidus analcite.

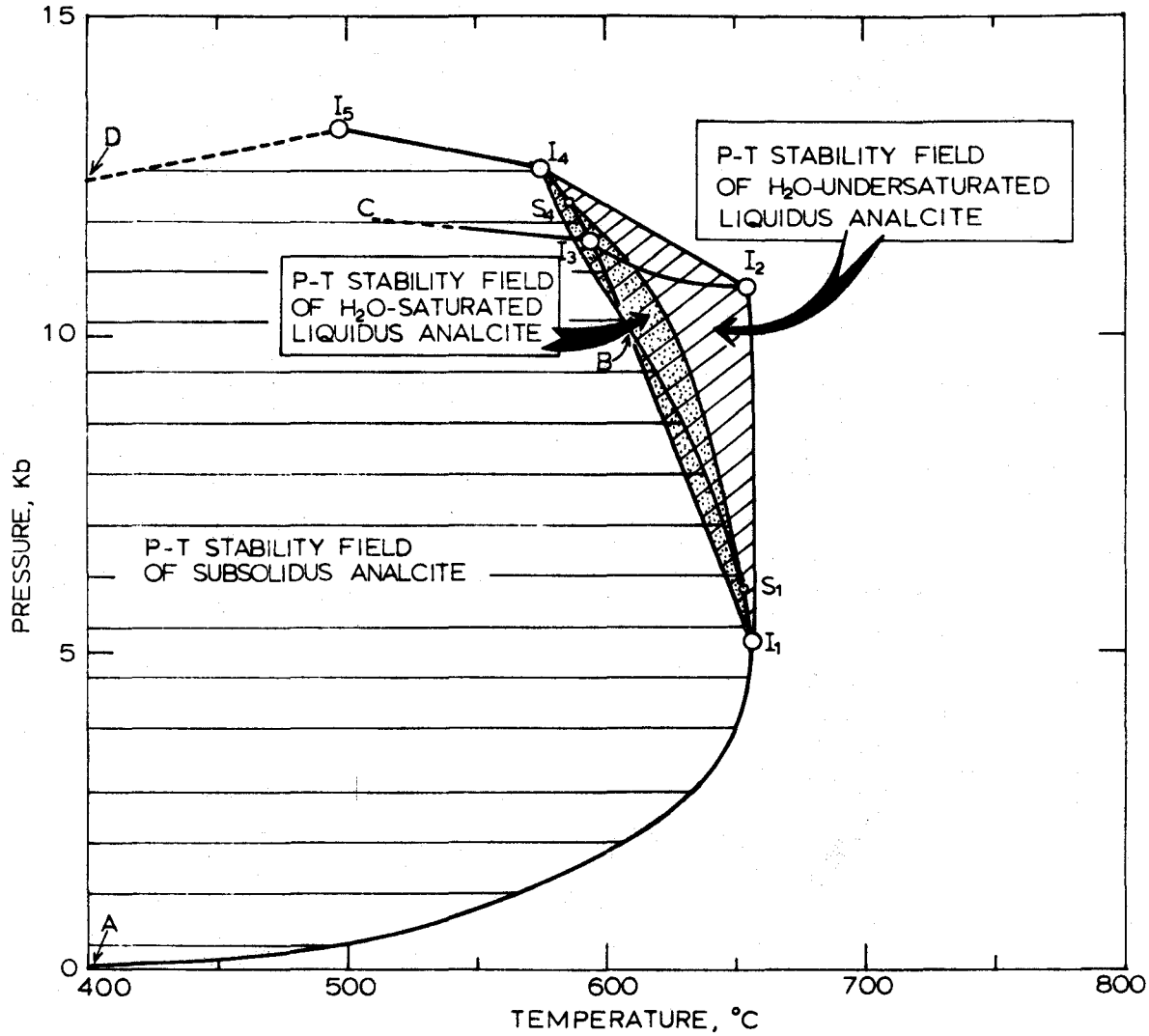

FIG.28 P-T STABILITY FIELD OF ANALCITE IN THE SYSTEM $NaAlSi_3O_8$-$NaAlSiO_4$-H_2O.

The stability field of analcite is deduced on the basis of phase relations presented in Fig. 27.

A horizontally hatched large area: maximum stability field of subsolidus analcite.

An obliquely hatched triangular area: maximum stability field of liquidus analcite and also that of H_2O-undersaturated liquidus analcite.

A stippled spindly area: maximum stability field of H_2O-saturated liquidus analcite.

1. Subsolidus Analcite

The subsolidus analcite is stable in a large P-T region enclosed by the various univariant curves joining A, I_1, S_1, B, I_3, S_4, I_4, I_5 and D (see Fig. 28). This P-T region represents a maximum range for the stability of subsolidus analcite. The P-T region does, of course, further extend towards the lower temperature regions. The P-T stability field of subsolidus analcite is more or less modified depending on the bulk composition (or the kind of co-existing phases).

When a bulk-composition is rich in the albite-component the analcite-stability field is represented as a P-T region defined by points, A, I_1, B, I_3 and C. When a bulk-composition is rich in the nepheline-component, then the stability field is defined by points A, I_1, S_1, B, I_4, I_5 and D. These stability fields can be further restricted, of course, depending on coexisting phases with the analcite. Attention is called to the fact that the P-T stability field of subsolidus analcite is enormously large, whereas that of liquidus analcite is very much limited.

2. Liquidus Analcite

The maximum stability field of liquidus analcite is a triangular P-T region defined by three invariant points, I_1 (657°C,

5.15Kb), I_2 (650°C, 11Kb) and I_4 (575°C, 12.5Kb) (closely hatched area in Fig. 28). The liquidus analcite can be subdivided into two kinds, H_2O-saturated liquidus analcite and H_2O-undersaturated liquidus analcite, with respect to H_2O-content in a coexisting liquid.

2-1. H_2O-Saturated Liquidus Analcite.

An analcite which coexists with liquid and vapor and/or other phases is stable only in a very narrow range of temperature (at most, within 20°C) at any given pressure within 5.15-12,5Kb. The P-T stability field of the analcite is defined by a set of univariant curves joining two invariant points I_1 and I_4, i. e. the narrow region enclosed by points, I_1, S_1, S_4, I_4, B and I_1 (stippled spindly area in Fig. 28).

If a bulk-composition is richer in the albite than that of the analcite of the thermal divide, the P-T stability field of the analcite is restricted to an area defined by points, I_1, S_1, S_4, I_3, and I_1. If a bulk-composition is richer in nepheline-component than that of the analcite of the thermal divide, then the stability field of the analcite is defined by points, I_1, S_1, S_4, I_4, B and S_1.

In most cases, however, the former (albite-rich) is represented by a single curve joining several points, I_1, B & I_3 (or up to S_4 and I_4), and the latter (nepheline-rich) is also reduced to a single curve joining I_1, S_1, B and I_4, except for some special case (e.g. analcitite). Thus, H_2O-saturated liquidus analcite has a very limited chance to crystallize from a liquid (or magma ?) on cooling .

2-2. H_2O-Undersaturated Liquidus Analcite.

The P-T region in which an analcite coexists stably with H_2O-undersaturated liquid (magma ?) and/or other crystal phases is also represented by the triangular area defined by three points, I_1, I_2, and I_4.

If a bulk-composition is richer in albite-component than that of the thermal divide due to the analcite T-X stability peak, then the P-T stability field of the analcite is defined by I_1, I_2, I_3, and I_1, (a triangle). If a bulk-composition is richer in nepheline-component than that of the thermal divide due to the analcite peak, then the P-T stability field is defined by points, I_1, I_2, I_4, B, S_1, & I_1.

In fact, the P-T stability field of liquidus analcite shown in Fig. 28 is represented essentially for H_2O-undersaturated analcite. Thus it may be concluded that most liquidus analcite (e.g. primary analcite phenocryst) is attributed essentially to the crystallization

from H_2O-undersaturated liquid (or magma ?). Since an analcite can crystallize directly from a melt within a very limited P-T region, the liquidus analcite may also be used as an approximate geothermometer (575°C-657°C) within the range of pressure 5.15-12.5Kb. This P-T region may be further reduced depending on the phase assemblage of primary analcite-bearing rock and also by knowing one of the two variables, pressure and temperature.

REFERENCES CITED

BARRER, R.M. (1950), Ion-exchange and ion-sieve processes in crystalline zeolites, Jour. Chem. Soc., pp. 2342-50.

_____ and WHITE, E.A.D. (1952), The hydrothermal chemistry of silicates. Part II, Synthetic crystalline sodium aluminosilicates, Jour. Chem. Soc., pp. 1561-71.

_____, HINDS, L., and WHITE, E.A.D. (1952), The hydrothermal chemistry of silicates. Part III. Reactions of analcite and leucite, Jour. Chem. Soc., pp. 1466-74.

_____ and BAYNHAM, J.W. (1956), The hydrothermal chemistry of silicates. Part VII. Synthetic potassium aluminosilicates, Jour. Chem. Soc., pp. 2882-91.

_____, _____, BULTITUDE, F. W. and MEIER, W. M. (1959), Hydrothermal chemistry of the silicates. Part VIII. Low-temperature crystal growth of aluminosilicates, and of some gallium and Germanium analogues, Jour. Chem. Soc. (London), pp. 195-208.

BELL, P.M., and ROSEBOOM, E.H. Jr. (1965), Phase diagram for the system nepheline-quartz, Carnegie Inst. Washington Year Book 64 , pp. 139-41.

BIRCH, F. , and LECOMTE, P. (1960), Temperature-pressure plane for albite compositions, Am. J. Sci., v. 258, pp. 209-17.

BOETTCHER, A. L. and WYLLIE, P. J. (1968) Jadeite stability measured in the presence of silicate liquids in the system $NaAlSiO_4$-SiO_2-H_2O, Geochim. et Cosmochim. Acta, v. 32, pp. 999-1012.

_____ and _____ (1969), Phase relationships in the system $NaAlSiO_4$-SiO_2-H_2O to 35 kilobars pressure, Am. J. Sci., v. 267, pp. 875-909.

BOWEN, N. L. and SCHAIRER, J. F. (1929), The system leucite-diopside, Am. J. Sci. 5th ser., v. 58, p. 499.

_____ and TUTTLE, O. F. (1950), The system $NaAlSi_3O_8$-$KAlSi_3O_8$-H_2O, Jour. Geol., v. 58, pp. 489-511.

BOYD, F. R. and ENGLAND, J. L. (1956), Breakdown of nepheline under pressure(abs), Geol. Soc. America Bull., v. 67, p. 1674.

BURLEY, B. J. and FREEMAN, E. B. (1959), The effect of temperature on the lattice parameters of quenched synthetic analcime, Canadian Mineral., v. 6, pp. 372-79.

BURNHAM, C. W. and JALENS, R. H. (1962), A method for determining the solubility of water in silicate melts, Am. J. Sci., v. 260, pp. 721-45.

CHIRVINSKY, P.N. (1953), The average chemical composition of the principal minerals of eruptive, metamorphic, and sedimentary rocks, Lvov. Geol. Soc.

COOMBS, D.S. and WHETTEN, J.T. (1967), Composition of analcime from sedimentary and burial metamorphic rocks, Bull. Geol. Soc. Amer., v. 78, pp. 269-82.

DEER, W.A., HOWIE, R.A. and ZUSSMAN, J. (1963), Rock-forming minerals, v. 4, Framework Silicates, London; Longmans, Green & Co. Ltd.

EDGAR, A.D. (1964), Phase-equilibrium relations in the system Nepheline-Albite-Water at 1,000 Kg/cm, Jour Geol., v. 72, pp. 448-60.

_____ (1964), A note on the lattice parameters of nepheline hydrate I. Am. Mineral., v. 49, pp. 1139-41.

FUDALI, R. (1963) Experimental studies bearing on the origin of pseudoleucite and associated problems of alkalic rock systems. Bull. Geol. Soc. Am., v. 74, pp. 1102-26.

FYFE, W.S., TURNER, F.J. and VERHOOGEN, J. (1958) Metamorphic reactions and Metamorphic facies, Memoir. 73, Geol. Soc. America.

_____ and VALPY, G.W. (1959) The analcime-jadeite phase boundary; some indirect deductions, Am. J. Sci., v. 257, pp. 316-20.

GORANSON, R.W. (1931) The solubility of water in granite magmas, Am. J. Sci., v. 22, pp. 481-502.

GREENWOOD, H.J. (1961), The system $NaAlSi_2O_6$-H_2O-argon: Total pressure and water pressure in metamorphism, Jour. Geophys. Res., v. 66, pp. 3923-46.

GREIG, J.W. and BARTH, T.F.W. (1938) The system $Na_2O.Al_2O_3.2SiO_2$ (nephelite carnegieite) - $Na_2O.Al_2O_3.6SiO_2$(albite), Am. J. Sci., 5th ser., v. 35A, pp. 93-112.

GRIGGS, D.T., FYFE, W.S. and KENNEDY, G.C. (1955) Jadeite alalcite, and nepheline-albite equilibrium (abs): Geol. Soc. America. Bull., v. 66, p. 1569.

HAMILTON, D.L. and MacKENZIE, W.S. (1960) Nepheline solid solution in the system $NaAlSiO_4$-$KAlSiO_4$-SiO_2, Jour. Petrol., v. 1, pp. 56-72.

_____ and _____ (1965) Phase-equilibrium studies in the system $NaAlSiO_4$ (nepheline) - $KAlSiO_4$ (kalsilite) - SiO_2 - H_2O, Mineral Mag., v. 34, pp. 214-31.

HLABSE, T. and KLEPPA, O.J. (1968) The thermochemistry of jadeite. Am. Mineral., v. 53, p.1281-92.

KELLY, K.K., TODD, S.S., ORR, R.L., KING, E.G. and BONNICKSON, K.R. (1953), Thermodynamic properties of sodium-aluminium and potassium-aluminum silicates, U.S. Bur. Mines Rept. In v. 4955.

KENNEDY, G. C. and HOLSER, S. P. (1966) Specific volumes of water in handbook of physical anstants (Ed. Clark, S. P.), Geol. Soc. America Mem. 97, revised Ed., pp. 374-79.

KHITAROV, N. I., LEBEDEV, E. B., RENGARTEN, E. V., and ARSEM'EVA R. V. (1959) The solubility of water in basaltic and granitic melts, Geochemistry (Geokhimya), no. 5, pp. 479-506.

KUBO, Y., YAMAGUCHI, G. and KASAHARA, K. (1967), Hydrated sodium aluminosilicates relating to nepheline-carnegieite minerals: relations among the crystal lattices and thermal transformations, J. Ceram. Assoc. Japan, v. 75, pp. 183-92.

LARSEN, E. S. and BUIE, B. F. (1938), Potash analcime and pseudo-leucite from the Highwood Mountains of Montana, Am. Mineral., v. 23, pp. 837-49.

LUTH, W. C., and TUTTLE, O. F. (1963), Externally heated cold-seal pressure vessels for use to 10,000 bars and 750°C.

MacKENZIE, J. D. (1941) The Crowsnest volcanics, Geol. Sur. Can. Mus. Bull., No. 4, Geological Series, No. 20.

MacKENZIE, W. S. (1957), The crystalline modifications of $NaAlSi_3O_8$, Am. J. Sci., v. 255, pp. 481-516.

MORSE, S. A. (1969a), Syenites, Carnegie Inst., Washington Year-book 1967, pp. 112-20.

MORSE, S.A. (1969b), Feldspars, Carnegie Inst. Washington Yearbook 67, pp. 120-26.

NEWTON, M.S., and KENNEDY, G.C. (1968), Jadeite, analcite, nepheline and albite at high temperatures and pressures, Am. J. Sci., v. 266, pp. 728-35.

NEWTON, R.C., and SMITH, J.V. (1967), Investigations concerning the breakdown of albite at depth in the earth, Jour. Geol., v. 75, pp. 268-87.

PEARCE, T.H. (1970), The analcite-bearing volcanic rocks of the Crowsnest Formation, Alberta, Can. J. Earth Sci., v. 7, pp. 46-66.

PETERS, Tj., LUTH, W.C. and TUTTLE, O.F. (1966), The melting of analcite solid solutions in the system $NaAlSiO_4$-$NaAlSi_3O_8$-H_2O, Am. Mineral., v. 51, pp. 736-53.

ROBERTSON, E.C., BIRCH, F. and MacDONALD, G.J.F. (1957), Experimental determination of jadeite stability relations to 25,000 bars, Am. J.Sci., v. 255, pp. 115-37.

SAHA, P. (1959), Geochemical and X-ray investigation of natural and synthetic analcites, Am. Mineral., v. 44, pp. 300-13.

_____, (1961), The system $NaAlSiO_4$(Nepheline)-$NaAlSi_3O_8$ (Albite)-H_2O, Am. Mineral., v. 46, pp. 859-84.

SAHAMA, Th. G. (1952), Leucite, potash nepheline and clinopyroxene from volcanic lavas from South Western Uganda and adjoining Belgian Congo, Am. J. Sci., Bowen v., p. 457.

SAND, L. B., ROY, R., and OSBORN, E. F. (1957), Stability relations of some minerals in the Na_2O-Al_2O_3-H_2O system, Econ. Geol., v. 52, pp. 169-79.

SCHAIRER, J. F., and BOWEN, N. L. (1935), Preliminary report on equilibrium relations between feldspathoids, alkali - feldspars, and silica, Trans. Am. Geophys. Union Pt. I, pp. 325-8.

SCHAIRER, J. F. (1950), The alkali feldspar join in the system $NaAlSiO_4$-$KAlSiO_4SiO$, Jour. Geol., v. 58, pp. 512-7.

_____ and BOWEN, N. L. (1955), The system K_2O-Al_2O_3-SiO_2, Am. J. Sci., v. 253, p. 681.

SCHREINEMAKERS, F. A. H. (1915), In-, mono-, and divariant equilibria I & II K. Nederlandse Akad. Wetenschappen, v. 18, pp. 116-26 & 531-42

_____ (1916), In-, mono-, and divariant equilibria III, K. Nederlandse Akad. Wetenschappen, v. 18, pp. 820-8.

TILLEY, C. E. (1958), The leucite nepheline dolerite of Meiches, Vogelsberg, Hessen, Am. Mineral., v. 43, p. 759.

TUTTLE, O. F. (1949), Two pressure vessels for silicate - water studies, Geol. Soc. America Bull., v. 60. pp. 1727-9.

_____ and SMITH, J. V. (1953), The nepheline-kalsilite system, II. , Phase relations, Am. J. Sci., v. 256, pp. 571-89.

TUTTLE, O. F. and BOWEN, N. L. (1958) Origin of granite in the light of experimental studies in the system $NaAlSi_3O_8$-$KAlSi_3O_8$-SiO_2-H_2O. Geol. Soc. America Mem. 74.

WHETTEN, J. T. and COOMBS, D. S. (1965) Composition of low temperature analcite, Trans. Am. Geophys. Union, v. 46, pp. 181-2.

WILKINSON, J. F. G. (1962) Mineralogical, Geochemical, and petrogenetic aspects of an analcite-basalt from the New England District of New South Wales, Jour. Petrol., v. 3, pp. 192-214.

_____ (1963) Some natural analcime solid solutions, Min. Mag., v. 33, pp. 498-505.

_____ and WHETTEN, J. T. (1964), Some analcime-bearing pyroclastic and sedimentary rocks from New South Wales, Jour. Sed. Petrol., v. 34, pp. 543-53.

_____ (1965), Some feldspars, nephelines and analcimes from the Square Top Intrusion, Nundle, N. S. W., Jour. Petrol., v. 6, pp. 420-44.

_____ (1968), Analcimes from some potassic igneous rocks and aspects of analcime-rich igneous assemblages, Contr. Mineral. and Petrol., v. 18, pp. 252-69.

YODER, H. S. Jr., (1950), The jadeite problem, Am. J. Sci., v. 248. pp. 225-48 and pp. 312-34.

_____ (1954), Zeolites-analcite; Carnegie Inst. Washington, Yearbook 53, pp. 736-53.

YODER, H.S. Jr., (1954), The system diopside-anorthite-water, Carnegie Inst. Washington 53, pp. 106-7.

_____, STEWART, D.B. and SMITH, J.R. (1957) Ternary feldspars, Carnegie Inst. Washington Yearbook 57, p. 189-91.

_____, (1958) Effect of water on the Melting of silicates, Carnegie Inst. Washington Yearbook 57, pp. 189-91.

_____, (1965) Diopside-anorthite-water at five and ten kilobars and its bearing on explosive volcanism., Carnegie Inst. Washington Yearbook 64, pp. 82-9.

ZEN, E-an, (1966) Construction of pressure-temperature diagrams for multicomponent systems after the method of Schreinemakers-A geometric approach, U.S.G.S. Bull. 1225,